

Oxidation of Sugars and Polyols for Sustainable Production of Value-added Chemicals

By © 2019

Honghong Shi

Ph.D., University of Kansas, 2019

M.Sc., University of Calgary, 2015

B.Eng., China University of Petroleum, 2011

Submitted to the graduate degree program in Department of Chemical and Petroleum Engineering and the Graduate Faculty of the University of Kansas in partial fulfillment of the requirements for the degree of Doctor of Philosophy.

Chair: Raghunath V. Chaudhari

Bala Subramaniam

Laurence Weatherley

Kevin C. Leonard

Ward, H. Thompson

Date Defended: 5 September 2019

The dissertation committee for Honghong Shi certifies that this is
the approved version of the following dissertation:

**Oxidation of Sugars and Polyols for Sustainable
Production of Value-added Chemicals**

Chair: Raghunath V. Chaudhari

Date Approved: 5 September 2019

Abstract

Biomass has attracted tremendous research attentions in the last few decades as one of the most promising renewable option to produce chemical products. To achieve efficiency and productivity similar to that demonstrated for the fossil-based routes, development of active and selective catalysts for biomass-to-chemicals conversion are highly demanded. In this dissertation, investigations on catalysis and kinetics of aqueous phase oxidation of ethylene glycol and glucose are presented as examples of biomass conversion to chemicals. Current state of development in these processes is reviewed in the Chapter 1 that demonstrates the research gap in designing a highly active oxidation catalyst for the selective production of carboxylic acid, especially under base-free conditions.

The screening of monometallic catalysts for the aqueous phase oxidation of ethylene glycol to glycolic acid was investigated as presented in the Chapter 2. The study employs an integrated approach of combining activity tests, surface characterization, and computational modeling. The effects of alkali promotion and the role of O_2 /water on ethylene glycol oxidation in the aqueous phase are discussed. NaOH as a base alone was found to catalyze EG oxidation, as also acting as a promoter in the presence of metal catalysts. O_2 was involved in producing OOH^* species that reacts with deprotonated EG to form glycolic acid, while producing H_2O_2 in the aqueous phase as a byproduct. Based on computational modeling, predictions of a volcano-type correlation between adsorption energy and reaction activity for various metals are presented that show trends consistent with the experimental results.

In the Chapter 3, experimental study on a highly active and selective bimetallic Pt-Fe alloy catalyst on CeO_2 support is presented along with screening of various bimetallic catalysts for the

aqueous phase oxidation of ethylene glycol. Selectivity with respect to glycolic acid as a product is discussed. The Pt-Fe nanoparticles are highly alloyed with a fcc type of crystal structure and a chemical state of Pt⁰/Fe⁰, as confirmed from XRD and EXAFS characterizations, respectively. Compared to the monometallic Pt catalyst prepared by an identical method, the Pt-Fe catalyst shows more than a 17-fold higher TOF achieving complete EG conversion in 4 hours at 70 °C and ambient O₂ pressure under alkaline conditions, with a selectivity of glycolic acid up to 62% on a carbon basis. From parametric effect studies, it can be concluded that the synergistic bimetallic effect occurs due to significantly changing the O₂ adsorption-dissociation characteristics on the catalyst surface. The addition of a base shows a promotional effect on both Pt and Pt-Fe catalysts at low NaOH concentrations but an inhibition effect on both catalysts is observed at sufficiently high NaOH concentrations. In contrast, HCO₃³⁻ and CO₃²⁻ ions were found to have an inhibition effect on the EG oxidation.

Oxidation of glucose to gluconic and glucaric acid using molecular O₂ in aqueous solution is an environmentally friendlier alternative to the conventional method that uses nitric acid as an oxidant. However, obtaining a satisfactory yield of the desirable product, glucaric acid, especially under base-free conditions, is still a challenge. In the Chapter 4, optimization of Pt based mono and bimetallic catalysts is reported by tuning four factors: support type, synthesis method, reductant used in synthesis, and choice of the second metal. All these four factors influence the glucaric acid selectivity. Among the tested combinations, the Pt-Cu/TiO₂ bimetallic catalyst showed ~60% glucaric acid selectivity in one-step glucose oxidation under base-free conditions at 90 °C and 15 bar O₂. The catalyst consists of Pt metal particles (~2.8 nm diameter on average) with a dominant presence of the alloyed Pt-Cu phase, as confirmed by XRD and TEM analyses. These results provide valuable insights for rational design of glucose oxidation catalysts.

It is of great interest to study the shape dependency on the catalytic activity of Pt catalysts in oxidation reactions. In the Chapter 5, one-pot synthesis strategy of supported Pt catalyst is discussed for synthesis of monodispersed nanocrystals enclosed by single lattice planes. The Pt and Pt-Cu nanocrystals with cubic, octahedral, and stellar morphologies were successfully synthesized, which were evaluated for their performance in glucose oxidation. It was found that the crystal facets of Pt-Cu nanoparticles play an important role in determining the catalytic activity and selectivity in the glucaric acid production. In addition, significant bimetallic effect was demonstrated an enhancement in the selective formation of glucaric acid (TOF increased for about 10 times regarding to glucaric acid production) .

Acknowledgments

Many people have earned my gratitude for their contribution to my Ph.D. degree. More specifically, I would like to thank three groups of people, without whom this dissertation could not have been finished: my thesis committee members, my colleagues and friends at the KU, and my family.

First, I am forever grateful to have Dr. Raghunath V. Chaudhari as my research advisor. It all started in spring 2016 when he offered me such a great opportunity to join the team in the Center for Environmentally Beneficial Catalysis (CEBC). Since my first day in the group, Dr. Chaudhari believed in me like nobody else and gave me endless support. Under his supervision, I learned how to find solutions to a scientific problem and finally publish the results. On the academic level, Dr. Chaudhari taught me fundamentals of conducting scientific research in catalysis and reaction engineering fields. On a personal level, Dr. Chaudhari inspired me by his healthy lifestyle, kindness and philosophy of being a lifetime learner. Without his help, I would not be able to become a positive and curious researcher.

Besides my advisor, I would like to thank the rest of my dissertation committee members: Dr. Bala Subramaniam, Dr. Franklin F. Tao, Dr. Kevin C. Leonard and Dr. Ward H. Thompson for their invaluable suggestions on my research work and inputs on shaping my dissertation. In the preliminary and comprehensive exams, the challenging questions from them inspired me to think through my research topic from diverse aspects. Moreover, I am so glad to have opportunities to discuss with them on various occasions as top experts in Chemistry and Chemical Engineering. At the same time, I would like to give special thanks to Dr. Ali Haider and his group in the Indian Institute of Technology in Delhi for their contributions to the computational works and insights for my works on the oxidation of ethylene glycol.

During the last four years, my colleagues and friends at KU gave me countless supports, making me feel that I am always be thought of and also be loved. I am very grateful to Dr. Xiaogang Yin and Dr. Xin Jin for their insightful comments, hands-on supports in lab and for sharing with me their experience in different technologies. I am thankful to Dr. Hongda Zhu, a fan of *Cthulhu Mythos* and an all-rounder who strives to excellence with a peaceful mind, for the inspiring thoughts and many helps in the lab. I am quite appreciative of Pallavi Bobba, Dr. Ziwei Song, Yuting Li, Dr. Yu Tang, Bhagyesha Patil, Dr. Priya Darshini Srinivasan, Anoop Uchagawkar, Dr. Luxi Chai, Chenxi Lin, and Lijun Chen for their help, caring and kindness. I also want to express my gratitude to all my colleagues working in CEBC, including Dr. Julian Silverman, Dr. Feng Niu, Dr. Michael Lundin, Dr. Kirk Snavely, Dr. Hyun-Jin Lee, Dr. Andrew Danby, Dr. Xiaobin Zuo, Dr. Claudia Bode, Nancy Crisp, Jane Johns, Ed Atchison, and Dr. Chris Lyon who helped me moment to moment during the last four years. In addition, I sincerely thank Dr. Prem Thapa, Dr. Luan Nguyen and Dr. Victor Day for their timely help with catalyst characterizations.

Finally, yet importantly, I would like to express my deepest gratitude to my parents and my husband. Positivity and kindness are a nature when I was a child, but they become my choices as an adult in front of the challenging moments and failures in life. The endless love received from my parents during my childhood and the good faith from them are the most important sources of strength supporting me. I am also grateful to my husband who gives our daughter and me the caring as much as he can and encourages me to finish my degree. His integrity, gifted eloquence, well-read habit and humor make me feel that I have encountered and married to a great man. This dissertation would not have been possible without the warm love and endless support from my family.

Dedication

This dissertation is dedicated to my family.

献给我的家人。

Table of Contents

Abstract	iii
Acknowledgments.....	vi
Dedication	viii
Table of Contents	ix
List of Figures	xiv
List of Tables	xix
Chapter One: Introduction & literature Review.....	1
1.1 Overview on biomass feedstock for chemicals	1
1.1.1 Biomass-to-Energy	1
1.1.2 Biomass-to-Fuels	3
1.1.3 Biomass-to-Chemicals	8
1.2 Summary of biomass-to-chemicals technologies	9
1.3 Catalysts Development on the Hydrogenolysis and Oxidation of Sugars and Polyols	16
1.3.1 Hydrogenolysis catalysts.....	16
1.3.2 Oxidation catalysts	21
1.4 Literature Survey on the Oxidation of Glucose and Ethylene Glycol to Value-added Products	26

1.4.1 Oxidation of Glucose	26
1.4.2 Oxidation of Ethylene Glycol	32
1.5 Objectives	35
Chapter 2: Aqueous Phase Oxidation of Ethylene Glycol using Supported Monometallic Catalysts	
2.1 Introduction.....	37
2.2 Experimental and Methodology.....	38
2.2.1 Catalyst Preparation	38
2.2.2 Catalyst Characterization	38
2.2.3 Catalyst Performance in Oxidation Reactions	39
2.3 Results and Discussions.....	39
2.4 Conclusion	49
Chapter 3: Liquid-phase Oxidation of Ethylene Glycol using Bimetallic Catalysts: Synergistic Effects and Reaction Mechanism.....	
3.1 Introduction.....	51
3.2 Experimental and Methodology.....	52
3.2.1 Catalyst Synthesis and Characterization.....	52
3.2.2 Performance Evaluation Catalysts for Oxidation	53
3.3 Results and Discussions.....	55

3.3.1 Performance Evaluation of Bimetallic Catalysts	55
3.3.2 Pt-Fe Bimetallic Effect and OH* Mediated Reaction Mechanism	60
3.3.3 Catalyst Characterization and Structure-Activity Relationship	61
3.3.4 Effect of Reaction Conditions.....	66
3.4 Conclusion	76
Chapter 4: Oxidation of Glucose using Mono and Bimetallic Catalysts in Base Free Conditions	77
4.1 Introduction.....	77
4.2 Experimental and Methodology.....	78
4.2.1 Materials	79
4.2.2 Catalyst Preparation	79
4.2.3 Catalyst Characterization	80
4.2.4 Activity Test.....	81
4.3 Results and Discussions.....	82
4.3.1 Screening of Mono Pt Catalysts.....	83
4.3.2 Bimetallic Catalysts	89
4.3.3 Characterization of Bimetallic Pt-Cu Catalyst.....	93
4.3.3 Effect of Reaction Conditions.....	103
4.4 Conclusion	107

Chapter 5: Synthesis of Monodispersed Pt-Cu Cubes, Octahedrons, Tetrahedrons on TiO ₂ for Glucose Oxidation: Facet Dependent Catalytic Activity and Selectivity	109
5.1 Introduction.....	109
5.2 Experimental and Methodology.....	111
5.2.1 Materials	111
5.2.2 Synthesis of TiO ₂ supported Pt and Pt-Cu Cubes	113
5.2.3 Synthesis of TiO ₂ supported PtCu octahedron.....	113
5.2.4 Synthesis of TiO ₂ supported PtCu stella octangula	114
5.2.5 Catalyst Characterization	114
5.2.6 Oxidation Reaction	115
5.3 Results and Discussions.....	115
5.3.1 Morphology and Structures.....	115
5.3.2 Evaluation of Catalytic Performance	123
5.4 Conclusion	128
Chapter 6: Conclusions and Recommendations for Future Work	129
6.1 Conclusions.....	129
6.1.1 Oxidation of Ethylene Glycol	129
6.1.2 Oxidation of Glucose	130
6.2 Recommendations.....	131

Notations	133
References	135
Appendix	160
Appendix I Supplementary Information for Chapter 2	160
Appendix II Supplementary Information for Chapter 3	166
Appendix III Supplementary Information for Chapter 4	170
Appendix IV Supplementary Information for Chapter 5	177
.....	177

List of Figures

Figure 1. Renewable energy consumption in major market, 2017 and 2023 (redrawn using the data from reference [4])	2
Figure 2. Global leading producers of bioethanol and biodiesel in 2018 (drawn by using the data from reference [9, 10])	5
Figure 3. Roadmap of chemical production from raw biomass materials	9
Figure 4. Chemical derivatives from glycerol by a variety of technologies	12
Figure 5. Comparison of different synthesis routes of 1, 6-hexanediol	14
Figure 6. Renewable synthesis of adipic acid from glucose	28
Figure 7. Oxidation of ethylene glycol and the products	33
Figure 8. TEM images of monometallics supported on CeO ₂	40
Figure 9. EDX images of (1) Fe/CeO ₂ (2) Au/CeO ₂ (3) Cu/CeO ₂	41
Figure 10. Effect of different initial EG concentrations on oxidation reaction using Pt catalyst	45
Figure 11. Scheme of -OH mediated oxidation mechanism in the aqueous phase, activation energies are cited from references [149] [150]	49
Figure 12. Concentration-time profiles on (a) Pt/CeO ₂ and (b) PtFe/CeO ₂ catalysts for aqueous phase ethylene glycol oxidation in the presence of alkali promoter. Reaction conditions: 0.58 mol/L initial EG conc., initial pH=13.9 (alkali added), EG:metal ratio = 5657:1 (mol:mol), 70 °C, 1atm O ₂ , 60 std mL/min gas flow	56
Figure 13. Concentration-time profiles on (a) Pd/CeO ₂ and (b) Pd-Fe/CeO ₂ catalysts for aqueous phase ethylene glycol oxidation in the presence of alkali promoter. Reaction conditions:	

0.58 mol/L initial EG conc., initial pH=13.9 (alkali added), EG:metal ratio = 5657:1 (mol:mol),
70 °C, 1atm O₂, 60 std mL/min gas flow 56

Figure 14. Concentration-time profiles on (a) Ag/CeO₂ and (b) Ag-Fe/CeO₂ catalysts for aqueous phase ethylene glycol oxidation in the presence of alkali promoter. Reaction conditions: 0.58 mol/L initial EG conc., initial pH=13.9 (alkali added), EG:metal ratio = 5657:1 (mol:mol), 70 °C, 1atm O₂, 60 std mL/min gas flow 57

Figure 15. Concentration-time profiles on (a) Au/CeO₂ and (b) Au-Fe/CeO₂ catalysts for aqueous phase ethylene glycol oxidation in the presence of alkali promoter. Reaction conditions: 0.58 mol/L initial EG conc., initial pH=13.9 (alkali added), EG:metal ratio = 5657:1 (mol:mol), 70 °C, 1atm O₂, 60 std mL/min gas flow 58

Figure 16. PtFe crystal structure: (a) disordered fcc; (b) ordered fct, and (c) X-ray diffraction pattern of the cerium oxide supported PtFe catalyst 63

Figure 17. (a) Fe K edge XAS spectra of Fe foil, ferric oxide, and PtFe catalyst (b)(c) Fourier-transformation of EXAFS 64

Figure 18. Oxygen pressure effect on EG oxidation with Pt catalyst (a) EG concentration-time (C-t) profiles under neutral conditions; (b) O₂ pressure effect on initial reaction rate under neutral conditions; (c) EG concentration-time profiles under alkaline conditions; (d) O₂ pressure effect on initial reaction rate under alkaline conditions. Reaction conditions: initial EG conc.=0.295 kmol/m³, 70 °C, P_{O2}=30 bar, initial NaOH conc.=1.458 kmol/m³ under alkaline conditions; no NaOH was added under neutral conditions, catalyst loading (Pt/CeO₂) = 2 kg/m³, initial reaction rate ($r_{i,EG}$) is calculated based on the data of EG conversion ≤ 15% 68

Figure 19. Initial EG concentration effect of EG oxidation on Pt catalyst (a) neutral conditions (no base added); (d) alkaline conditions (initial NaOH conc.=1.458 kmol/m³). Reaction

conditions: initial EG conc.=0.295 kmol/m³, 70 °C, P_{O2}=30 bar, catalyst loading (Pt/CeO₂)=2 kg/m³, initial reaction rate ($r_{i,EG}$) is calculated based on the data of EG conversion $\leq 15\%$ 69

Figure 20. Oxygen pressure effect on EG oxidation with Pt-Fe catalyst (a) EG concentration-time profiles under neutral conditions; (b) O₂ pressure effect on initial reaction rate under neutral conditions; (c) EG concentration-time profiles under alkaline conditions; (d) O₂ pressure effect on initial reaction rate under alkaline conditions. Reaction conditions: initial EG conc. = 0.295 kmol/m³, 70 °C, P_{O2}=30 bar, initial NaOH conc. = 1.458 kmol/m³ under alkaline conditions; no NaOH was added under neutral conditions, catalyst loading (Pt-Fe/CeO₂) = 2 kg/m³, initial reaction rate ($r_{i,EG}$) is calculated based on the data of EG conversion $\leq 15\%$ 72

Figure 21. Base effect on Initial Reaction Rate for EG oxidation with Pt Catalyst. Reaction conditions: initial EG conc. = 0.295 kmol/m³, 70 °C, P_{O2} = 30 bar, catalyst loading (Pt/CeO₂) = 2 kg/m³, initial reaction rate ($r_{i,EG}$) is calculated based on the data of EG conversion $\leq 15\%$ 73

Figure 22. Concentration-time Profiles of EG oxidation using different base with Pt catalyst. Reaction conditions: initial EG conc.= 0.295 kmol/m³, base-to-EG molar ratio=1:1, 70 °C, P_{O2} = 30 bar, catalyst loading (Pt/CeO₂) = 2 kg/m³ 75

Figure 23. Conversion of glucose (%) and selectivity of products (%). Reaction conditions: time=12 h, 15 bar O₂, initial pH=7, 80 °C, initial glucose concentration = 0.278 mol/L. 83

Figure 24. XRD pattern of 5% Pt-Cu (1:1)/TiO₂-a (WC-2, NaBH₄) 93

Figure 25. TEM images of Pt-Cu/TiO₂ catalysts by different synthesis methods: (a, b) impregnation; (c, d) solvothermal; (e, f) wet chemistry method (WC-1) 96

Figure 26. TEM images of Pt-Cu/TiO₂ catalysts by wet chemistry method (WC-2) using different reducing agents: (a, b) AB; (c, d) Me₂AB 97

Figure 27. TEM image and particle size distribution of 5% Pt-Cu /TiO ₂ -a (WC-2, NaBH ₄)	98
Figure 28. HRTEM and EDX images of 5% Pt-Cu/TiO ₂ -a (WC-2, NaBH ₄)	98
Figure 29. Pt 4f and Cu 2p XPS spectra of new (a-b) and used (c-d) Pt-Cu/TiO ₂ catalyst	100
Figure 30. Cu 2p XPS curve fitting results of Pt-Cu/TiO ₂ catalyst after reaction	101
Figure 31. Recycle test results of Pt-Cu/TiO ₂ catalyst; Reaction conditions: 15 bar O ₂ , initial pH=7, T=90 °C, initial glucose concentration = 0.278 mol/L, catalyst Pt-Cu/TiO ₂ -a prepared by WC-2.....	105
Figure 32. Concentration-time profile of glucose oxidation under neutral condition using the semi-batch reactor. Reaction conditions: 15 bar O ₂ , initial pH=7, T=90 °C, initial glucose concentration = 0.278 mol/L, catalyst Pt-Cu/TiO ₂ -a prepared by WC-2 method using NaBH ₄ as reducing agent. The C ₂ -C ₃ products include oxalic acid, tartronic acid, glyoxal, glyceric acid, glycolic acid and acetic acid.	106
Figure 33. Scheme of one-pot synthesis of shape controlled nanocrystals.....	112
Figure 34. TEM images of shape-controlled Pt and Pt-Cu nanoparticles on TiO ₂ support	118
Figure 35. STEM/EDX images of Pt-Cu cube.....	119
Figure 36. STEM/EDX images of Pt-Cu octahedron	120
Figure 37. STEM/EDX images of Pt-Cu stella octangula	120
Figure 38. XRD patterns of Pt and Pt-Cu nanocrystals and crystal structure of Pt-Cu alloy	121
Figure 39. XPS of Pt and Pt-Cu nanoparticles.....	122

Figure 40. Concentration-time profile of glucose oxidation on Pt cube catalyst.....	123
Figure 41. Concentration-time profile of glucose oxidation on Pt-Cu cube catalyst.....	123
Figure 42. Concentration-time profile of glucose oxidation on Pt-Cu octahedron catalyst	124
Figure 43. Concentration-time profile of glucose oxidation on Pt-Cu stella octangula catalyst	124
Figure 44. Selectivity of main products from glucose oxidation on Pt and Pt-Cu catalysts	127
Figure 45. Activity of Pt and Pt-Cu nanocatalyst on glucose oxidation.....	127

List of Tables

Table 1. Comparative GHG emissions from passenger cars using different fuels	4
Table 2. Advantages and disadvantages of using biodiesel compared to petroleum-based diesel [16-18]	7
Table 3. Literature reports on catalysts for glucaric acid by aqueous phase oxidation of glucose	Error! Bookmark not defined.
Table 4. Metal content and particle size of monometallic catalysts.....	42
Table 5. Ethylene glycol (EG) oxidation over monometallic catalysts under alkaline conditions ^a	43
Table 6. Ethylene glycol (EG) oxidation over monometallic catalysts under neutral conditions ^a	46
Table 7. Diagnostic experiments on EG oxidation	47
Table 8. EG Oxidation over Pt and PtFe catalysts under alkaline or neutral conditions .	60
Table 9. Concentration of H ₂ O ₂ during the EG Oxidation in Alkaline Solution over Pt and Pt-Fe Catalysts	61
Table 10. Base Effect on Product Selectivity for Pt Catalyst.....	74
Table 11. Physical properties of the monometallic Pt catalysts	85
Table 12. Synthesis method and bimetallic effects on glucose oxidation ^a	86
Table 13. Effect of the Pt:Cu atomic ratio in precursor on glucose oxidation ^a	89
Table 14. Reducing agent effect on glucose oxidation ^a	91
Table 15. Theoretical XRD calculations for Pt-Cu alloy structure	94
Table 16. Quantification results of Cu 2p XPS curve fitting using CasaXPS	101

Table 17. Glucose oxidation results at different temperatures using 5% Pt-Cu/TiO ₂ -a ^a	103
Table 18. Glucose oxidation results at different O ₂ pressures using 5% Pt-Cu/TiO ₂ ^a ...	104
Table 19. Glucose oxidation results at different initial glucose concentrations using 5% Pt-Cu/TiO ₂ ^a	104
Table 20. Metal composition and particle size of the Pt and Pt-Cu nanoparticles.....	119

Chapter One: Introduction & literature Review

1.1 Overview on biomass feedstock for chemicals

Biomass is a category of organic materials that comes from plants and animals. Due to its renewable feature and abundant availability, it is considered as one of the most important alternatives to petroleum in the production of energy, fuels and chemicals. In 2004, the Department of Energy (DOE) in the United States (US) described that biomass utilization for fuels, products and power is a critical component in the nation's strategic plan to address the continued dependence on volatile supplies and prices of imported oil. [1] In this chapter, the multiple uses of biomass and their end applications are reviewed to explain the background and motivation for this study.

1.1.1 Biomass-to-Energy

The history of energy derivation from biomass can date back to million years ago when fire was employed by humans to provide heat. So far, the major use of biomass in rural and developing countries is still in this traditional form.[2] For example, more than 90% of total primary energy supply of renewable energy sources in Africa is from biomass, predominantly for cooking and heating. [3] In Brazil, biomass is considered as the top three energy sources due to the abundance of forestry biomass in the nation. In a modern biomass power plant, agricultural/ forestry biomass and municipal solid wastes are combusted to provide heat to drive the steam turbines for electricity production. From environmental perspective, biomass is considered as a carbon neutral material because the production of forestry biomass through photosynthesis is still the most efficient way to consume CO₂ with zero environmental footprint. From economic and

political perspectives, the development of a country is directly linked to its energy supply, thus it is critically important for a nation to develop a diversified energy to meet the expanding demands and decrease in its dependence on fossil fuels [2]. Due to these crucial reasons, the bioenergy is considered as the most important renewable energy source in many developed countries and areas.

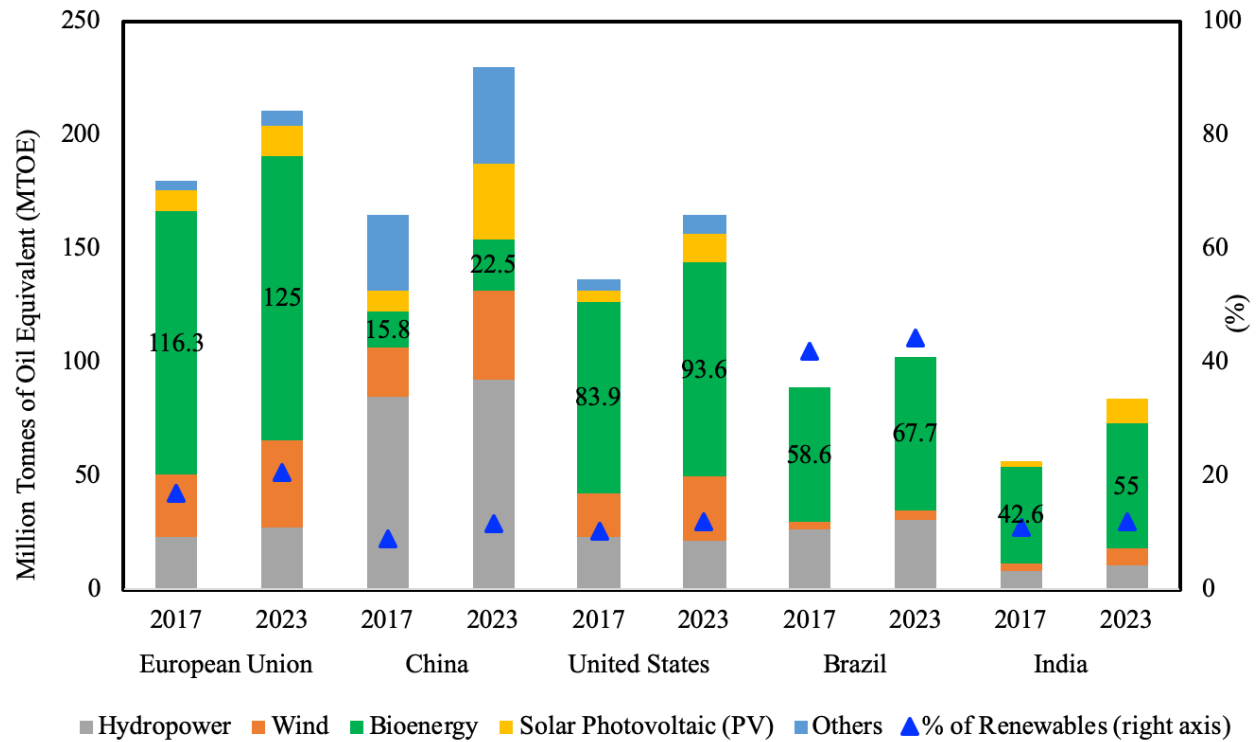


Figure 1. Renewable energy consumption in major market, 2017 and 2023 (redrawn using the data from reference [4])

Figure 1 illustrates the renewable energy consumption worldwide by the year-end of 2017 and the predicted values in 2023. It can be seen that the European Union (EU) is ranking as the number one area/country in consuming bioenergy (116.3 MTOE in 2017), followed by the US (83.9 MTOE), Brazil (58.6 MTOE) and India (42.6 MTOE) on a yearly basis. Unlike these countries, bioenergy is currently not the major renewable energy source in China. Instead, the

hydropower and wind energy are the two most important sectors. In addition, the solar photovoltaic industry is expected to grow fast in China that a growth from 8.9 MTOE in 2017 to 33 MTOE in 2023 was estimated. It is reported that the Total Primary Energy Supply of biomass worldwide is 56.5 EJ in 2016 that accounts for 70% of the share among all renewable energy sources, while the second large is hydropower (18%). [3] However, the global renewable energy share of total final energy consumption is still not significant (16.6% in 2010) and grows very slowly (17.5% in 2016).

To improve this situation, renewable energy from biomass should make further gains in its efficiency sector. So far, the biomass energy efficiency for heat or heat-led combined heat and power facilities (CHP) is approximately 75-80%, while generation of electricity is only about 20-25%, and conversion to liquid fuels for transportation sectors are even less efficient overall. In 2015, all United Nations Member States adopted “affordable and clean energy” as one of the 17 Sustainable Development Goals (SDGS) [5] to ensure access to affordable, reliable, sustainable and modern energy for all. Much higher ambition is required with regard to improving the efficiency of using biomass as an energy source, including the power generation and transportation fuel sectors to meet the goals.

1.1.2 Biomass-to-Fuels

Compared to biomass power plant with single desired end-product, “bio-refinery” is a more integrated upgrading facility that applies multiple techniques to obtain fuels, power and value-added chemicals from biomass, resulting in little or even no waste while maximizing the value derived from the biomass feedstock.[6] The biofuels include bioethanol, biodiesel and biomethane that serve the transportation sector. Between 2010~2012, the EU performed a research project

called “Biograce” aiming at the life-cycle analysis of using biofuels and calculations of the Green House Gas (GHG) emissions.[7] Part of the results are shown in **Table 1**. It can be seen that the biodiesel has the highest GHG emission in the group of biofuels. However, its saving in GHG emissions is still significant compared to all categories of fossil fuels. In addition, the GHG emissions of using the biogas is significantly lower compared to that of the biodiesel and bioethanol. Methane is another energy-rich compound found in both biogas and natural gas. In addition, it also contains considerable amounts of CO₂ (35~50%).[7] The primary method of biogas production is the anaerobic digestion (AD) that is a biological breakdown of organic material in the absence of oxygen. The obtained biogas is upgraded by a variety of methods (adsorption, absorption, membrane filtration, cryogenic separation) to obtain >95% methane which can be injected into the existing NG grid for use.[8]

Table 1. Comparative GHG emissions from passenger cars using different fuels

Name	Category	GHG in g CO ₂ eq/km
Gasoline	Fossil Fuels	164
Diesel	Fossil Fuels	156
LPG	Fossil Fuels	141
Nature gas (EU-mix)	-	124
Biomethane (from maize)	Biofuels	66
Biomethane (from liquid manure)	Biofuels	33
Biomethane (from organic waste)	Biofuels	48
Ethanol (wheat, residual materials: animal feed)	Biofuels	111
Biodiesel (rape seed, residual materials, animal feed)	Biofuels	95
Hydrogen (EU electricity mix, electrolysis on-site)	Electronic Motors	174
Hydrogen (100% wind electricity, electrolysis on-site)	Electronic Motors	8
E-Mobility (EU electricity mix)	Electronic Motors	75
E-Mobility (100% wind electricity)	Electronic Motors	5

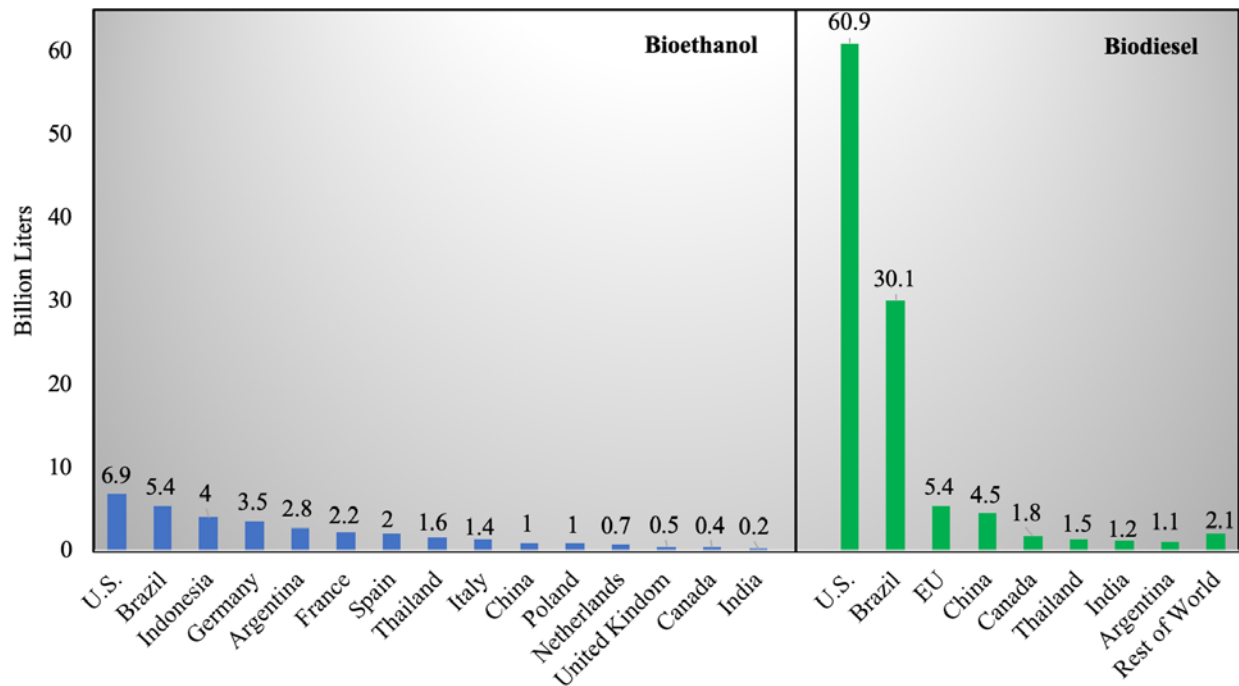


Figure 2. Global leading producers of bioethanol and biodiesel in 2018 (drawn by using the data from reference [9, 10])

The production of liquid hydrocarbon fuels for the transportation sector is one of the most important targets for a current bio-refinery that has experienced sustainable growth over the past two decades. [3] Bioethanol and biodiesel are currently the most important products within this scope. They are usually blended with gasoline and diesel for the use in flexible-fuel vehicles. **Figure 2** shows the global leading producers of bioethanol and biodiesel in 2018. It is interesting to see that biodiesel output is significantly higher than the bioethanol output in the US and Brazil, while in other countries/area the difference is less remarkable. In addition, the US, Brazil and EU are ranking as the top three producers in both bioethanol and biodiesel worldwide. In 2009, the annual biodiesel production in the US and EU are 516 and 2330 million gallons respectively.[11, 12] In the US, the biodiesel production in 2011 creates a new milestone (967 million gallons) due

to the release of the Renewable Fuel Standard by Environmental Protection Agency (EPA) that sets an 800-million gallons production target. In the same year (2011), the biodiesel production in EU still maintains a similar level (2763 million gallons) compared to that of 2009. According to the data in 2018, US has become the first-place biodiesel producer globally that the production exceeds 60.9 billion litres (**Figure 2**, equivalent to around 16,088 million gallons) that achieves more than 16-times growth from 2011 to 2018.

As for biodiesel production, the most commonly used technology is the transesterification of vegetable oil which was first studied by Patrick Duffy on 1853.[13] In the year of 1989, Gaskoks, an Australian company built the first industrial-scale biodiesel plant with a capacity of 30, 000 tons of rapeseed oil per annum.[14] To decrease the dependence on the use of oil crops (food source), the second and third generations of biodiesel production are available from non-food feedstocks (waste vegetable oil or animal fat, algae, halophytes or sewage sludge) through various biochemical or thermochemical pathways. Similar to bioethanol, the biodiesel is a fuel blended with the petroleum diesel (B2 ~ 2% biodiesel, B5 and B20). In addition, it can also be used directly in the automotive designed for the biodiesel (B100). Extensive work has been reported on the techno-economic evaluation and life-cycle assessment of biodiesel.[15] A summary of the pros and cons of using biodiesel is listed in the **Table 2**.

Table 2. Advantages and disadvantages of using biodiesel compared to petroleum-based diesel [16-18]

Advantages	Disadvantages
Domestically produced from renewable resources	Use of blends above B5 not yet approved by many automakers
Can be used in most diesel engines, especially newer ones	Lower fuel economy and power (10% lower for B100, 2% for B20)
Less exhaust emissions, including less unburned hydrocarbons (HC), CO, sulfates, polycyclic aromatic HC and particulate matter (PM) and less greenhouse gas emissions (e.g., B20 reduces CO ₂ by 15%)	Currently more expensive
Biodegradable	B100 generally not suitable for use in low temperatures
Non-toxic	Concerns about B100's impact on engine durability
Safer to handle	Slight increase in nitrogen oxide emissions in some circumstances

By the report from International Energy Agency, the annual ethanol production in 2017 was 6.9 billion gallons that United States and Brazil are the main contributor accounting for more than 80% of global output.[4] Currently, most of the bioethanol is produced from food-crops such as corn, sugar canes or wheat by biochemical routes. However, different routes are being developed to make ethanol from lignocellulose biomass especially agricultural residues or industrial waste materials. For example, using gasification to obtain methane and carbon monoxide first then apply the F-T synthesis. In another example, the researchers at the University of Borås, Sweden developed a process that uses phosphoric acid to break down the lignocellulose wastes and an edible filamentous fungus for the fermentation route to ethanol.[19] The produced residues can be used as animal feed with minimal pretreatment.

1.1.3 Biomass-to-Chemicals

In the last few decades, there has been political and technical focus on producing transportation fuels from biomass, while much less attention has been given to conversion of biomass-to-chemicals. This also happened to the petrochemical industry wherein the crude oil consumed by nonfuel chemical production only takes a small proportion compared to the transportation section. However, the situation is expected to be reversed soon. By predictions from the BP's 2018 Energy Outlook, the share of the average oil barrel dedicated to transportation fuel will peak at 58% in 2025 and begin to decline whereas the chemicals will continue to grow, from 16% of oil demand in 2020 to 20% by 2040.[20] In U.S., the agricultural and forestry biomass sources can renewably supply a billion tons per year of lignocellulosic feedstocks which will not satisfy U.S. fuel demands but could theoretically replace fossil fuels for chemical production.[21]

Biomass is not the only renewable energy source; however, it is the only renewable organic resource.[22] It is essential to develop suitable technologies for converting a certain type of biomass into value-added chemical streams. During 1945-1950, 66% of n-butanol and 10% of acetone in the U.S. were produced by fermentation of molasses and starch.[22] Other chemicals such as acetic acid, citric acid, lactic acid and itaconic acid were also produced from fermentation in the early 20th century in the U.S. [23] Later on, increased prices of sugar feedstock and decreased prices of petrochemical feedstock ended these fermentative productions until recent years. By 2016, a report from the National Renewable Energy Lab (NREL) [24] estimated that the market share of bio-based chemicals in the global chemical industry will increase from 2% to 22%.

1.2 Summary of biomass-to-chemicals technologies

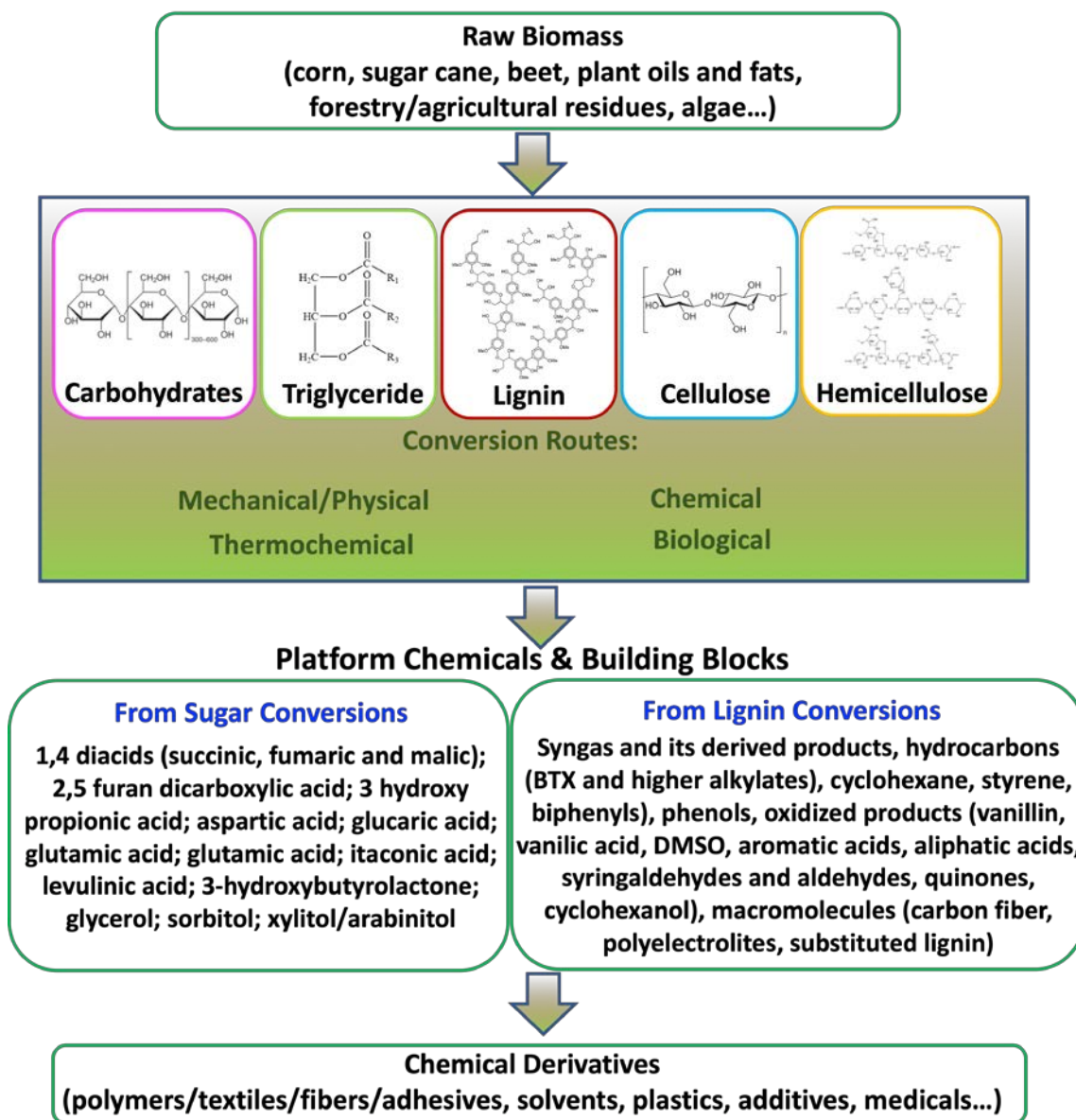


Figure 3. Roadmap of chemical production from raw biomass materials [25] [26]

According to the sources, biomass has a very versatile nature. it is a mixture of cellulose, hemicellulose, lignin and carbohydrates in the forestry or agricultural sourced biomass. In addition, some biomass such as municipal solid waste or industrial waste may also contain proteins, fats, waxes, organic acids and inorganic minerals. In the seeds of oil crops and algae, the main ingredients consist of triglycerides which are esters composed of three fatty acid unites linked to glycerol (**Figure 3**). The technical feasibility for converting biomass, based on their main characteristics and main constituents, have been extensively studied and reviewed.[23] In fact, the chemical structure of a renewable feedstock has been the first factor considered for the possibility of producing a target chemical. For instance, lignin is one of the few renewable sources to produce aromatic compounds due to its aromatic biopolymer structure that is rarely found in other biomass resources.[27] As another example, cellulose is a long-chain homopolymer of D-glucose units linked by β —1,4-glycosidic bonds, which is linear and contains amorphous and crystalline portions, with extensive intra molecular hydrogen bonding networks. This chemical and structural characteristic makes it possible to provide a series of important building blocks: levulinic acid, 5-hydroxymethylfurfural (HMF), C5-C6 sugars.[28]

For downstream processing, various pretreatment methods have been used to convert the sorted raw biomass into a variety of low-molecular-mass feedstock. For example, the depolymerization process to break down lignin and the hydrolysis/hydration/dehydration processes to decompose the cellulose/hemicellulose belong to chemical approaches.[29] The thermochemical pretreatments are mainly pyrolysis and gasification both requiring significant energy inputs. The biological pretreatments are defined as processes that employ microorganisms for the degrading under aerobic or anaerobic conditions. In 2007, the US Department of Energy's report - "Top Value-Added Chemicals from Biomass "identifies twelve building block chemicals

that can be produced from sugars via biological or chemical conversion as listed in the **Figure 3**.^[25] The report also mentions that the screenings of potential opportunities are more difficult for the lignin due to its high degree of structural variability and less stable thermally/oxidatively compared to other biomass streams.^[26] However, the macromolecules, aromatics and miscellaneous monomers that fit medium-term or long-term opportunities have been presented (as listed in **Figure 3**).

In the next step, numerous chemical derivatives such as polymers, textiles, fibers, adhesives, solvents, plastics, additives, and medicals are produced from these platform chemicals or building blocks using existing technologies. The full utilization of triglyceride is a good example to show the technologies in the biomass-to-chemicals workflow (**Figure 4**). One mole of triglyceride reacts with one moles of methanol to produce one mole of methyl-esters (crude biodiesel component) and one mole of glycerol theoretically. Based on the stoichiometric calculations, the biodiesel production will generate about 10%(w/w) glycerol as the main byproduct.^[30] The feasible routes for the range of products from glycerol are listed in **Figure 4**.

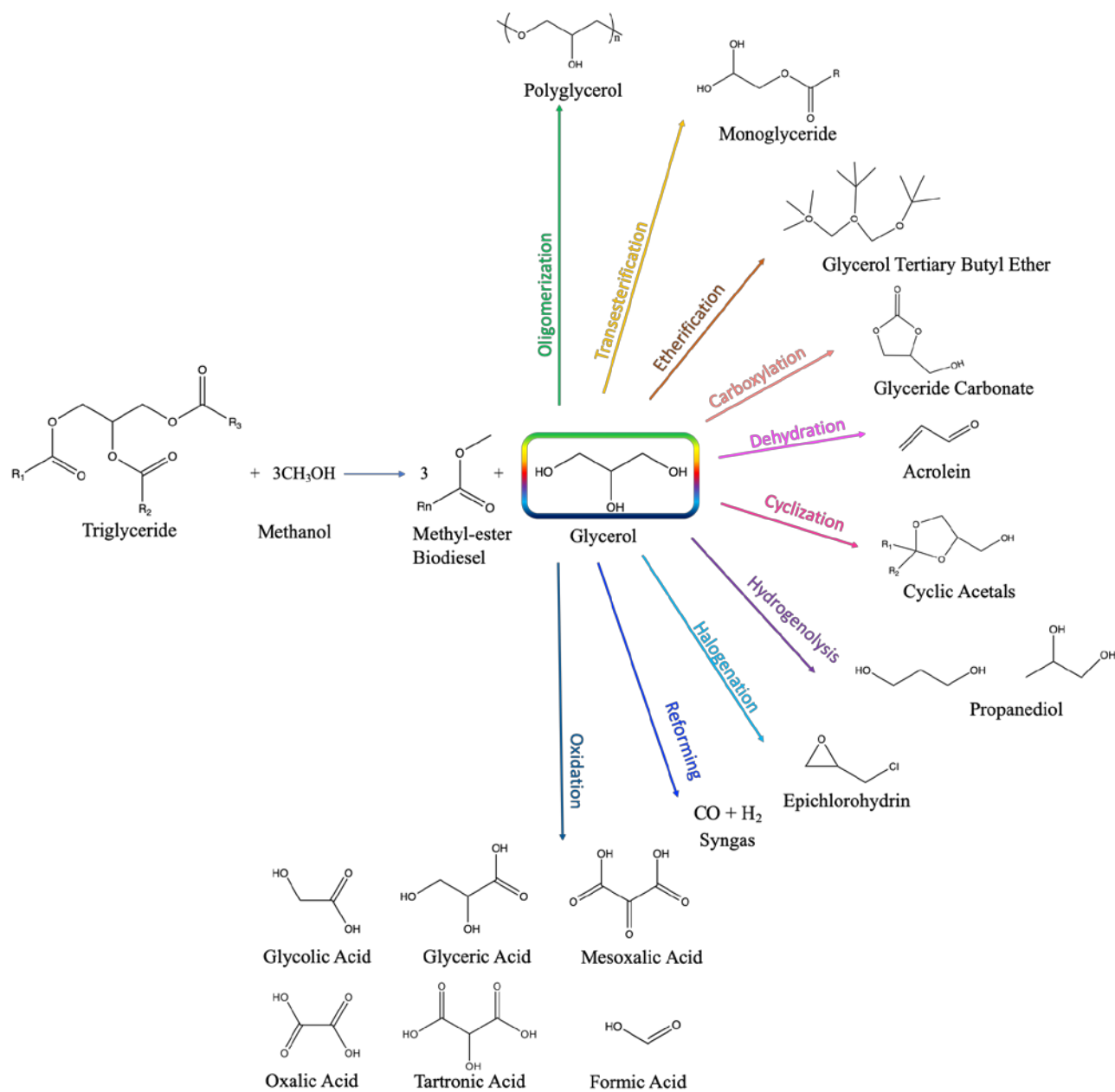


Figure 4. Chemical derivatives from glycerol by a variety of technologies [31]

The renewable chemical production using biomass as feedstock is technically more straightforward compared to conventional petrochemical synthesis for some cases such as the production of 1,6-hexanediol (HDO). 1,6- HDO is a high-value commodity chemical with low toxicity, a market price of \$4400 per ton [32] and an annual market size of 138,000 tons [33]. The dual hydroxyls as the terminal groups make it an ideal monomer for the synthesis of polymers. The polyesters made from HDO show superior performance in flexibility, surface hardness and hydrolytic stability due to their longer carbon chain, compared to the polyethylene terephthalate (PET) made from ethylene glycol [34]. Conventionally, 1,6-HDO is derived from the hydrogenation of adipic acid or its esters [35]. Producing adipic acid commercially is a 4-step procedure (**Figure 5**): (i) hydrogenation of benzene to cyclohexane, (ii) oxidation of cyclohexane to KA oil (a mixture of cyclohexanol and cyclohexanone), (iii) oxidation of KA oil with the aid of large amount of nitric acid together with copper and ammonium metavanadate catalysts, (iv) hydrogenation of adipic acid to 1,6-HDO. However, the renewable synthesis route only requires 2-steps. In the first step, 5-hydroxymethylfurfural (HMF) can be prepared in high yield from dehydration of fructose, glucose dehydration or even directly from the cellulose [36]. Then, the HMF is hydrogenated by H_2 to obtain the 1,6-HDO. So far, the highest yield of 57.8% has been obtained at 100 °C and 70 atm by using a Pd/SiO₂ and Ir-Re/SiO₂ double-bed catalysts in a tubular reactor. In addition, formic acid was found to replace the H_2 gas as an alternative hydrogen source for this reaction on the Pd/ZrP catalyst.

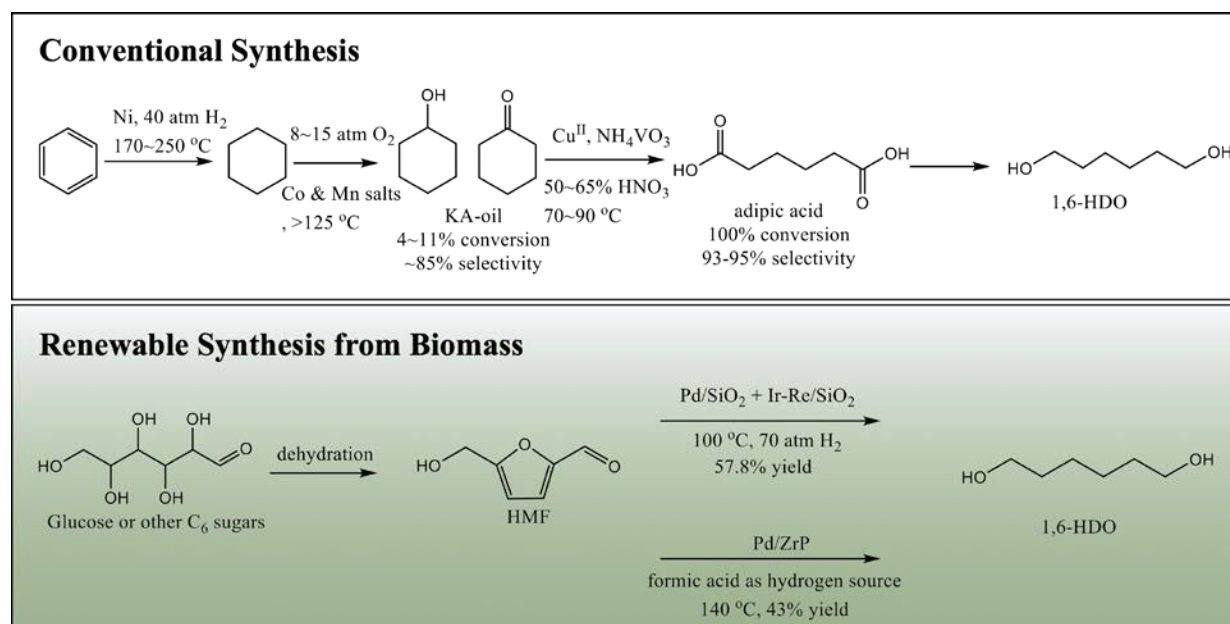


Figure 5. Comparison of different synthesis routes of 1, 6-hexanediol

Unlike the biofuels, the environmental and economic feasibilities of biomass-based chemistry for specific products are not widely assessed in the existing literature. [37] This is probably because most of the biochemistry technologies are still not technically mature for large-scale manufacture. In addition, the current production cost of bio-based chemicals are heavily dependent on the availability and price of the feedstock.[38] The green chemistry metrics (GCMs) and life-cycle assessment (LCA) are two widely used techniques for the environmental and economic impact evaluations. During the last decades, a variety of GCMs was proposed include the measurements of effective mass yield, E-factor, atom economy, mass intensity, reaction mass efficiency (RME), carbon efficiency. Some of them such as E-factor has been widely adopted by the fine chemicals and pharmaceutical industries.[39] However, none of them is sufficient by itself to drive business or innovations towards sustainable practices.[40] In several recent works by Roger A. Sheldon and Johan P.M. Sanders, four sustainability metrics for quickly evaluating the production of

commodity chemicals from renewable sources. They applied this method for comparing the sustainability of the production of seven commodity chemicals – lactic acid, 1-butanol, propylene glycol, succinic acid, acrylonitrile, isoprene and methionine – from biomass in comparison with the traditional chemical synthesis. Considering the mass efficiency and production costs, the productions of succinic acid, methionine, butanol, and lactic acid from biomass are competitive to those of traditional petrochemical synthesis, whereas the fermentative production of succinic acid is apparently cheaper (€85~1045/MT) compare to the traditional maleic anhydride route (€2554/MT).[41-46] However, the petrochemical routes have apparent advantages in less land use for all the seven commodity chemicals. The energy inputs/efficiency comparison between biomass-based or petrochemical synthesis does not have a clear pattern. As a multi-criteria approach, the LCA is a more comprehensive assessment to sustainability within the defined domains, e.g. from cradle-to-gate, cradle-to-grave and gate-to-gate. D. Cespi et al. evaluated the environmental performance of two different processes of butadiene production based on bio-ethanol (the one-step Lebedev process and the two-steps Ostromisslensky process), compared to the fossil-based route from naphtha.[47] They focus on five indicators in the LCA: the cumulative energy demand, the carbon footprint, the water depletion, a mid-point oriented analysis and an economic index. Overall, the ReCiPe single-score analysis showed the sustainable sequence of these processes is: Lebedev process > naphtha cracking > Ostromisslensky process. The existing LCA studies on chemical production from biomass also include the production of ethyl levulinate from lignocellulosic residues [37], the production of polyethylene furandicarboxylate (PEF) from corn starch [48], the production of partial bio-based high density polyethylene (HDPE) and polyethylene terephthalate (PET) from sugar crops [49-51], and the production of succinic acid from corn [52].

1.3 Catalysts Development on the Hydrogenolysis and Oxidation of Sugars and Polyols

1.3.1 Hydrogenolysis catalysts

Hydrogenolysis is one of the most critical technologies in upgrading sugars and polyols to platform chemicals. It is a process that undergoes carbon-carbon/carbon-oxygen single bond cleavage as well as hydrogenation in a hydrogen abundant environment. For instance, the hydrogenolysis of glycerol can produce 1,2-propanediol (PDO), 1,3-PDO, and EG. It is comparable to the hydrocracking and hydrotreating in the area of oil refining which is used for the removal of various heteroatoms in the crude oil. Therefore, the catalysts in this area are initially adopted from the known successful applications in the same context of upgrading fossil feedstocks. Several review articles have been published recently to have an overall look at the catalysis development progress in the hydrogenolysis of sugars and polyols with different focuses. A.M. Ruppert and et al. reviewed the catalysts on the hydrogenolysis of glycerol, sugar alcohols, mono-/disaccharides, and polysaccharides by classifying the active metals.[53] To date, platinum group metals (Pt, Pd, Os, Ir, Ru, and Rh) are the most dominant metal catalysts studied in this area coupled with the investigations of a large variety of possible supports (carbon, metal oxide and zeolites). The non-noble metals are studied to limited content with results published mainly on using Ni and Cu based catalysts.

The global challenge of hydrogenolysis is the selective cleavage of C-O or C-C bond that is reflected in two aspects: (1) the difficulty in minimizing the C-C bond cleavage, and (2) the challenge in creating C-O bond cleavage selectively at the desired positions. The first challenge is particularly important in the area of producing liquid alkanes from biomass. Pt-based catalysts

have been reported frequently for the one-pot conversion of sugar and sugar polyols to n-alkanes. For example, the hydrogenolysis of glycerol on Pt is used to produce propane; however, the CO₂ and ethane are usually formed that makes the yield of propane less than 40%. [54, 55] Similarly, Dumesic and coworkers reported that the Pt/SiO₂-Al₂O₃ catalyst can produce C₆H₁₄ from sorbitol; but with a considerable amount of cracking products that the yield of gasoline products was only 60% (based on carbon numbers). [56] One pathway to depressing the C-C cleavage is to adjust the concentration and strength of the acid sites on the bifunctional catalyst. Huber and coworkers have tested a series of different solid acid catalysts with the same Pt loading (4 wt%) for the hydrogenolysis of sorbitol/xylitol and found that Pt/ZrP showed almost twice the C₅ and C₆ alkane selectivity compared to previous reported Pt/SiO₂-Al₂O₃ and the gasoline product yield reaches up to 73%. [57] Another strategy is to involve the non-noble catalyst in the catalytic system, by either using monometallic non-noble catalyst or bimetallic catalysts. Generally, the noble metals such as Pt or Ru are more active species than the non-noble metals such as Cu, Re, and Ni in the hydrogenation or hydrogenations reactions. However, the non-noble metal is not the active site for catalyzing the C-C bond cleavage; therefore benefits for promoting only the C-O cleavages. Two successful examples demonstrating both the strategies mentioned as above are: the Ir-ReO₂/SiO₂ catalyst coupled with HZSM-5 developed by K. Chen [58], and the Ni/HZSM-5 modified with silica MCM-41 developed by Q. Zhang. [59] High yield (>95% C) of n-hexane and n-pentane were obtained by hydrogenolysis of sorbitol and xylitol respectively on the Ir-ReO₂/SiO₂ catalyst combined with HZSM-5 as a cocatalyst and n-dodecane as a cosolvent. The activity and selectivity of Rh and Ir catalysts to C-O cleavage was found to be greatly enhanced by the modification with Re. In addition. The promotion effect of HZSM-5 was found to improve the dehydration of secondary alcohols, which enhances the hydrogenolysis of secondary alcohols to alkanes. The

number of hydroxorhenium sites (Re-OH) on the catalyst surface was also increased by the addition of HZSM-5. As for the case of using Ni/HZSM-5 catalyst in sorbitol hydrogenolysis, the appropriate addition of MCM-41 (40 wt%) demonstrates an increase in sorbitol conversion from 40% to 67.1% and a selectivity increase from 35.6% to 98.7 % for the liquid alkanes. The dramatic support effect by combining HZSM-5 and MCM-41 was found due to the enhanced surface area, H₂ adsorption capacity, and tuned amount/distribution of acidic sites which favors for only C-O hydrogenolysis in the sorbitol.

X. Jin and et al. reviewed the hydrogenation/hydrogenolysis and oxidation catalysts of cellulosic biomass to chemicals.[60] Unlike the previous review, this article was not focused on classifying the metal types or discussing the process evolutions in converting specific reactants; however, it targets on introducing the novel nanostructured catalysts in the field of biomass conversion. As stated, the novel nanostructured catalysts have been exploited in the electrochemistry and electrocatalysis though not primarily studied yet in the field of biomass conversion. It was mentioned in this review that three general strategies in novel catalyst design are emerging to improve the catalytic upgrading of cellulosic biomass through hydrogenolysis and oxidation reactions: (1) morphology control of the nanoparticles; (2) building hybrid materials with core-shell or hierarchical structures; (3) using bimetallic or trimetallic nanocatalysts with unique interfacial properties.

The hydrogenolysis of polyols, especially the glycerol, was recently reviewed by J.T. Dam and U. Hanefeld.[61] The production of 1,3-PDO from the selective hydrogenolysis of glycerol is an excellent example to see how researchers tackle the challenge of the selective C-O cleavage. The primary hydroxyl group is more easily hydrogenated than the secondary hydroxyl group; therefore 1,2-PDO is preferentially produced from the hydrogenolysis of glycerol but 1,3-PDO is

a more commercially interesting product which can be used in the production of polypropylene terephthalate (PPT). In the selective conversion of glycerol to 1,3-PDO, Bronsted acid sites on the catalyst surface were found to play a vital role and more advantageous than Lewis acid sites [62]. It is known that secondary carbocation is more stable than the primary carbocation. Also, a secondary hydroxyl has stronger proton affinity than the primary hydroxyl, as shown by theoretical calculations [63]. Therefore, the secondary hydroxyl group in the glycerol could be more easily activated by the protons provided by the Bronsted acid sites the catalyst surface to go through a process similar to dehydration. Then the hydrogen species created by the heterolytic cleavage of hydrogen molecules will be added to form 1,3-PDO as explained in the literature [64, 65]. The Bronsted acidity is available by adding metal additives such as tungsten [66], using acidic support or adding liquid acids (such as sulfuric acid) [61] as a promoter to improve the selectivity to 1,3-PDO. In a very recent work [67], Single/pseudo-single atom Pt catalyst was prepared on mesoporous WO_x that provides large surface area and abundant oxygen vacancies for the Pt dispersion and stabilization. Outstanding hydrogenolysis activity under low H_2 pressure (1 MPa) with a very high space–time yield towards 1,3-propanediol ($3.78 \text{ g}_{\text{Pt}}^{-1} \text{ h}^{-1}$) was delivered by this Pt–W catalysts. The high selectivity towards 1,3-propanediol was attributed to the heterolytic dissociation of H_2 at the interface of Pt and WO_x following the dehydration–hydrogenation reaction mechanism as described above.

Initially, the hydrogenolysis studies were performed in the presence of hydrogen by default. However, the production of hydrogen is energy-intensive and not renewable (from fossil fuels by gasification and steam reforming). This triggers a series of studies in recent years using in-situ generated hydrogen for the polyol hydrogenolysis. Overall, the in-situ generated hydrogen can be from two sources: aqueous phase reforming (APR) or catalytic transfer hydrogenation

(CTH). During the APR, glycerol or other polyols itself serves as the hydrogen source by its reaction with water to produce CO_2 and H_2 . A. Martin and the coworkers reviewed the hydrogenolysis of glycerol into propanediol using in situ generated hydrogen by aqueous phase reforming.[68] The platinum group metals were considered as essential for both C-C bond cleavage and C-O cleavage so that the H_2 can be produced by the reforming reaction and consumed by the hydrogenolysis afterward. In a previous work by Roy et al. [69] an admixture of 5%Ru/ Al_2O_3 -5%Pt/ Al_2O_3 was reported to deliver ~50.1% glycerol conversion with a 1,2-PDO selectivity of ~47.2% at 493K, when no external H_2 was used. It was shown that glycerol hydrogenolysis in the presence of added hydrogen (41 bar), at otherwise identical operating conditions, gave lower selectivity to 1,2-PDO (31.9%) compared to the run without added hydrogen (47.2%). It has been found that the presence of external hydrogen at higher pressure promotes the formation of methane and other alkanes, adversely affecting the 1,2-PDO selectivity. Nickel (Ni) was considered as the most favored candidate to replace the noble metal for the in-situ hydrogenolysis reactions, either mono- or bimetallic catalysts such as Ni-Co or Ni-Cu catalysts.[68] The Ra-Ni₁₄Sn/ Al_2O_3 catalyst showed 100% conversion and 76% 1,2-PDO selectivity from the in-situ hydrogenolysis of glycerol at 538 K and 51.9 bar inert pressure.[70] In addition to glycerol, the APR has successful applications in converting xylitol and sorbitol to alkanes on the Pt- and Ni- based catalyst.[56, 71] The CTH is a process in which hydrogen is transferred from an additional hydrogen donor molecule to glycerol or other polyols. The hydrogen donors that have been experimentally investigated are: the simple molecules such as cyclohexene, hydrazine and formic acid; the alcohols like 2-propanol (2-PO) or methanol.[72, 73] Pd was found as the most active metal catalyst for this type of reaction although other noble metals such as Pt and Rh are also showed some moderate activity; and the transition metals such as Ni and Cu were

reported to be active only at high temperatures. Overall, the in-situ hydrogenolysis of polyol provides a new pathway to produce biomass-derived platform chemicals with minimal H₂ dependency. However, the applications to higher polyols (C₄ and above) or sugar alcohols are still scarce. In addition, the selective production of 1,3-PDO from the in-situ hydrogenolysis of glycerol has not been reported yet.

1.3.2 Oxidation catalysts

Among the various transformation technologies of converting biomass-based sugars and polyol, oxidation is of particular interest since it does not consume costly H₂ source and maintains most of the valued O-containing functional groups in the final products. The obtained aldehydes and aldonic or carboxylic acids from the oxidation of sugars and polyols are widely used in the cosmetics, pharmaceutical, food, and paper industries. In addition, the mild reaction conditions and satisfying yields make this route very attractive for the carbohydrate chemistry. For example, the oxidation of D-glucose to D-gluconic acid using Pd catalysts in aqueous alkaline solution is able to compete economically with the generally applied biochemical oxidations.[74]

The heterogeneous catalysts for the oxidation reaction usually consist of three main components: active metal, a second metal (as promoter or co-catalyst) and support material. In the beginning, Pt and Pd are selected as the active metal for this type of reaction. In 1997, Prati et al. created a milestone that Au is also an excellent active metal for the liquid-phase oxidation.[75] It was claimed that Au is a more stable metal to over-oxidation or O₂ poisoning problems as observed in some cases of using Pt and Pd catalysts. Later, a large number of works surrounding Au catalysts on the selective oxidation of biomass-derived platforms have been established during the last two

decades. Prati's group published a review article for the Au-based catalysts for selective oxidation reactions in the year of 2007.[76] Very recently, the same group reported a new review article to state the configuration of the recent development in the Au catalysts for the oxidation of three biomass-derived platforms, namely glucose, 2,5-hydroxymethylfurfural, and glycerol.[77] The optimization of catalysts has been performed mainly by following some general rules in the heterogeneous catalysis, such as tuning the particle size, changing support materials and also the introduction of a second metal for the oxidation reactions to achieve the better activity, selectivity, and stability. Some crucial findings for selective oxidation in the aqueous phase on Au, Pt and Pd catalysts are highlighted as below:

Significant metal particle size effect was observed for the monometallic catalyst, though the reported trends are sometimes contradictory. The decrease in Pt particle size depressed the rate of methanol and d-glucose oxidation; however, accelerates the oxidation of 5-hydroxymethylfurfural (HMF).[74] As for the glucose oxidation reaction to produce gluconic acid, Comottie et al. prepared the Au nanoparticles of different sizes supported on active carbon within the range of 3-6 nm and found an inversely proportional relationship between the particle size and catalyst activity.[78] However, a contradictory trend has been reported as well: Megias-Sayago and co-workers found that the TOF of Au nanoparticles supported on active carbon increases with the increase of particle size from 4nm to 23 nm.[79] For the reaction of glycerol oxidation in alkaline solutions, Dimitratos et al. studied the effect of particle size on mono- and bimetallic Au and Pd on carbon.[80] They found that larger metal particles led to lower catalytic activity but higher selectivity to sodium glycerate. As for the monometallic, different synthesis method can create variations in metal particle size. For instance, Dimitratos et al. also found that high-temperature calcination can facilitate the formation of larger Au particles on the TiO₂ (ranged from

5 nm to 25 nm).[81] On the contrary, smaller particles in the range of 2-5 nm can be formed by the low-temperature chemical reduction method.

Using a different support material is one of the most easily available methods in tuning the catalyst formulation but possible in achieving a better catalyst performance due to the additional acidic/basic sites on the support, space effect or potential metal-support interactions. A variety of commercially available support materials (activated carbon, graphite, TiO_2 , Al_2O_3 , SiO_2 , CeO_2 and zeolites) combined with Au catalyst have been systematically studied for the oxidation of glycerol and glucose to produce glyceric acid and gluconic acid respectively.[77] Cai et al. prepared Au nanoclusters of 1 nm encapsulated in HY zeolite which shows superior oxidation performances due to the interaction between the hydroxyl groups in the supercage of the zeolite and the alter of the electronic structure of Au nanoclusters by the support.[82] In most of the sugar/polyol oxidation studies, base promoters such as NaOH, KOH, and Na_2CO_3 are often added to enhance oxidation kinetics on the metal-catalyst surface.[60] Due to this reason, the basic supports such as hydrotalcite and MgO were developed and found to benefit the selective oxidation of HMF to FDCA on Au catalyst, even in the base-free solutions. More applications, such as Pt nanoparticles immobilized on anion exchange resins, nitrogen-doped carbon nanotube, and mesoporous carbon nitride show synergistic activity during glycerol oxidations.[60] Such metal-solid base pairs are found to be effective in accelerating the activation of O-H bond in glycerol molecules and tune surface electron reconfigurations of the active metals for promoting the oxidation reactions.

Developing novel multimetallic catalyst is one of the most critical strategies to improve the catalyst performance for the oxidation of sugars and polyols. For instance, the monometallic Au, Pt and Pd on carbon catalysts showed weak activity in the aqueous phase oxidation of D-sorbitol to gluconic acid. However, a synergistic effect between Au, Pt and Pd has been observed

that the Au-Pt and Au-Pd bimetallics exhibited a significant enhancement in both activity and selectivity compared to the monometallics.[83] However, it is not economically efficient to build bimetallics of two noble metals. Attempts have been made to develop new bimetallic catalyst which contains at least one non-noble metal species. The transitional metals are known for their homogeneous and heterogeneous catalytic activity, which is ascribed to their ability to borrow or lose electrons when alloyed with the noble metals. The bimetallic alloys of combining Pt with 3-d transitional metals such as Fe, Mn and Cu showed superior oxidation performance in producing dicarboxylic acids from the oxidation of glycerol and glucose by decreasing the activation energy in the secondary oxidation step (oxidation of monocarboxylic acid to dicarboxylic acid).[84-87]

Morphology control to develop bimetallics with novel structures was investigated to a limited extent for the aqueous phase oxidations though some important findings have been achieved. For instance, the Au-Pd bimetallic catalyst was synthesized by galvanic replacement method to create a novel crown-jewel structure that Au atoms were selectively replaced by Pd in low coordination positions such as top, edge, and face sites.[88] The catalysts showed up to 30 times higher than monometallic Au particles and 8-10 times higher activity than the Au-Pd alloyed particles of similar size. Jerome and co-workers reported the synthesis of CuO nano-leaves by a sonochemical synthesis method, which was found to be highly selective to the production of dicarboxylic acid from glycerol oxidation under base-free conditions using the H_2O_2 as oxidant (78% selectivity of tartronic acid and oxalic acid).[89] To date, the Bimetallic catalysts with tailored nanostructures have been synthesized and tested widely in the electrooxidation fields, but still not yet widely applied in the catalytic conversion of sugars and polyols.

As a summary, monometallic Pt, Pd and Au catalysts and some bimetallic combinations of these noble metals are well studied by following the general rules for correlating the catalytic properties with the composition of the catalyst. However, some technical challenges are still apparent. For instance, the rational design of selective oxidation is still very difficult, for example, the direct production of glucaric acid from glucose is more difficult than the formation of gluconic acid, because the aldehyde group is naturally easier to be oxidized compared to the hydroxyl group. In another example of glycerol oxidation, glyceraldehyde and glyceric acid are easier to be produced than the production of tartronic acid. In addition, the C-C cleavage relations are uncontrollable to form smaller molecules that affects the selectivity of the final product. There is a strong tendency of decarboxylation over Pt, Pd and Au catalysts so that the production of glyceric acid with high yield is still a grand challenge in the oxidation of glycerol. These problems are hardly to be solved by simply tuning the compositional parameters in the monometallic catalysts. By merging many complementary contributions, it is expected to create new and more efficient nanostructured catalysts, which embody a balanced amount of activity, selectivity and stability for challenging applications in organic synthesis.[76] The novel catalyst designs should be implemented along with mechanism studies (such as accurate kinetic investigations or theoretical works) to understand the experimental behavior of active metal and the promoters (second metal, novel support materials or alkalis) in the selective oxidation. In addition, precise morphology control such as decorating the second metal precisely at active sites (edges or corners), or the synthesis of bimetallic alloys with well-shaped structures (polyhedron, cage, nanotube) is expected to bring in electronic effect and structural effects for the new oxidation pathways.

1.4 Literature Survey on the Oxidation of Glucose and Ethylene Glycol to Value-added Products

Compared to fossil-based feedstock, biomass is oxygen rich due to presence of multiple hydroxyl groups and oxygenated compounds. Thus, hydrogenolysis or hydrogenation are usually adopted to get rid of the extra oxygen (de-oxygenation) from biomass. On the contrary, oxidation is a technology that does not rely on expensive hydrogen source and maintains most of the oxygen-containing functional groups during the reaction. Oxidation of biomass derived sugars and polyols has recently attracted significant interest as a renewable alternative to petroleum route for making a wide range of industrial chemicals. Compared to gas-phase oxidation, the aqueous phase oxidation does not require the removal of water from the crude sugars and polyols. In this dissertation, glucose and ethylene glycol were selected as model materials for the catalysis studies on the oxidation of sugars and polyols. In this section, a literature survey on the aqueous phase oxidation of glucose and ethylene glycol is presented and challenges for future research opportunities in this field identified.

1.4.1 Oxidation of Glucose

Glucose is a versatile feedstock that can be produced in nature in large quantities through photosynthesis. From the structural perspective, the aldehyde and hydroxyl groups at the two ends of the glucose molecule provide a possibility of its oxidation to value added carboxylic acid products (gluconic acid, GA; **Figure 6**) or even dicarboxylic acid (glucaric acid; **Figure 6**). Since the oxidation rate of the aldehyde group is faster than that of the hydroxyl group, gluconic acid is easier to obtain compared to glucaric acid.

Gluconic acid has a large number of industrial applications. It is widely used as a food additive (e.g., an acidity regulator in juices and wine manufacturing). Its salts, especially zinc and calcium gluconates are commonly used as injection or oral doses, for the treatment of calcium or zinc deficiency. The calcium gluconate, in the form of a gel, is also used to treat burns from hydrofluoric acid. Moreover, gluconic acid has a high sequestering capacity (reacts with metal ions to form soluble complexes) that can be applied as an important, low toxic detergent for industrial metal cleaning. [90] Two general pathways involving biochemical and chemical conversion for the synthesis of gluconic acid are known. Boutroux discovered the feasibility of using microorganisms to produce gluconic acid in 1880. In 1922, M. Molliard detected gluconic acid in cultures of the 'aspergillus Niger' [91]. Today, the submerged fermentation with the use of aspergillus Niger that obtains high yield of the product (as high as 98%) is still the main route for gluconic acid production in industry [90]. However, the biochemical conversion is so far a discontinuous process (batch or fed batch), which limits the productivity per unit of time (around 15 g/L·hr) [90]. Consequently, the manufacturing cost is high. Chemical conversion can be classified into two routes: electrochemical synthesis and catalytic synthesis. The electrochemical synthesis in the presence of bromide ions is a paired process that always produces a side product – sorbitol. The catalytic process with aid of heterogeneous catalyst employs a cheap and environmentally acceptable oxidant – molecular oxygen/air and occurs at a mild reaction condition. However, the low selectivity of glucoric acid used to be uneconomical for industrial purpose. Thus, the key question of chemical conversion is to find a commercially feasible catalyst with better product yield and selectivity for glucose to glucaric acid. Catalytic conversion of glucose to gluconic acid with the platinum (Pt), palladium (Pd), and their combinations (Pt-Pd) has been extensively investigated. Addition of bismuth (Bi) has significant promotional effects on the catalyst reactivity

and stability [92]. A high gluconic yield of 97% can be obtained using Pt/C catalyst [93]. Gold (Au) and its combination with other metals attracted significant interest in the past decade because of following advantages [94, 95]: (1) Au catalysts are active in various forms – either supported metal or nano-metric colloidal particles (gold sol) in oxidation reactions; (2) they can be used over a wide range of pH conditions (from alkaline to acidic); (3) high Turnover Frequency (TOF). However, relatively lower glucoric acid yield makes the Au catalysts difficult to be competitive compared to Pt catalysts at this stage.

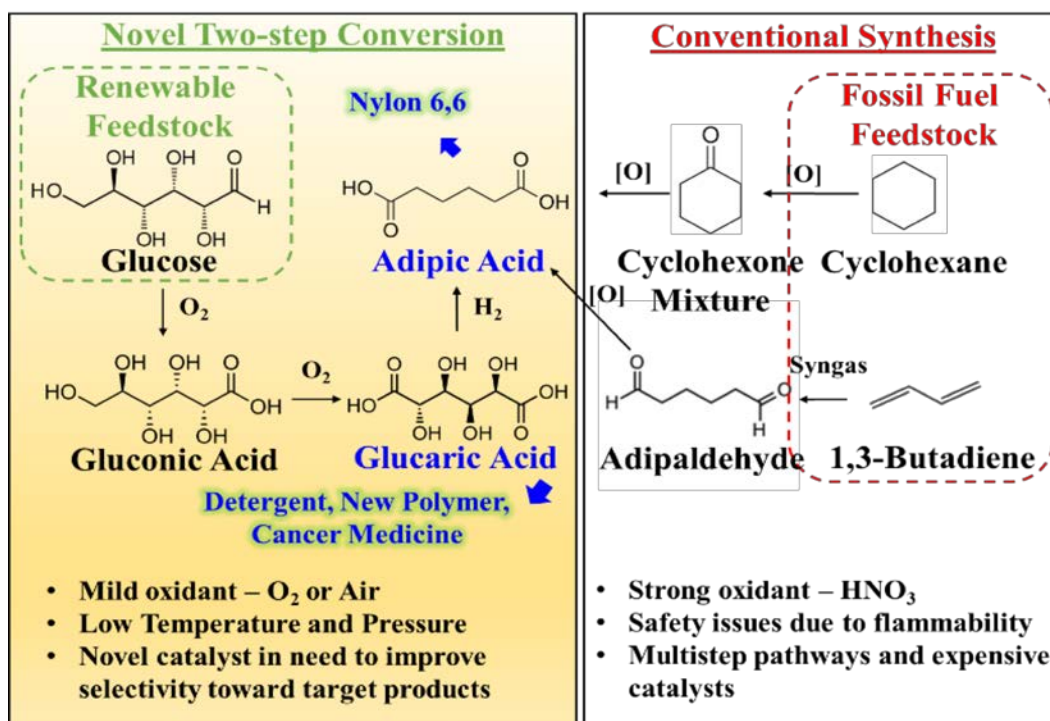


Figure 6. Renewable synthesis of adipic acid from glucose

Glucose oxidation to produce glucaric acid is important for several reasons though it is considered as a more difficult process: 1) Glucaric acid and its derivatives are used as oral supplements for either cancer prevention or to control the progression of breast, prostate, and colon cancers;^[96-100] 2) glucaric acid is identified as one of the top 12 building block chemicals by US

Department of Energy that can be transformed into a wide range of commodity chemicals;[101]

3) oxidation catalysts developed for glucose-to-glucaric acid conversion can be potentially applied to a wide range of other biomass derived sugars and polyols, such as xylose, arabinose, glycerol, ethylene glycol, and sorbitol to value added products.[101]

Conventional oxidation of glucose to glucaric acid with nitric acid has been demonstrated on a pilot plant scale,[102] although this process has never been commercialized due to environmental safety concerns associated with use of corrosive nitric acid and products and difficulties in temperature control caused by strongly exothermic reaction.[103] Another drawback is that the nitric acid usage generates N_2O that has 180 times greater global warming potential compared to CO_2 . [103] TEMPO (2,2,6,6-tetramethylpiperidin-1-oxyl radical) mediated glucose oxidation is reported to give high yields (up to 90%) of glucaric acid using bleach solution or sodium/potassium hypochlorite as an oxidant.[104] However, the high cost and toxicity of the by-products are major drawbacks of this route.

Heterogeneous catalytic glucose oxidation studies reported in the literature employ molecular O_2 as an inexpensive and environmentally friendly oxidant at mild reaction conditions (35-80 °C, ambient pressure, aqueous media). Dirkx et al. reported oxidation of gluconic acid in aqueous solution (at pH 8-11 and 45-65 °C) using Pt/C catalyst with molecular O_2 , obtaining a glucaric acid yield of 50-55%.[105] Besson et al. and Xin et al. studied Pt/C catalyzed glucose oxidation and found that glucaric acid production starts only after glucose is completely converted.[106]·[107] This phenomenon was attributed to the C=O bond in glucose adsorbing and interacting strongly with the catalyst surface inhibiting further oxidation of gluconic acid to glucaric acid.

Alkali promoter is known to accelerate glucose/polyol oxidation rates to carboxylic acids. However, the base also promotes side reactions leading to C-C and C-O cleavage that adversely affects the selectivity of glucaric acid.[107] Stoichiometric consumption of base promoter and difficulties in isolating glucaric acid from its alkali salt are other disadvantages of the base promoted oxidation. In this context, the development of new catalysts that enable glucose oxidation under base-free conditions is receiving significant interest. Gold catalyst is reported to be selective toward gluconic acid rather than glucaric acid in the absence of alkali.[108-113] However, in one of the reports, Au-Pt/ZrO₂ bimetallic catalyst is shown to give 50% yield of glucaric acid at 100 °C, 40 bar O₂ without the addition of alkali.[114] In a few patents,[115, 116] Pt catalysts supported on activated carbon, SiO₂ and ZrO₂ by simple impregnation method are claimed to provide more than 60% yield of glucaric acid during glucose oxidation. However, the experiments were performed in a high throughput catalyst screening equipment with small amounts of catalyst, and reproducibility of these results is not established on a higher scale. In a recent work, Lee et al. reported 74% glucaric acid yield by using Pt/C catalyst at pH=7.2, 80 °C and 13.8 bar O₂. [117] Several pH effect studies of either glucose or gluconic acid oxidation on Pt catalysts show that the absence of alkali does not lead to significant catalyst poisoning but promotes selectivity to glucaric acid by suppressing the C-C bond cleavage.[106][117]

Table 3. Literature reports on catalysts for glucaric acid by aqueous phase oxidation of glucose

T (°C)	Gas	P (bar)	pH value	Catalyst	Substrate	Initial		Substrate/Pt ratio (mol/mol)	Reaction Time (hr)	Yield	Ref.
						Substrate Conc. (mol/L)	Substrate				
55	O ₂	1	at constant pH=10	Pt/C	glucose	0.2	glucose	19.5	2	50-55% at 100% conversion	[105]
56	O ₂	2	controlled at constant pH=11	Pt/C	gluconic acid	0.2	gluconic acid	19.5	1.5	50-55% at 100% conversion	[105]
60	air	1	controlled at constant pH=7	Pt/C	glucose	2	glucose	787	24	50% at 100% conversion	[106]
60	air	1	controlled at constant pH=7	Pt/C	gluconate	2	gluconate	787	24	55% at 97.2% conversion	[106]
55	O ₂	1	controlled at constant pH=8	Pt/C	gluconic acid	0.2	gluconic acid	19.5	0.7	50% at 100% conversion	[118]
80	O ₂	13.8	No base added	Pt/C	glucose	0.55	glucose	54	10	74% at 99% conversion	[117]
60	O ₂	1	Base added (NaOH)	Pt-Au/TiO ₂	gluconic acid	0.53	gluconic acid	5367	4	32.3% at 100% conversion	[86]
45	O ₂	1	Base added (NaOH)	Pt-Au/TiO ₂	glucose	0.56	glucose	5678	24	25.4% at 100% conversion	[86]
35	O ₂	1	Base added (NaOH)	Pt-Pd/TiO ₂	glucose	0.28	glucose	2976.2	72	44.3% at 100% conversion	[107]
119	O ₂	27.6	Base added (NaOH)	Au-Pt/TiO ₂	glucose	10 wt%	glucose	42	3	71%	[69]
90	O ₂	5.2		Pt/C	glucose	N/A	glucose	N/A	8	60%	[67]
90	O ₂	5.2		Pt/ZrO ₂	glucose	N/A	glucose	N/A	5	59%	[67]
90	O ₂	5.2		Pt/SiO ₂	glucose	N/A	glucose	N/A	8	66%	[67]
80	O ₂	5.2	Initial pH < 7	Pt/Al ₂ O ₃	glucose	N/A	glucose	N/A	5	31%	[67]
90	O ₂	5.2		Pt/CeO ₂	glucose	N/A	glucose	N/A	5	17%	[67]
100	O ₂	5.2		Pt/Zeolite	glucose	N/A	glucose	N/A	5	39%	[67]
100	O ₂	5.2		Pt/TiO ₂	glucose	N/A	glucose	N/A	5	30%	[67]

Situation and Key Challenges in Glucose Oxidation

In general, the oxidation of glucose to produce gluconic acid has been extensively studied; nevertheless, the direct formation of glucaric acid is still a grand challenge especially under base-free conditions. The general strategies such as tuning the support material or particle size, introducing a second metal, changing the synthesis method have not been systematically discussed for the glucose oxidation under the base-free conditions. Moreover, the metal catalysts with tailored structures (morphology-controlled nanoparticles) or theoretical works on shape dependency have not been explored for this reaction.

1.4.2 Oxidation of Ethylene Glycol

Ethylene glycol (EG) is the smallest polyol molecule that can be produced by hydration of ethylene oxide or hydrogenolysis of biomass (cellulose).[119] It is mainly used as a precursor for the manufacture of polyesters and as an antifreeze/coolant in automobiles and aircrafts. Significant research has been reported on the electro-oxidation of ethylene glycol due to its higher boiling point (189 °C) and higher energy density compared to ethanol and methanol. However, in this fuel cell application, EG is preferably converted into CO₂ in order to harvest the maximum amount of energy. Catalytic conversion of EG into chemical precursors is attractive since a number of EG derivatives such as glyoxal, formic acid and glycolic acid (**Figure 7**) are valuable commodity chemical precursors with versatile applications. Partial oxidation of EG on silver and copper catalysts in a flow reactor is practiced commercially for glyoxal manufacture.[120-122] However, there are only few reports on producing glycolic acid from EG.[123-131]

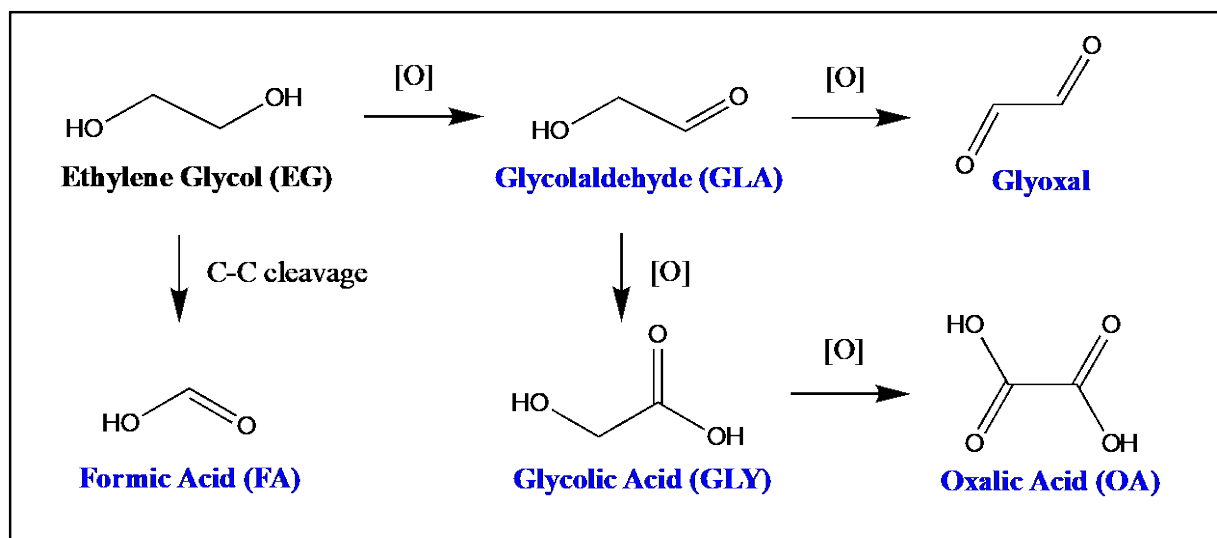


Figure 7. Oxidation of ethylene glycol and the products

Glycolic acid (GA) is an essential additive in skin care products, textile industry and food processing that received considerable commercial interests. The current industrial process for glycolic acid involves hydrolysis of monochloroacetic acid or carbonylation of formaldehyde.[123] Approximately 94% GA yield is reported by reacting formaldehyde with CO and water.[132] However, the use of strong acid catalysts (concentrated sulfuric acid or chloric acid), and harsh reaction conditions (200 °C, 900 atm CO pressure) demand safer and greener alternative pathways. Glycolic acid from EG oxidation is also demonstrated biochemically using microorganisms, via electrooxidation or chemo-catalytically in aqueous solution. While microbial conversion provides high selectivity, it is a slow process providing 88-92% GA yield only after 120 hours.[133] As for electrooxidation, Ni based catalysts have been developed to achieve the goal of CO₂ free power generation.[134, 135] However, obtaining high selectivity in glycolic acid

is still a challenge since oxalic acid is the main oxidation product in previous work but less value-added.[134]

Glycolic acid can also be produced from the aqueous-phase oxidation of ethylene glycol selectively on the monometallic Au,^[136] [123] Pd, [124] Ni,[137] Cu[137] and Pt[138] [125] catalysts but with low activity. The Au catalyst is reported to produce GA selectively.[136] [123] For example, Berndt et al. have reported high GA selectivity (>95%) on a 1% Au/Al₂O₃ catalyst during EG oxidation in aqueous alkaline medium at atmospheric pressure and low temperatures (50-70°C).[136] Interestingly, Case and co-workers reported that while carbon supported Au is inactive for EG oxidation at similar reaction conditions, [123] Au supported on Al₂O₃ showed high selectivity to glycolic acid; however, the mechanism for this support effect was not revealed. Besides Au, the Pd metal was also reported to show good glycolic acid selectivity (100%) under alkaline conditions, but provide low activity (45 h⁻¹) and low EG conversion in aqueous solution(<20% at 5 hours) [124] In addition, carbon nanofiber supported Cu were also studied for the EG oxidation under alkaline conditions at 150-180 °C showing better selectivity for glycolic acid (~96%) compared to the Ni catalyst (~31%). However both of these catalysts showed very low activities (TOF=11 h⁻¹ and 14 h⁻¹ for Ni and Cu respectively).[137]

Situation and Key Challenges in Ethylene Glycol Oxidation

Overall, the heterogeneous catalysts for the production of glycolic acid from the oxidation of ethylene glycol are investigated to a limited content; and they all showed poor activity. A systematic screening of different monometallics under the same experimental conditions is highly desirable to select a suitable active metal for this reaction. Developing new bimetallic catalysts

should be applied as an essential strategy to promote the activity for this slow oxidation reaction. In addition, fundamental studies on reaction mechanisms regarding the role of the second metal are critical to understand the catalysis in the aqueous phase oxidation. Although most of the reported works were conducted using soluble alkali as a promoter, the knowledge on the promotion effect of soluble alkali is still lacking. Meanwhile, the concentration effect of the alkali has not been discussed yet for an optimization purpose.

1.5 Objectives

The literature review on catalysis of oxidation of polyols and sugars indicates while the oxidation route can be highly promising to develop a greener and environmentally compatible process for industrially useful carboxylic acid products, there is a need to develop active, selective and stable catalysts to meet the economic demands for commercialization. This in turn requires fundamental understanding of parameters in design of catalysts, reaction mechanism and kinetics. This dissertation focuses mainly on aqueous phase oxidation of ethylene glycol and glucose using mono and bimetallic catalysts. The specified objectives are summarized below:

- To achieve selective oxidation under base-free conditions for the production of glucaric acid on Pt based catalyst, a systematic study on the effects of support material, metal composition, the second metal, catalyst synthesis method and experimental conditions should be performed for the catalytic system optimization.
- To meet the gap of utilizing shape-controlled nanostructures in the catalytic conversion of glucose-to-glucaric acid, Pt based catalysts with specific morphologies will be synthesized. This part of the study is also for testing two hypotheses: (1) the one-pot

synthesis of metal oxide supported Pt nanoparticles with tailored structure is approachable; (2) the glucose oxidation under base-free conditions is a structure sensitive reaction. The Pt nanoparticles enclosed by single crystal facets, namely (100) facet and (111) facet will be synthesized by using solvothermal technique with suitable solvent, capping agent/template and metal precursors. The obtained catalysts will be tested under the same conditions to compare their activity, selectivity and stability for the glucose oxidation.

- To select the best active metal candidate for the ethylene glycol oxidation, a systematic evaluation of various metals will be performed. This part of work will be conducted by both experimental studies demonstrated in the main part of this thesis and computational works through cooperation with Dr. Ali Haider's group from the Indian Institute of Technology (IIT, Delhi).
- To meet the desire of designing a highly active catalyst, several bimetallic pairs will be selected based on the monometallic maps obtained from the investigations described above. Detailed characterizations coupled with the kinetics study will be conducted to understand the activity enhancement (if any) of the bimetallic catalyst. Moreover, the potential promotion effect of using the base promoter will be discussed for both the monometallic and bimetallic catalysts to gain more fundamental understandings on the reaction mechanism.

Chapter 2: Aqueous Phase Oxidation of Ethylene Glycol using Supported Monometallic Catalysts

2.1 Introduction

As described in the Chapter 1, oxidation of polyols in aqueous solution is receiving increased attention in the context of transforming biomass-derived platform chemicals into higher value products.[139] Ethylene glycol (EG) is the smallest polyol molecule that can be produced by hydration of ethylene oxide or hydrogenolysis of biomass (cellulose).[119] The development of suitable catalytic systems for EG oxidation will not only benefit for the production of glycolic acid, but also bring insights to a broader area of the oxidation of other polyols. To achieve the goal of rationally designing novel catalysts for ethylene glycol to glycolic acid conversion, experimental results on the catalytic performance of different monometallic catalysts, role of promoters, supports, surface characterization of catalysts are discussed. An array of monometallic (Pt, Pd, Rh, Ag, Au, Ru, Fe, Cu) were synthesized by a one-pot solvothermal method and evaluated for aqueous phase EG oxidation under the same conditions for parallel comparisons. In addition, the experiments were performed under either neutral or alkaline conditions to understand the role of alkali promoter and its influence on the reaction mechanism. A group of diagnostic experiments was also conducted to discuss the role of NaOH, metal catalyst and O₂ individually.

The experimental results on catalyst performance is also compared with predictions using computational modeling (based on density functional theory) performed in the group of Professor M. Ali Haider at the Indian Institute of Technology (Delhi, India). For this purpose, *ab initio* microkinetic model (MKM) is constructed to yield a two-descriptor volcano plot for understanding

reactivity and selectivity trends for monoacid (GA) versus di-acid (OA) production in oxidation of ethylene glycol.

2.2 Experimental and Methodology

2.2.1 Catalyst Preparation

N, N-dimethylformamide (DMF, HPLC grade, >99.9%), cerium oxide nanopowder (<50nm, BET), and metal precursors including Pt(acac)₂, Fe(acac)₃, Ag(acac)₂, Pd(acac)₂, Ru(acac)₃, Rh(acac)₃, Cu(acac)₂ (acac = acetylacetonate) were all purchased from Sigma Aldrich. All materials were used without further purification.

All monometallic catalysts were prepared using a solvothermal method described elsewhere.[85, 87] In a typical synthesis, the precursor M(acac)_n (M = metal, n = metal coordination number) was first mixed with 1.2 g cerium oxide (CeO₂) powder and 20 mL N,N-dimethylformamide in a 75 mL autoclave. The molar ratio of metal precursor to CeO₂ is 1:113 for all the catalysts. The mixture was purged with N₂ and heated to 200 °C under 10 bar N₂ atmosphere. After 12 hours of vigorous stirring, the autoclave was cooled to room temperature. The M/CeO₂ catalyst was washed several times with ethanol/water (volume ratio = 2:1) solution before transferring to a vacuum oven for drying overnight at 60 °C.

2.2.2 Catalyst Characterization

Bulk compositional information was obtained for the synthesized catalysts by inductively coupled plasma (ICP-OES, Horiba J-Y 2000) analysis. The particle size of metal nanoparticles was determined by high-resolution transmission electron microscopy (HR-TEM). The TEM

samples were prepared by suspending the catalyst powder in anhydrous ethanol using ultrasonic agitation. Approximately 10 μL of this ethanol suspension was placed onto a copper or nickel mesh grid with the lacey carbon film (Ted Pella Inc.) and air dried for TEM examination.

2.2.3 Catalyst Performance in Oxidation Reactions

Oxidation experiments were performed following the procedure described elsewhere.[85] Briefly, a mixture of aqueous solution of ethylene glycol (25 mL, 0.58 mol/L) and 0.05 g catalyst was heated to 70°C in a 100 mL three-neck flask equipped with an overhead condenser. The flask was placed in an oil bath for precise temperature control. The O_2 flow was maintained at 60 std mL/min. All the catalysts were tested under both neutral and basic conditions. Approximately 1.7 g NaOH was mixed with the reaction solution to attain basic conditions ($\text{pH} \approx 13.9$) while the pH was approximately 7 (“neutral condition”) with no base added. A small amount of liquid sample was taken from the reactor and diluted with sulfuric acid for composition analysis using high-performance liquid chromatography (Shimadzu HPLC, Shodex SH1011 column). A 0.005N aqueous H_2SO_4 solution was used as the mobile phase and the column temperature was maintained at 70 °C. The retention times and calibration curves for the observed products were determined by injecting standards with known concentrations.

2.3 Results and Discussions

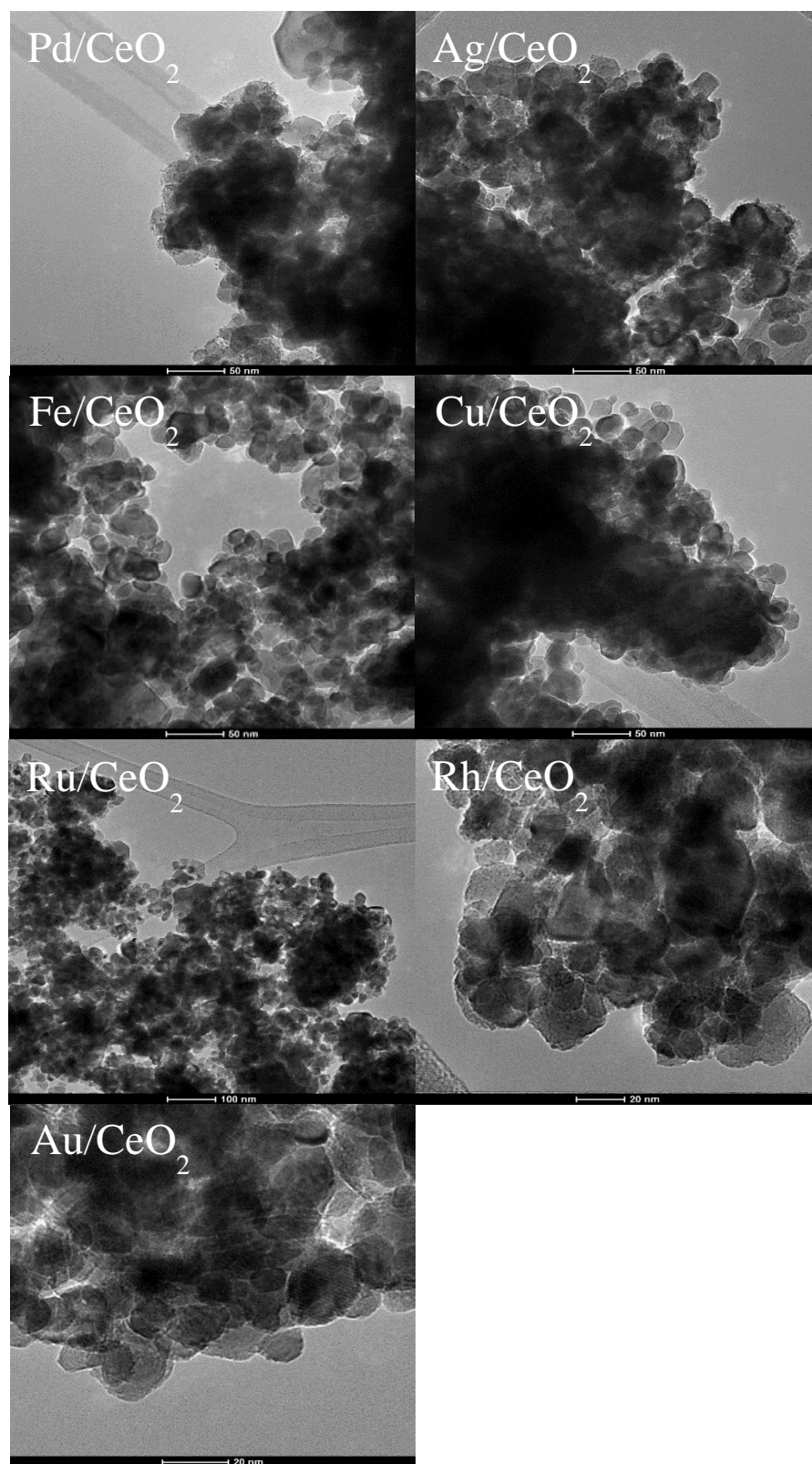


Figure 8. TEM images of monometallics supported on CeO_2

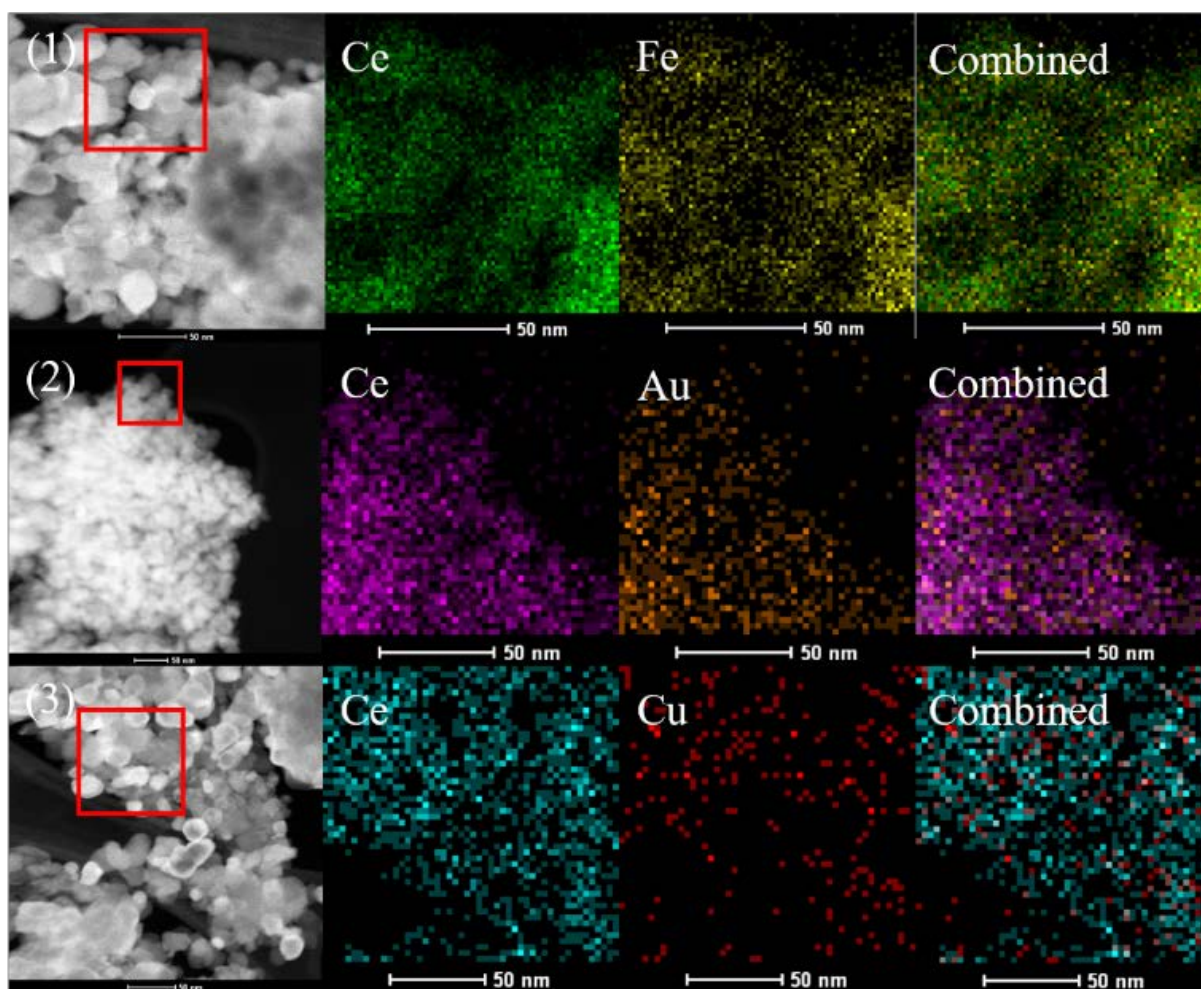


Figure 9. EDX images of (1) Fe/CeO₂ (2) Au/CeO₂ (3) Cu/CeO₂

Table 3. Metal content and particle size of monometallic catalysts

Metal	Weight (%) ^a	Average Particle Size (nm)	FE (Metal Dispersion) ^b
Pt	1.09	11.8 ± 3.8	0.08
Pd	0.61	3.9 ± 1.5	0.37
Ag	0.56	3.2 ± 1.2	0.42
Ru	0.52	2.5 ± 0.6	0.54
Fe	0.25	-	1.00
Rh	0.53	2.4 ± 0.8	0.55
Au	1.01	-	1.00
Cu	0.33	-	1.00

^ametal loading (wt%) was obtained from the ICP analysis

^bmetal dispersion number (FE) calculations are based on an empirical correlation [140]: if metal particles have small size (nanoparticle size < 24 × atom diameter), $FE = \frac{2.64}{(\frac{nanoparticle\ size}{atom\ diameter})^{0.81}}$; if metal particles are large (nanoparticle size > 24 × atom diameter), $FE = \frac{5.01}{(\frac{nanoparticle\ size}{atom\ diameter})}$

Figure 8 shows the TEM images of synthesized monometallic catalysts deposited on a commercial cerium oxide support with a surface area of 30 m²/g and a diameter ≤ 50 nm. The TEM image of Pt/CeO₂ has been demonstrated in our previous publication showing an average Pt metal particle size of 11.8 ± 3.8 nm and a shape of non-uniform polyhedron.[87] In general, Pt nanoparticles show a larger size (11.8 ± 3.8 nm) compared to other monometallics - Pd, Ag, Ru and Ru (**Table 4**). Moreover, the Au, Fe and Cu nanoparticles exhibit a size of about 1 nm or even less which is hardly observable in the TEM image. Again, the STEM images of Fe, Au, and Cu also show smooth CeO₂ surface without the presence of significant nanoparticles or clusters (**Figure 9**). Further, the elemental mapping results clearly demonstrate the existence of these metals (Au, Fe, and Cu) on the CeO₂ surface with a uniform metal distribution. In addition, the ICP results in **Table 4** also confirm the successful deposition of these metals on CeO₂ support with

expected metal loadings. During catalyst synthesis, the metal precursor (metal-acetylacetonate) concentration, temperature, pressure, amount of solvent (DMF), stirring rate and heating rate /duration are all maintained constant for all the catalysts synthesis. However, the synthesized catalysts still have a varied size from sub-nanometer scale to about 10 nm. This can be explained by the different decomposition rates of the metal precursors in DMF that affects the initial nucleation and the subsequent crystal growth. Furthermore, the metals have different atomic radius and packing patterns that may also influence the final particle size. The metal dispersion numbers (FE) are calculated based on the metal particle size using an empirical correlation as described in a previous publication.[140] Considering the small particle size of Au, Cu and Fe nanoparticles, their dispersion is assumed to be one for the TOF calculations.

Table 4. Ethylene glycol (EG) oxidation over monometallic catalysts under alkaline conditions^a

	TOF _{EG} × 10 ² (sec ⁻¹) ^d	TOF _{GLY} × 10 ² (sec ⁻¹) ^d	X (%) ^b	S (%) ^b				CB (%)
				GLY ^c	OA ^c	FA ^c	Others	
Pt	111	83	69	70	6	9	6	94
Pd	45.4	32	77	73	8	0	0	85
Ag	5.0	3.3	16	78	0	0	0	96
Ru	2.9	2.0	19	76	0	3	0	96
Fe	3.0	1.5	22	46	0	0	0	88
Rh	4.0	3.3	30	63	22	2	13	100
Au	3.7	1.7	35	61	17	10	12	100
Cu	2.9	2.4	18	78	0	0	19	99

^areaction condition: 0.58 mol/L initial EG conc., initial pH=13.9, EG:metal ratio = 5657:1 (mol:mol), 70 °C, 1atm O₂, 60 std. mL/min

^bconversion (X), selectivity (S) and carbon balance (CB) data are based on values at 12 h using formula shown in SI Section 7

^cglycolic acid (GLY), oxalic acid (OA), formic acid (FA)

^dinitial TOF values are based on experimental data at EG conversion 2-13%

The experimental results of testing the monometallic catalysts under alkaline conditions are presented in **Table 5**. Catalytic activity is expressed as the TOF values calculated from EG conversion and GLY production data respectively under differential conditions. Pt and Pd supported catalysts showed significantly higher TOFs than other metals by nearly one order of magnitude. In addition, the activity of Pt is higher than two times compared to that of Pd. The overall activity trend of different metals is $\text{Pt} > \text{Pd} > \text{Ag} \approx \text{Rh} > \text{Ru} > \text{Cu} > \text{Au} > \text{Fe}$. For all the monometallics, glycolic acid is the main product that has the highest selectivity (61~78%). Similar trend of higher glycolic acid selectivity for the transition metals was also observed in the MKM analysis (shown in **Figure A - 1**, Appendix). In addition, Rh and Au supported catalysts are observed to promote oxalic acid production compared to other catalysts. As also seen in this study, the experimental and theoretical predictions of activity trends for different monometallic catalysts fit satisfactorily. However, the experimental TOF values are higher than DFT calculated values by orders of magnitude. This is because actual supported metal catalyst is more complex than a well-defined crystal surface assumed in the computational modelling. In addition, promotional effect of the alkali can result in an order of magnitude increase in the reaction rates.[141][142]

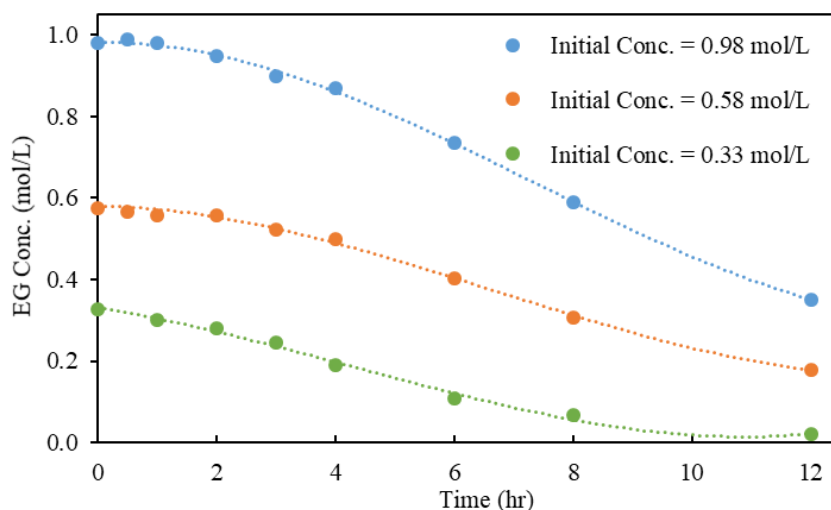


Figure 10. Effect of different initial EG concentrations on oxidation reaction using Pt catalyst

Reaction conditions: initial pH=13.9, 0.05 g Pt/CeO₂ catalyst, 70 °C, 1atm O₂, 60 mL/min

Table 5 shows that the trend regarding EG conversion (%) at 12 h which is a little different from the one with respect to activity (TOF): Pd > Pt > Au > Rh > Fe > Ru > Cu > Ag. This is understandable since in an integral batch reactor, the final conversion is influenced not only by catalyst activity, but also by potential inhibition effects caused by adsorption of reactant, intermediates and products and kinetics of sequential steps. The effect of initial EG concentration was studied using Pt catalyst under alkaline conditions. The EG concentration-time profiles are shown as **Figure 10**. A rate inhibition with EG at the initial stage of reaction is observed for Pt catalyst especially at higher EG concentration (0.98 mol/L).

Table 5. Ethylene glycol (EG) oxidation over monometallic catalysts under neutral conditions^a

	TOF _{EG} (s ⁻¹) × 10 ^{3 d}	TOF _{GLY} (s ⁻¹) × 10 ^{3 d}	X (%) ^b	S (%) ^b		CB (%)
				GLY ^c	GLA ^c	
Pt	200	71	12	45	55	97
Pd	8.3	2.7	2	55	45	99
Ag	5.3	1.0	4	32	68	99
Ru	7.1	1.1	2	31	69	100
Fe	7.0	1.8	4	32	62	100
Rh	19	7.7	8	51	48	99
Au	6.5	1.5	6	51	49	99
Cu	6.1	1.8	5	37	63	99

^areaction condition: 0.58 mol/L initial EG conc., initial pH=7 (no alkali added), EG:metal ratio = 5657:1 (mol:mol), 70 °C, 1atm O₂, 60 mL/min

^bconversion (X), selectivity (S) and carbon balance (CB) data are based on values at 12 h using formula shown in SI Section 7

^cglycolic acid (GLY), glycolaldehyde (GLA)

^dinitial TOF values are based on experimental data at EG conversion 2-13%

The same catalysts (consisting of various supported metals) were also tested under base-free conditions. Results are summarized in **Table 6**. In general, the TOFs for all the catalysts were lower by one order of magnitude compared to those obtained under alkaline conditions. The reaction was slow such that conversions of EG at 12 h were no more than 10% for most of the catalysts. However, Pt and Pd catalysts still show higher catalytic activity compared to the other tested metals. It is worthy to mention that the product distribution changed significantly under base-free conditions with glycolaldehyde and glycolic acid as the only products. In addition, the selectivity of glycolaldehyde is higher than that of glycolic acid for most of the monometallics under neutral conditions

Table 6. Diagnostic experiments on EG oxidation

No.	Conditions	Observations at 12 h
#1	NaOH + O ₂	EG conversion is 16.2%, selectivity for glycolic acid is 74%
#2	NaOH + N ₂	no EG conversion
#3	NaOH + N ₂ + H ₂ O ₂	Glycolic acid and formic acid were detected, but quantification is not possible
#4	Pt catalyst + H ₂ O ₂ + N ₂	H ₂ O ₂ decompose fast as it touches the Pt catalyst, no EG conversion at end
#5	H ₂ O ₂ + O ₂	EG conversion is 6.3%, selectivity for glycolic acid is 22%

To discuss the role of NaOH as a promoter and probe the reaction mechanism we conducted several diagnostic experiments, as shown in **Table 7**. When comparing the following two sets of reaction data: (1) using only NaOH without the metal catalyst that is entry #1 shown in **Table 7**, and (2) using only the Pt metal catalyst without base, shown in **Table 6**, it is apparent that NaOH catalyzes the reaction faster than the Pt catalyst alone. In addition, glycolic acid is still the dominant product (~74% selectivity) when using only NaOH. This result is similar to those as shown in Table 5 under alkaline conditions. However, using only the Pt metal catalyst is more selective to glycolaldehyde production (~55% selectivity) with less glycolic acid formed (~45% selectivity). Similar phenomenon was observed by Yuan et al. showing that NaOH alone was found to be a homogeneous catalyst for selective aerobic oxidation of alcohols in water.[143] However, in the presence of both Pt and alkali (as shown in **Table 5**), EG conversion is significantly higher than the cases of using only the metal or the base. Since NaOH is known as an excellent catalyst for hydrogen transfer,[144] it can act as a promoter to facilitate deprotonation of EG. Kwon et al. discussed the role of both the base and the metal as possible catalysts for electrocatalytic oxidation of alcohols in alkaline solution.[145] They suggested that the first deprotonation of alcohols is base catalyzed, and the second deprotonation is metal catalyzed. Since the first deprotonation (Eq. i) is a slower step compared to the second deprotonation (Eq. ii), the addition of alkali is expected

to accelerate the overall reactivity significantly. In addition, it was reported that Na^+ attached on the metal surface can promote the adsorption of electron acceptors (O_2) while inhibiting the adsorption of the electron donor (EG). [146, 147] By moderating the relative adsorption strengths, the alkali metals allow more O_2 to be adsorbed on the active sites, leading to an acceleration of the reaction.

Our experiments also showed that under N_2 environment even with the presence of NaOH , EG conversion at 12 hours is still negligible, which suggests that O_2 presence is essential for this reaction. This result provides evidence that O_2 plays a crucial role in generating OOH^* (**Figure 11**Eq. iii in proposed mechanism), therefore producing OH^* to form carboxylic acid (Eq. iv and v). Under N_2 atmosphere, OH^* cannot be provided easily from deprotonation of H_2O and hence the reaction proceeds slowly. Moreover, O_2 is a suitable electron acceptor [148] that removes electrons of OH^- on the metal surface to provide OH^* (Eq. vii). The OH^* subsequently reacts with deprotonated EG species (HOCH_2CO^*) to form the glycolic acid. This theory also helps in explaining the phenomenon of NaOH acting as a catalyst or a promoter for EG oxidation reaction because the base can continuously provide supplementary hydroxyl species for the aqueous phase oxidation.

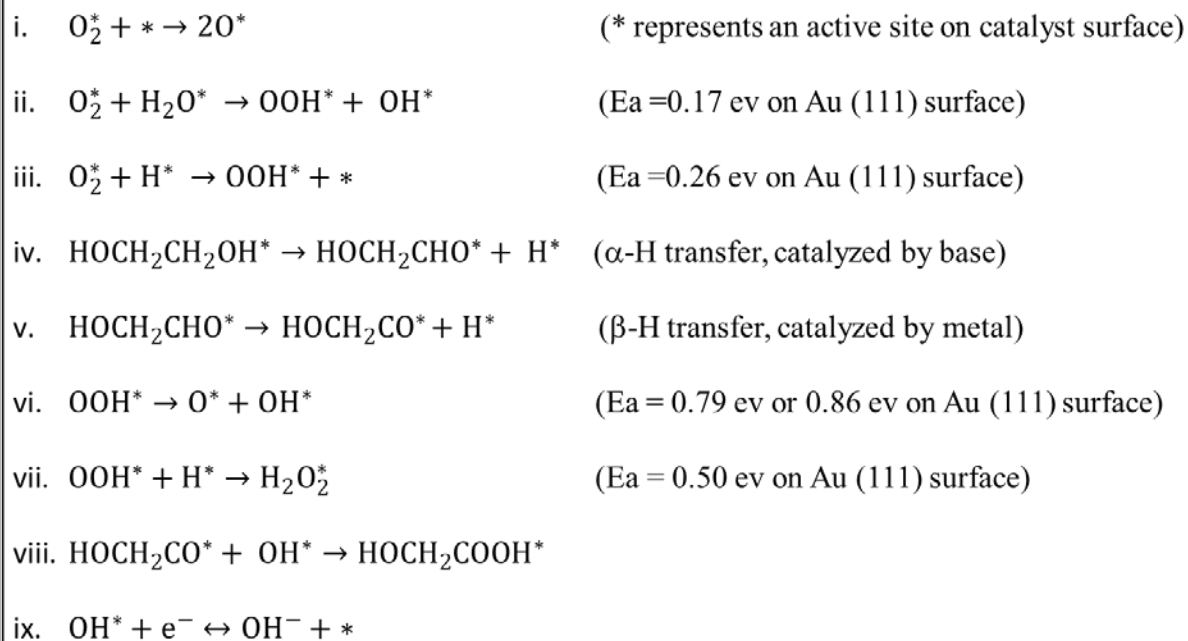


Figure 11. Scheme of -OH mediated oxidation mechanism in the aqueous phase, activation energies are cited from references [149] [150]

2.4 Conclusion

Oxidation of ethylene glycol in water using eight different monometallic catalysts was investigated experimentally in this work that shows good agreement with the micro-kinetic modelling. Pt shows the best TOF for glycolic acid formation under both neutral and alkaline conditions, followed by Pd. The alkali promotion effect was found for all the metal catalysts investigated in this work. Based on experimental observations and literature reports, this alkali promotion is explained in terms of the following three aspects: (a) alkali promotes hydrogen transfer; (b) Na^+ interacts with the Pt surface enhancing O_2 adsorption and decreasing EG adsorption, and (c) OH^- is an extra source for continuous formation of OH^* species that reacts

directly with deprotonated EG to form glycolic acid. A volcano plot was built from DFT calculations and micro-kinetics study to show the catalytic activity vs. adsorption energy relationship. The activities from the micro-kinetics modelling fits well with the experimental findings in testing different monometallics. The active sequence of different metals in alkaline solutions is: $\text{Pd} > \text{Pt} > \text{Au} > \text{Rh} > \text{Fe} > \text{Ru} > \text{Cu} > \text{Ag}$.

Chapter 3: Liquid-phase Oxidation of Ethylene Glycol using Bimetallic Catalysts: Synergistic Effects and Reaction Mechanism

3.1 Introduction

The introduction of a second metal as a promoter has been demonstrated to be successful in maximizing the activity and selectivity to desired products for many reactions in the field regarding biomass conversion.[151] The general bimetallic effect can be divided into five phenomena: geometric effect, electronic effects, stabilizing effects, synergistic effects and bifunctional effects. As demonstrated in the literature survey part of this thesis (Section 1.4.3), the bimetallic catalysts for the aqueous phase oxidation of EG are not widely studied. In addition, the activities demonstrated by the current catalysts are not high enough for their commercial applications.

In the previous publications, alloying of Pt with 3d transitional metals has shown successes in the oxidation of sugars and polyols. For instance, the anisotropic Pt-Mn catalysts with nanobud and nanoflower morphologies showed remarkable eight-fold enhancement in the catalytic activity for the oxidation of glycerol-to-tartronic acid.[85] In another example, the bimetallic Pt-Fe nanoclusters with high-index numbers has been prepared to exhibit an unprecedented six-fold enhanced catalytic activity on glycerol oxidation and threefold higher selectivity towards tartronic acid, in comparison with the monometallic Pt catalyst.[87] From the kinetics modelling works, it was found that the presence of Fe in Pt catalysts sufficiently enhanced the rate of oxidation and decreases the activation barrier for the primary and secondary oxidation steps.

From the experimental studies on monometallics as shown in the Chapter 2, it was found that Pt is the most active metal for the aqueous phase oxidation of EG. By the volcano-plot obtained from the computational works as demonstrated in the Appendix I, Pt is a strong surface for EG adsorption while Fe is a weak surface. Therefore, the combination of Pt and Fe has potential to create a moderate surface for the EG adsorption for tuned oxidation activity. This “interpolation” strategy has been demonstrated for designing the Co-Mn bimetallic catalyst with enhanced activity for the reaction of ammonia synthesis.[152] In this Chapter, the bimetallic Pt-Fe catalyst was then synthesized to test the hypothesis of the synergistic effect of Pt and Fe. As for comparison, other bimetallics such as Au-Fe, Ag-Fe and Pd-Fe were also synthesized and tested under the same experimental conditions. Detailed catalyst characterizations and parametric effect study was also performed on the Pt-Fe catalyst to discuss the reaction mechanism.

3.2 Experimental and Methodology

3.2.1 Catalyst Synthesis and Characterization.

The monometallic 1%-M/CeO₂ and bimetallic 1% M-Fe/CeO₂ catalysts were prepared following the method reported previously, where M is the selected noble metal (Au, Ag, Pd, Pt).[87] For the bimetallic M-Fe/CeO₂ catalysts, the molar ratio of M : Fe : CeO₂ is (1:1:113). N-dimethylformamide (DMF, HPLC grade, > 99.9%), cerium oxide nanopowder (< 50 nm, BET), Pt(acac)₂ and Fe(acac)₃, (acac = acetylacetonate) were all purchased from Sigma Aldrich and used without further purification.

Powder X-ray diffraction pattern for the bimetallic Pt-Fe catalyst was obtained on a Bruker D8 powder diffractometer with a copper target (Cu K α radiation) operating at 40 kV and a current of 40 mA. X-ray absorption spectroscopy (XAS) was performed at the SPring-8/BL36XU in Japan. Data analysis of EXAFS (extended X-ray absorption fine structure) was performed using the IFEFFIT package using standard procedures.[153] The Fe K-edge spectrum of the bimetallic PtFe/CeO₂ catalyst was measured in fluorescence mode under ambient conditions. The Fe K-edge spectrum of a metallic Fe foil was collected simultaneously in the reference mode for X-ray energy calibration and data analysis. The sizes of Pt and Pt-Fe nanoparticles are 11.8 ± 3.8 nm and 17.3 ± 4.9 nm, respectively, as inferred from transmission electron microscopy (TEM) micrographs. [87]

3.2.2 Performance Evaluation Catalysts for Oxidation

The catalytic performance was evaluated in a stirred reactor setup as described previously (see Appendix, **Figure A - 6**).[85] In a typical example, an aqueous solution (25 mL, 0.58 mol/L) of ethylene glycol (anhydrous, 99.8%, Sigma-Aldrich), and 0.05 g catalyst were placed in a 100 mL three-neck flask and heated to 70 °C under magnetic stirring. The flask was equipped with an overhead condenser and placed in an oil bath for precise temperature control. O₂ was bubbled into the aqueous solution with gas flow maintained at 60 std mL/min. The Pt and Pt-Fe catalysts were tested under both neutral (pH ~ 7 with no base addition and and basic conditions. 1.7 g NaOH were dissolved in the reaction solution prior to reaction to attain basic condition (pH \approx 13.9). Approximately 0.5~1 mL reaction solution was sampled from the reactor and neutralized with

sulfuric acid for compositional analysis using high-performance liquid chromatography (Shimadzu HPLC, Shodex SH1011 column) to obtain concentration-time profiles.

Hydrogen peroxide formation during the reaction was detected and quantified by a colorimetric method using the UV-vis spectroscopy (Lambda 850 UV-vis Spectrometer, Perkin Elmer). [154] 2 mL of reaction solution was sampled from the reactor and mixed immediately with 2 mL of diluted H_2SO_4 aqueous solution (1 mol/L) and 0.2 mol of $\text{TiO}(\text{SO}_4)$ indicator (15 wt% in dilute H_2SO_4 , purchased from Sigma Aldrich). 30 wt% H_2O_2 purchased from Fisher Scientific was used for preparing a series of H_2O_2 aqueous solutions of known concentrations for calibration purposes. The peak height corresponding to H_2O_2 absorbance at 405 nm is used for quantification purposes. The lower limit of H_2O_2 detection by this method is approximately 0.005 mM as reported previously.[154]

Experimental data on the effects of reaction conditions were collected using a 100 mL semi-batch reactor equipped with precise temperature and pressure control (SI, Scheme S2). The experimental conditions are: $T=70\text{ }^\circ\text{C}$; catalyst loading = 2 kg/m^3 ; $P_{\text{O}_2}=10\sim 50\text{ bar}$; initial EG concentration = $0.15 - 0.60\text{ mol/L}$ in aqueous solution; (NaOH:EG molar ratio) = $0 - 4.8$. The absence of heat and mass transfer limitations was confirmed by estimating gas-liquid, liquid-solid, and intraparticle mass-transfer limitations using the criteria described by Ramachandran and Chaudhari.[155] Intraparticle heat transfer limitations were quantified based on the Mears criterion.[156]

3.3 Results and Discussions

3.3.1 Performance Evaluation of Bimetallic Catalysts

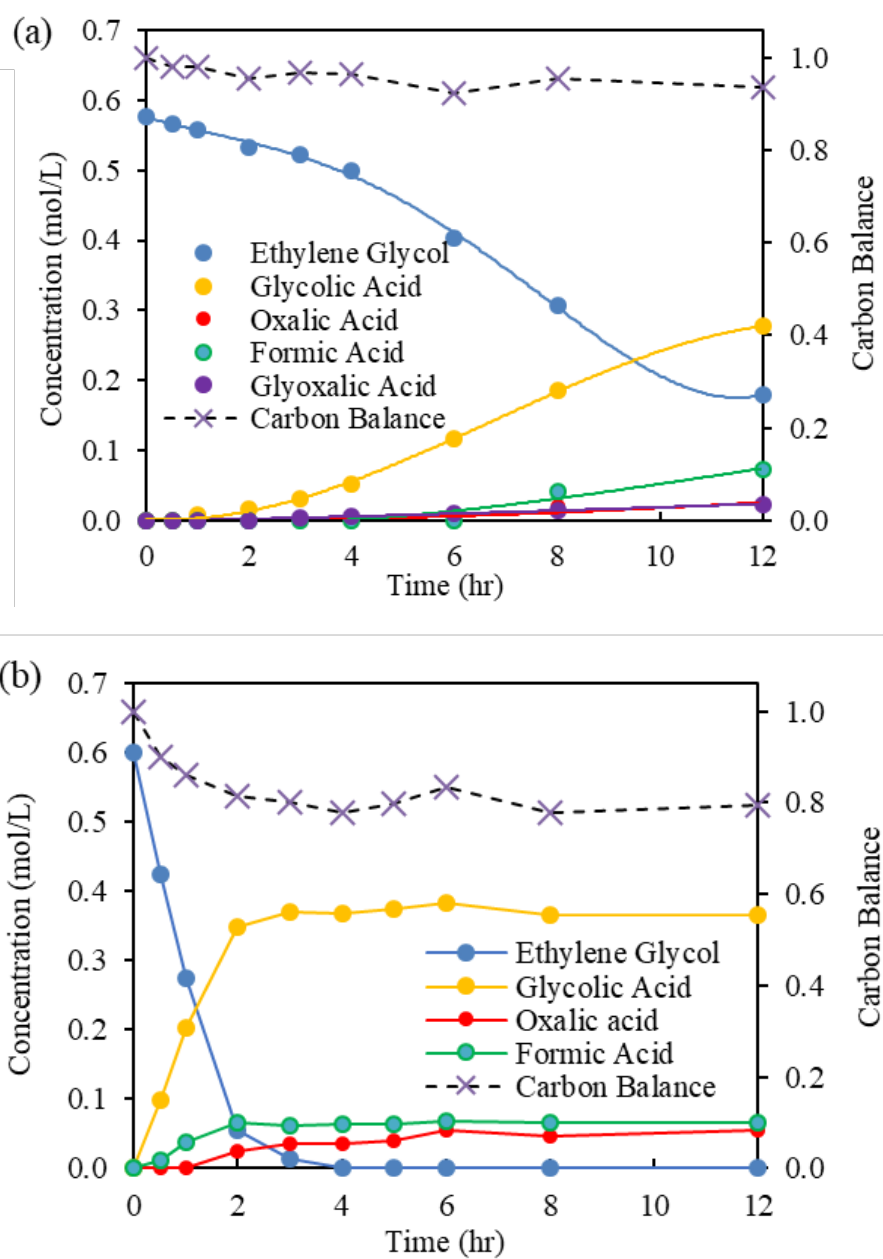


Figure 12. Concentration-time profiles on (a) Pt/CeO₂ and (b) PtFe/CeO₂ catalysts for aqueous phase ethylene glycol oxidation in the presence of alkali promoter. Reaction conditions: 0.58 mol/L initial EG conc., initial pH=13.9 (alkali added), EG:metal ratio = 5657:1 (mol:mol), 70 °C, 1atm O₂, 60 std mL/min gas flow

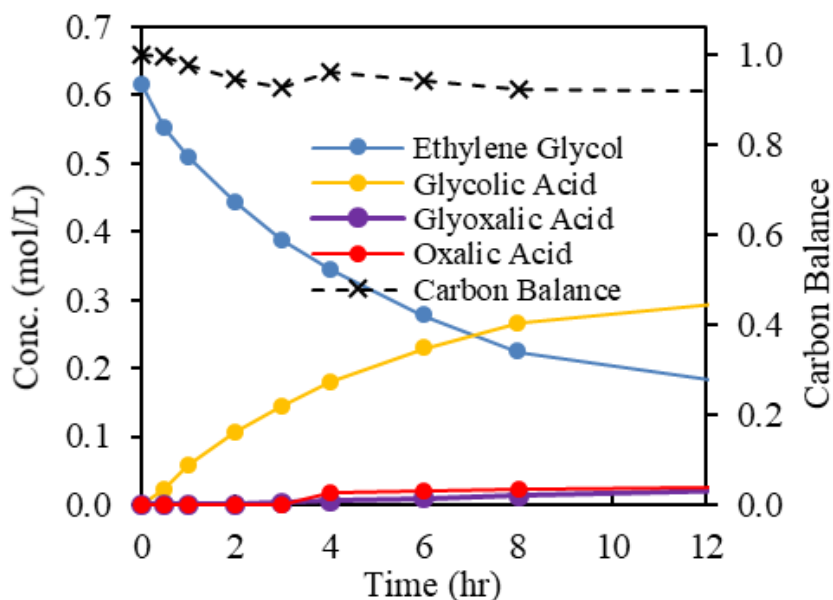
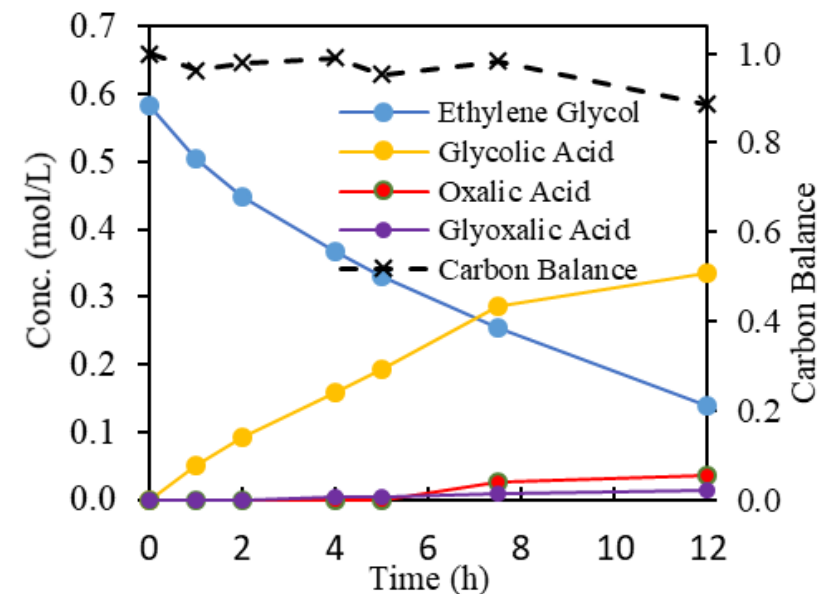


Figure 13. Concentration-time profiles on (a) Pd/CeO₂ and (b) Pd-Fe/CeO₂ catalysts for aqueous phase ethylene glycol oxidation in the presence of alkali promoter. Reaction conditions: 0.58 mol/L initial EG conc., initial pH=13.9 (alkali added), EG:metal ratio = 5657:1 (mol:mol), 70 °C, 1atm O₂, 60 std mL/min gas flow

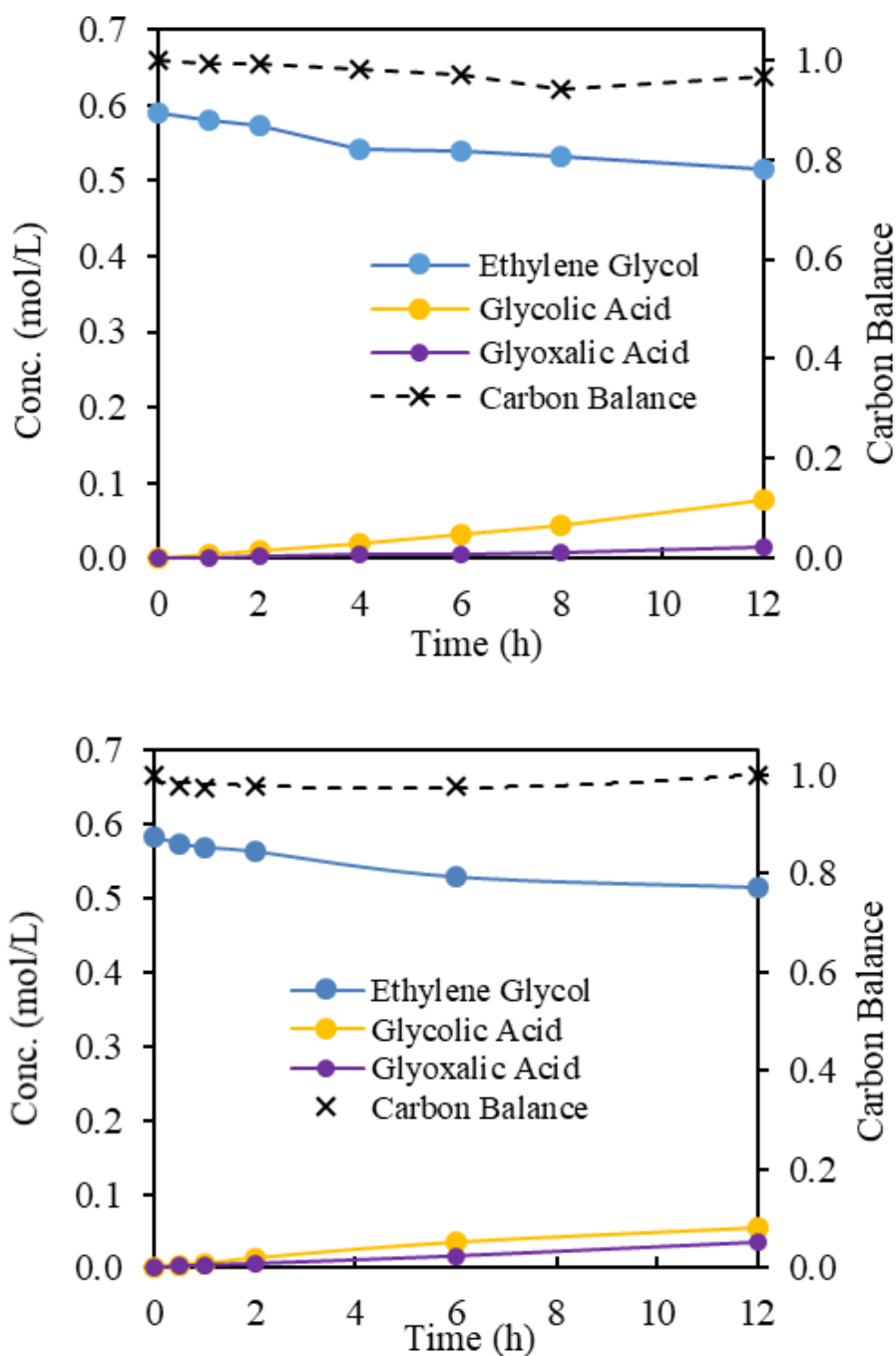


Figure 14. Concentration-time profiles on (a) Ag/CeO₂ and (b) Ag-Fe/CeO₂ catalysts for aqueous phase ethylene glycol oxidation in the presence of alkali promoter. Reaction conditions: 0.58 mol/L initial EG conc., initial pH=13.9 (alkali added), EG:metal ratio = 5657:1 (mol:mol), 70 °C, 1atm O₂, 60 std mL/min gas flow

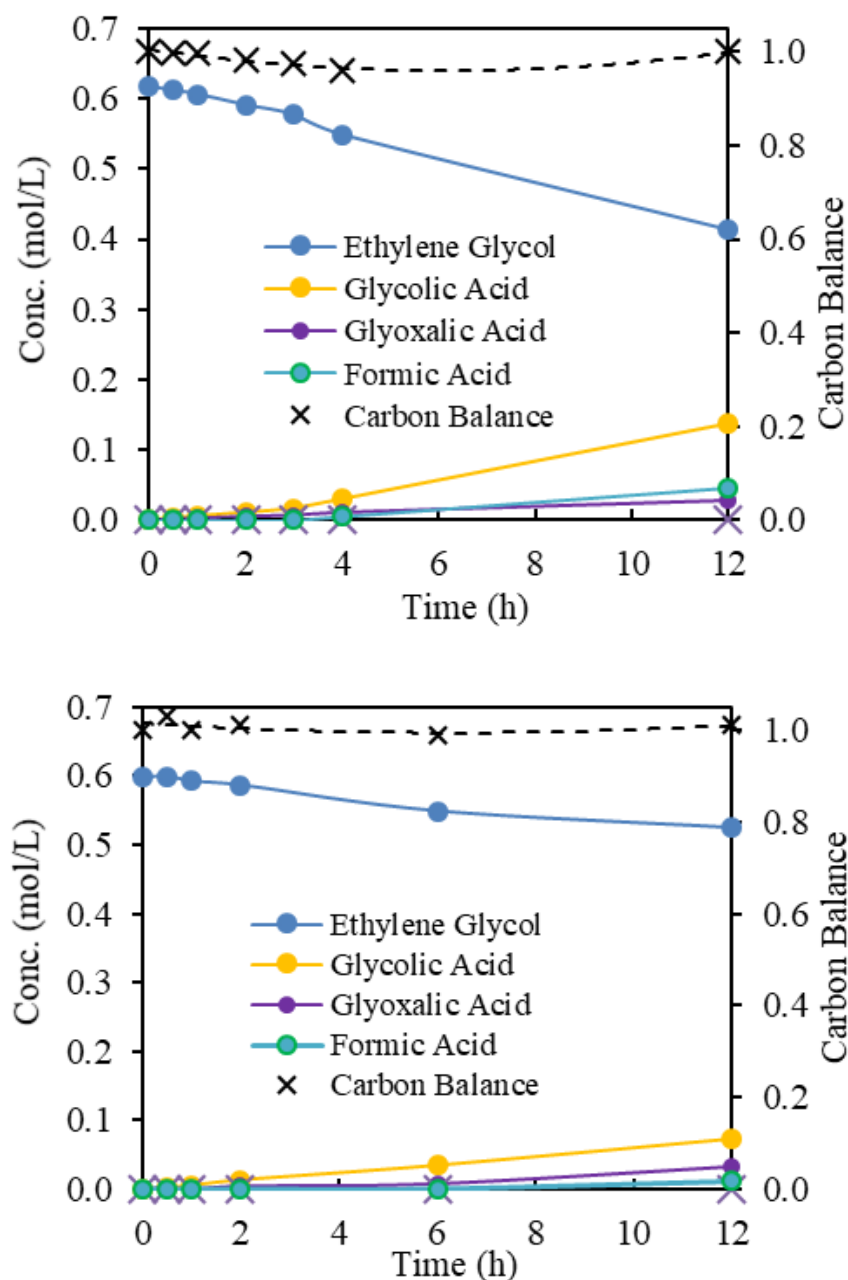


Figure 15. Concentration-time profiles on (a) Au/CeO₂ and (b) Au-Fe/CeO₂ catalysts for aqueous phase ethylene glycol oxidation in the presence of alkali promoter. Reaction conditions: 0.58 mol/L initial EG conc., initial pH=13.9 (alkali added), EG:metal ratio = 5657:1 (mol:mol), 70 °C, 1 atm O₂, 60 std mL/min gas flow

The bimetallic 1% Pt-Fe/CeO₂, 1% Au-Fe/CeO₂, 1% Pd-Fe/CeO₂ and 1% Ag-Fe/CeO₂ catalysts were synthesized under similar conditions and tested for the aqueous phase oxidation of EG. The concentration-time profiles of all the bimetallic catalysts compared with the monometallic catalysts were shown as **Figure 12** to **Figure 15**. As can be seen from the results, the Pd-Fe and Ag-Fe did not show significant difference in comparison with the Pd and Ag monometallic catalysts. In addition, the activity of Au-Fe is observed to be slight lower than that of Au catalyst. only the bimetallic Pt-Fe catalyst gives a dramatic higher activity compared to the monometallic Pt catalyst. The EG was completely consumed within 4 hours with bimetallic Pt-Fe catalyst. Therefore, not all the bimetallics on the basis of the interpolation principle theory showed a better catalytic performance in aqueous phase oxidation reaction. It would be meaningful to discuss the reaction mechanism of Pt-Fe and explore the underlying reasons for the significant bimetallic effect.

In fact, the promotional effect of transition metal addition to Pt metal for alcohol and CO oxidations has been reported in many publications.¹⁻⁶ In this regard, the oxophilic character of Fe with its high O/OH binding energy makes it an attractive metal to alloy with Pt in order to enhance catalytic activity. Based on this hypothesis, parametric effect studies were performed for aqueous phase oxidation of ethylene glycol over Pt and Pt-Fe catalysts under either neutral or alkaline conditions to provide insights into the underlying bimetallic effect and to understand the role of alkali promoter.

3.3.2 Pt-Fe Bimetallic Effect and OH* Mediated Reaction Mechanism

Table 7. EG Oxidation over Pt and PtFe catalysts under alkaline or neutral conditions

		TOF _{EG} (sec ⁻¹) ^a	X (%) ^b	S (%) ^b					CB (%) ^b
				GLY ^c	GLA ^c	OA ^c	FA ^c	Others	
Pt	Alkaline	1.1	69	70	-	6	9	6	94
	Neutral	0.2	12	45	55	-	-	-	97
Pt-Fe	Alkaline	19.1	100	62	-	9	8	-	79
	Neutral	2.8	40	42	-	-	-	-	77

^areaction condition: 0.58 mol/L initial EG conc), EG:metal ratio = 5657:1 (mol:mol), 70 °C, 1atm O₂, 60 std mL/min, initial turn-over frequency (TOF) values are based on experimental data at EG conversion 5-25%

^bconversion (X), selectivity (S) and carbon balance (CB) data are based on values at 12 h using formula shown in SI; CB data is calculated on the basis of liquid products only.

^cglycolic acid (GLY), glycolaldehyde (GLA), oxalic acid (OA), formic acid (FA)

Catalytic performance metrics including activity (TOF), EG conversion and product selectivity under both neutral and alkaline conditions are presented in **Table 8**. The support material (CeO₂) alone was also tested but showed no activity for EG oxidation. The base (NaOH) acts as a promoter for both Pt and Pt-Fe catalysts showing 5~6 times higher TOF compared to the values under neutral conditions for monometallic Pt. The bimetallic Pt-Fe catalyst shows a significantly higher activity compared to the monometallic Pt catalyst under both neutral and alkaline conditions. The calculated initial TOF for Pt-Fe is about 19.1 sec⁻¹, which is more than 17 times higher than that of Pt catalyst (TOF=1.11 sec⁻¹) in the presence of a base promoter. As can be seen from **Error! Reference source not found.**, EG is entirely converted during 4 hours using Pt-Fe catalyst while the Pt catalyst gives much less conversion in the same duration. However, significant carbon deficit in liquid phase products was observed due to over-oxidation (CO₂ formation) when Pt-Fe catalyst is used.

Based on the theoretical works for the aqueous phase oxidation of glycerol, Davis and co-workers reported that O₂ dissociation on Au or Pt surface is not facile. [148, 149, 154] By using

isotope labelling experiments, they proved that O_2 was involved in the reaction by taking H from water or glycerol to form OOH species, which reacts with deprotonated glycerol to form the glyceric acid, producing H_2O_2 as a byproduct. To verify if the EG oxidation in water follows a similar mechanism, possible H_2O_2 formation as a byproduct was measured with results shown in **Table 9**. It was found that H_2O_2 was indeed formed during EG oxidation, and the H_2O_2 concentration change correlates with the change in the reaction rate as observed from **Table 9**. It is worth mentioning that the H_2O_2 formation with Pt-Fe catalyst is less pronounced. The instantaneous H_2O_2 concentration in the reaction solution with Pt-Fe catalyst is an order of magnitude lower than that observed with the Pt catalyst. This suggests that increase in reaction rate with the Pt-Fe catalyst follows a different reaction mechanism that does not promote the formation of OOH species during reaction.

Table 8. Concentration of H_2O_2 during the EG Oxidation in Alkaline Solution over Pt and Pt-Fe Catalysts

Time (h)	H_2O_2 conc. (mol/L)	
	Pt	PtFe
0.5	5.0E-04	2.4E-04
1	1.3E-03	2.2E-04
2	1.5E-03	8.3E-05
4	8.3E-04	6.4E-05
12	4.2E-04	-

3.3.3 Catalyst Characterization and Structure-Activity Relationship

To interpret the bimetallic effect and draw conclusions based on surface chemistry, detailed characterization studies were performed to discuss the structure-performance correlations for the Pt-Fe catalyst. In the previous publication using the same synthesis method, it is shown that the bimetallic Pt-Fe nanoparticle exhibits an alloyed structure.[87] To derive more structural

information for this bimetallic alloy, X-ray diffraction analysis was used to characterize the Pt-Fe/CeO₂ catalyst used in this work. Two crystal structures of Pt-Fe alloy are known in the literature:[157] (1) disordered faced centered cubic-fcc (A1 phase, **Figure 16**) and (2) ordered face centered tetragonal phase-fct (L1₀ phase, **Figure 16**). The XRD spectra of CeO₂ supported Pt-Fe catalysts of different metal loadings are shown in **Figure 16**. The sample with metal loading at 1 wt% did not show any clear diffraction peaks besides the peaks of CeO₂ due to the sensitivity limitation of the XRD instrument. At increased metal loadings of 5 wt% or 10 wt%, the characteristic diffraction lines of PtFe alloy at $2\theta = 23.0^\circ$, 40.4° , and 82.8° are well defined, indicating that the Pt-Fe catalyst belongs to a fcc crystal structure with a calculated lattice constant $a = 0.386$ nm (Appendix, **Table A - 1**). The peaks representing Pt crystal or Fe crystal were not found in the spectra, indicating that our catalyst is highly alloyed. Dominance of the fcc disordered phase occurs in most of the current PtFe nanoparticle preparation techniques without thermal treatment. Post-deposition annealing at a temperature around 600 °C is usually required to achieve the formation of ordered fct structure of Pt-Fe alloy according to the phase diagram of Pt-Fe system.[84]

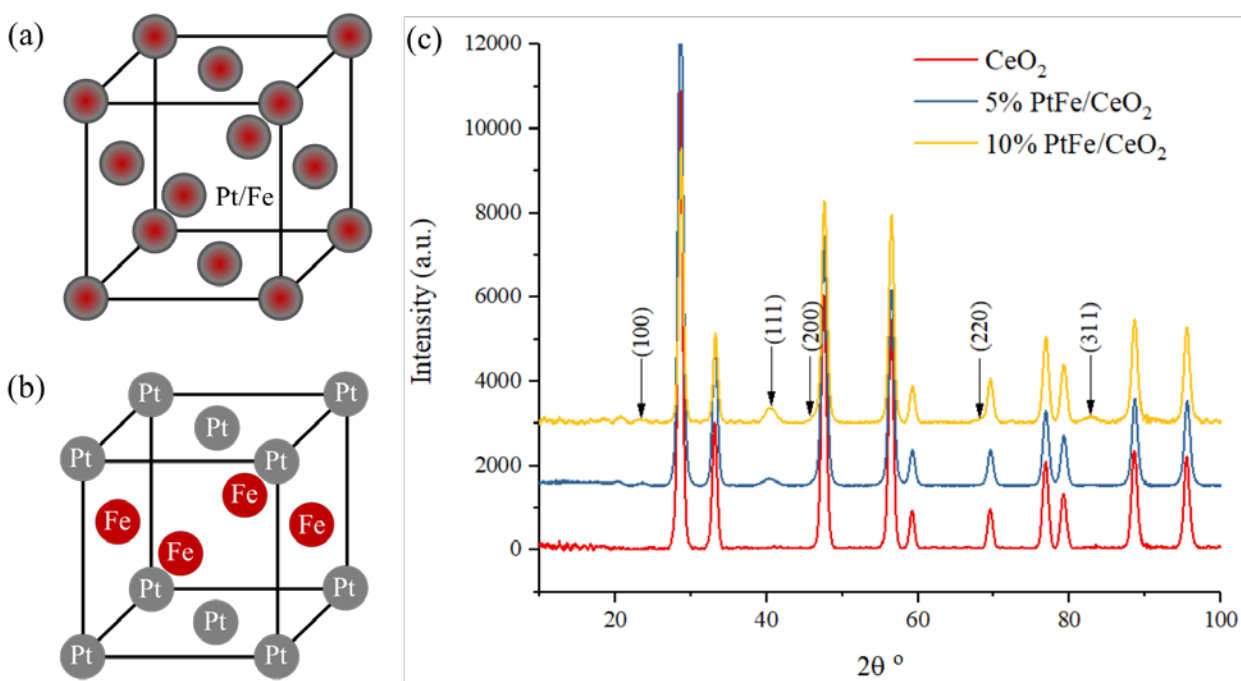


Figure 16. PtFe crystal structure: (a) disordered fcc; (b) ordered fct, and (c) X-ray diffraction pattern of the cerium oxide supported PtFe catalyst

The XPS results shown in previous work revealed that the Pt maintains metallic state before or even after oxidation reaction.[87] However, the oxidation state of Fe in Pt-Fe alloy has not been previously reported. In this paper, used Pt-Fe catalyst after one12 h run of EG oxidation was investigated with the EXAFS technique to discern more information about the Pt-Fe alloy structure. As shown in **Figure 17**, the Pt-Fe catalyst's absorption edge curve is more in line with that of Fe foil, instead of Fe₂O₃ standard sample. Besides, no Fe-O coordination was found in the r-space figure, as shown in **Figure 17**. In other words, the Fe element in the Pt-Fe alloy remains in reduced state (Fe⁰).

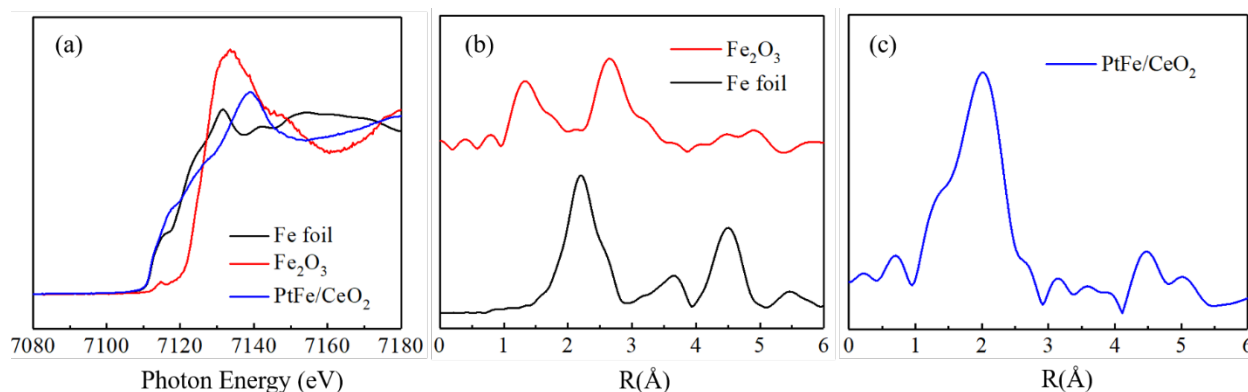


Figure 17. (a) Fe K edge XAS spectra of Fe foil, ferric oxide, and PtFe catalyst (b)(c) Fourier-transformation of EXAFS

Given that Fe metallic nanoparticle can be easily oxidized in an O₂ and moisture rich environment, the above finding seems unexpected. In the EXAFS study of Pt-Fe/zeolite by Kotobuki, even after hydrogen reduction treatment, Fe center atom was coordinated by not only Pt and Fe but also by O.[158] However, researchers also found that noble metals like Pt can enhance the reduction of iron by intimately contacting with them in the supported bimetallic catalysts,[159] due to the strong hybridization of Pt 5d bands with highly polarized Fe 3d bands. It has been found that the reduced state of Fe depends largely on the degree of its alloying with Pt. Although pure Fe surfaces are known to be highly reactive with O₂ such that the surface metallic Fe can be oxidized to form FeO, the surface alloyed Fe can remain stable even when exposed to O₂-rich reaction conditions. In an O₂/CO adsorption study combined with XPS characterization by Xu et al.,[160] the Pt-Fe alloy after adsorption of O₂ displayed similar O 1s intensity compared to that of the Pt nanoparticle. Also, Fe 2p^{3/2} positive shift is found almost negligible (0.2 eV), indicating that Fe in a highly-alloyed structure was resistant to oxidation and still highly active to

CO oxidation.[160] Considering the highly alloyed structure of our Pt-Fe catalyst as observed from XRD spectra, the conclusion that the assignment of the Fe^0 state is reasonable.

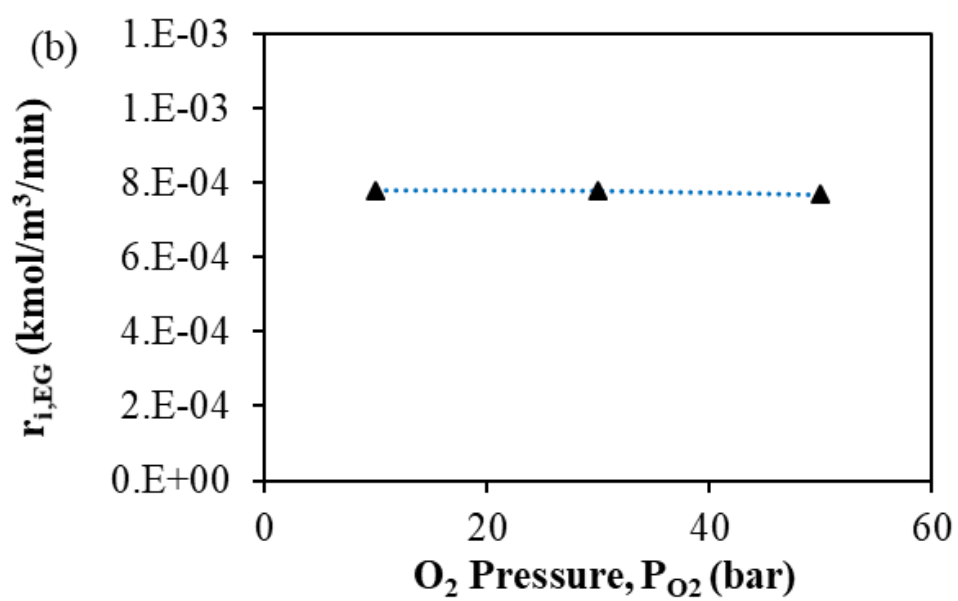
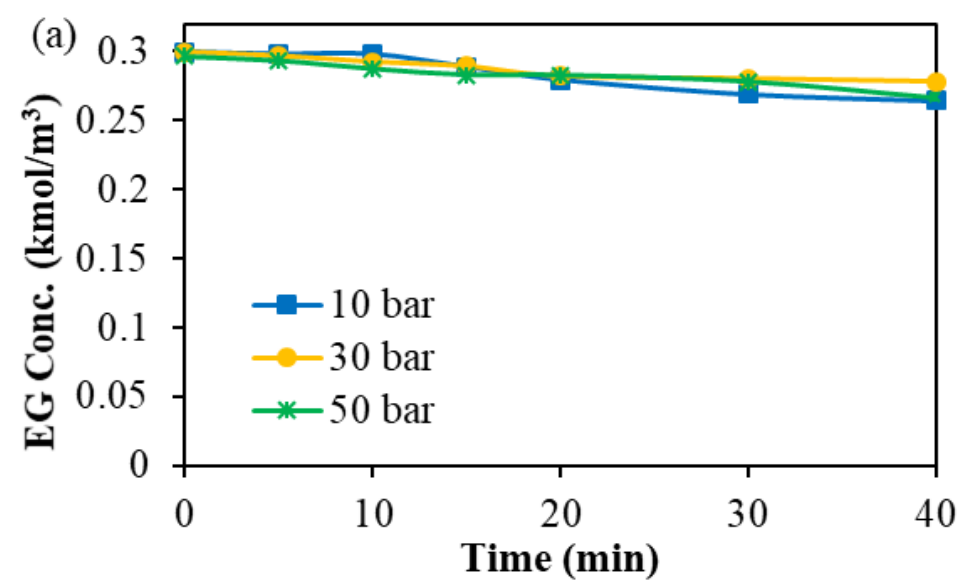
Pt alloys involving 3d metals are usually found to be better catalysts than Pt because the d band of the Pt atoms on the surface of these alloys are modified.[161] Based on the d-band theory, catalyst activity depends on the strength of adsorbate-metal bond interaction to a large extent, which in turn depends on the position of the metal d states relative to the Fermi level.[162] In our study, the crystalline lattice spacing reduction (lattice constant of Pt = 0.392 nm is decreased to 0.386 nm in Pt-Fe alloy, see **Table A - 1** for details) can result in the downward shifting of the d-band center, weakening the bonding between Pt and adsorbent (EG) and therefore tuning the catalytic performance.

Due to the difference in electronegativity of Pt and Fe, electron transfer from Fe to Pt occurs upon the formation of Pt-Fe bonding in the alloyed structure nanocrystal.[160] This electron transfer from Fe to Pt on the surface can modify the adsorption energy of EG or O_2 on the Pt metal surface. In addition, DFT calculations show that the existence of alloyed Fe atoms can improve O_2 dissociation.[163] It has been found that the reaction energy barrier of O_2 dissociation on atomically dispersed Fe sites in the Pt-Fe alloy is very low, around 0.32 eV, and the O adsorption energy is also much lower (-1.63 eV) than the adsorption energy of other Fe surfaces.[163] Therefore, the phenomenon of less pronounced H_2O_2 formation with Pt-Fe catalyst is explained as follows. Part of the O_2 does not react with water to generate OOH species like it does on the Pt surface. However, the O_2 dissociates on the Pt-Fe surface and then reacts with the adsorbed EG to form the glycolic acid. Oxidation by this pathway cannot form H_2O_2 as a byproduct. To verify this proposed mechanism, we performed the following parametric effect studies.

3.3.4 Effect of Reaction Conditions

The O₂ pressure effect on the initial reaction rate was studied with monometallic Pt catalyst for both neutral and alkaline conditions while keeping other reaction parameters constant. The concentration-time profiles are shown as **Figure 18** (a) and (c). The initial reaction rate for EG conversion at various O₂ pressures is shown in **Figure 18** (b) and (d). While the EG oxidation rate does not change with O₂ pressure under neutral conditions, it shows a linear dependence with O₂ pressure under alkaline conditions. In other words, the reaction order with respect to O₂ pressure is increased from zero to one by the base promotion effect.

Effect of initial EG concentration on the EG reaction rate with Pt catalyst is also dramatically different for the neutral and alkaline conditions (**Figure 19**). Under neutral conditions, the reaction rate increases very rapidly with an increase in initial EG concentration from 0.15 - 0.6 kmol/m³ but remains constant at EG concentrations greater than 0.6 kmol/m³. In contrast, a strong inhibition effect was observed for the EG oxidation rate under alkaline conditions with respect to EG concentration. The EG oxidation rate continuously decreases with an increase in initial EG concentration in the 0.15-1.2 kmol/m³ range, suggesting strong EG adsorption on the catalyst surface when compared to O₂. This inhibition effect may also be observed from the results in **Figure 10**. A “slow” oxidation period exists during the first four hours of reaction, following which the reaction accelerates due to the alleviation of rate inhibition upon EG consumption.



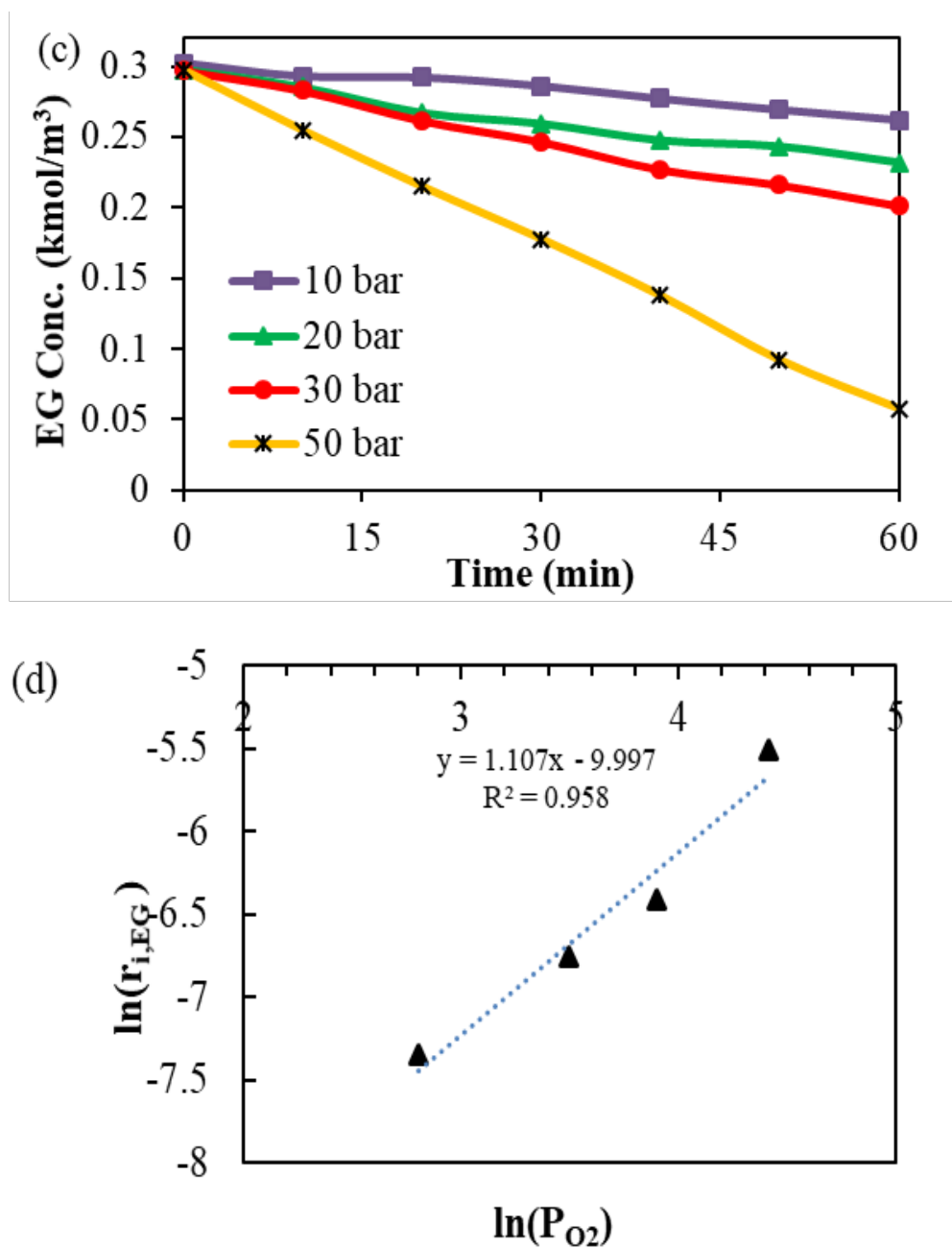


Figure 18. Oxygen pressure effect on EG oxidation with Pt catalyst (a) EG concentration-time (C-t) profiles under neutral conditions; (b) O_2 pressure effect on initial reaction rate under neutral conditions; (c) EG concentration-time profiles under alkaline conditions; (d) O_2 pressure effect on initial reaction rate under alkaline conditions. Reaction conditions: initial EG conc.=0.295 kmol/m³, 70 °C, P_{O_2} =30 bar, initial NaOH conc.=1.458 kmol/m³ under alkaline conditions; no NaOH was added under neutral conditions, catalyst loading (Pt/CeO₂) = 2 kg/m³, initial reaction rate ($r_{i,EG}$) is calculated based on the data of EG conversion $\leq 15\%$

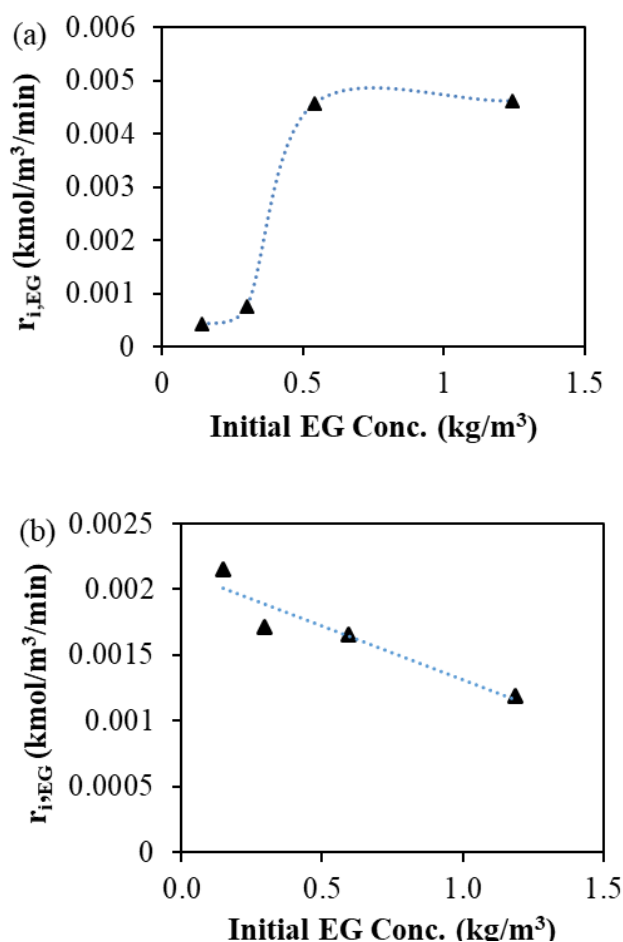


Figure 19. Initial EG concentration effect of EG oxidation on Pt catalyst (a) neutral conditions (no base added); (d) alkaline conditions (initial NaOH conc.=1.458 kmol/m^3). Reaction conditions: initial EG conc.=0.295 kmol/m^3 , 70 °C, P_{O_2} =30 bar, catalyst loading (Pt/CeO₂)=2 kg/m^3 , initial reaction rate ($r_{i,EG}$) is calculated based on the data of EG conversion $\leq 15\%$

Similar effects of O₂ pressure and initial EG concentration dependence on the reaction rates for the Pt-Fe bimetallic catalyst are shown in **Figure 20**. Interestingly, the reaction order with respect to O₂ is markedly different for the bimetallic catalyst compared to the monometallic Pt catalyst. Under neutral conditions, the reaction rate increases linearly with the O₂ pressure yielding a reaction order close to one as observed from the $\ln(r_{i,EG})$ and $\ln(P_{O_2})$ plot (**Figure 20 (a)**). This

confirms that O_2 is involved in the rate-determining step for EG oxidation in the case of the Pt-Fe catalyst. Further, the O_2 reaction order was increased to around two as observed from **Figure 20 (b)**. The effect of initial EG concentration on the Pt-Fe catalyst is similar to that observed with the Pt catalyst. A mixed order dependence (first order at low EG concentration and zero order at higher EG concentrations) was observed under neutral condition while EG inhibition was observed under alkaline conditions. Thus, the adsorption characteristics of EG do not appear to have changed significantly on the bimetallic catalyst.

The observed O_2 reaction order change can be caused by the promoted O_2 -dissociation on the catalyst surface due to the alloy structure as explained earlier. In addition, the O_2 adsorption on the surface is likely to be enhanced by the Fe species in the catalyst. Kotobuki et al. reported CO, H_2 , and O_2 chemisorption measurements of mordenite supported Pt, Fe, and Pt-Fe catalysts, demonstrating that Pt sites act as adsorption sites for only CO and H_2 , while Fe or FeO sites are primarily responsible for O_2 adsorption.[164] Consistent with these observations, a dual site mechanism was proposed in their work to explain the effect of adding Fe to the catalytic system for PROX (Preferential Oxidation of CO in H_2) reaction. Pt acts as CO adsorption site, while Fe is responsible for O_2 dissociative-adsorption site. Herein, we invoke a similar reaction mechanism for EG oxidation over Pt-Fe catalyst.

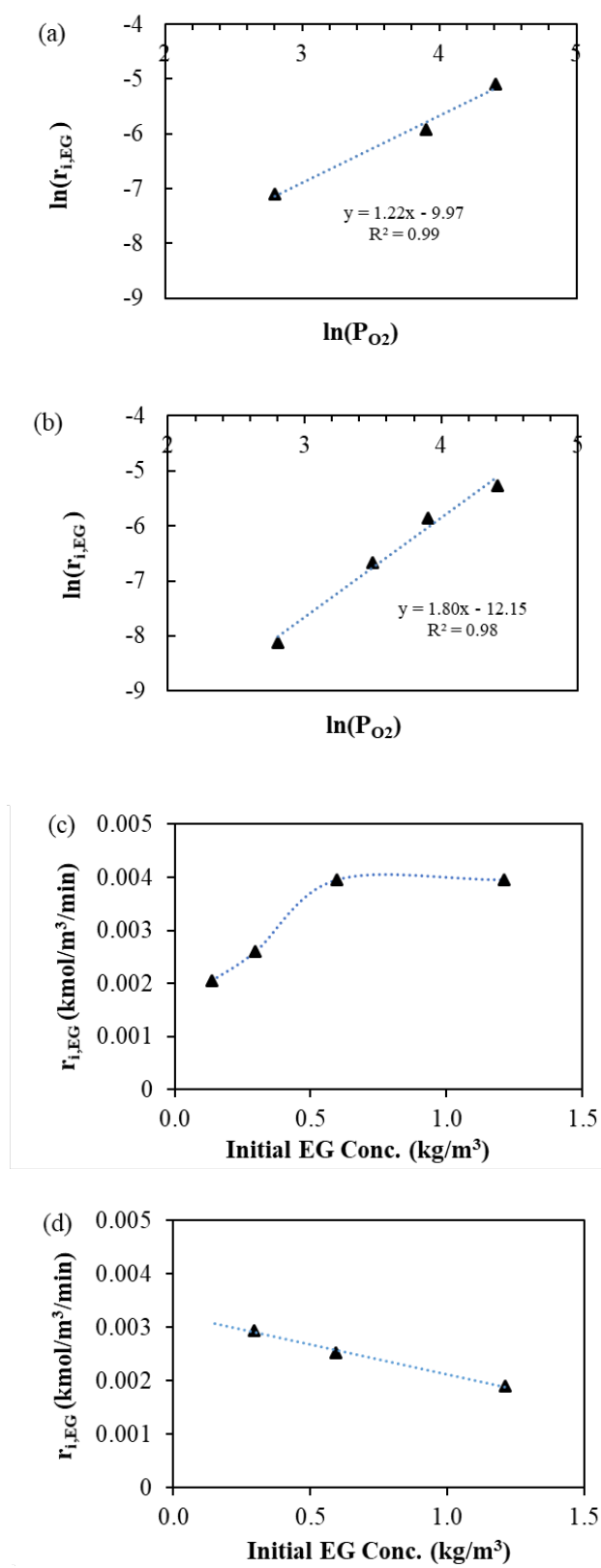


Figure 20. Oxygen pressure effect on EG oxidation with Pt-Fe catalyst (a) EG concentration-time profiles under neutral conditions; (b) O₂ pressure effect on initial reaction rate under neutral conditions; (c) EG concentration-time profiles under alkaline conditions; (d) O₂ pressure effect on initial reaction rate under alkaline conditions. Reaction conditions: initial EG conc. = 0.295 kmol/m³, 70 °C, P_{O₂}=30 bar, initial NaOH conc. = 1.458 kmol/m³ under alkaline conditions; no NaOH was added under neutral conditions, catalyst loading (Pt-Fe/CeO₂) = 2 kg/m³, initial reaction rate ($r_{i,EG}$) is calculated based on the data of EG conversion $\leq 15\%$

We also investigated the effect of base for both Pt and Pt-Fe catalysts while keeping other reaction parameters constant (**Figure 21**). Contrary to our expectation, the base (NaOH) not only acts as a promoter as previously claimed in the literature [154] but is actually an inhibitor at sufficiently high concentrations. This phenomenon was not previously reported for the oxidation of polyols or carbohydrates most likely because previous studies were typically conducted at fixed NaOH concentrations. The trend of reaction rate vs. base concentration was observed to be similar for the Pt and Pt-Fe catalysts. However, the promotion effect of base under optimum conditions is more significant when bimetallic catalyst is used, which implies a stronger synergistic effect between the bimetallic catalyst and the base.

Not only does the reaction rate change with the amount of base, the product selectivity is also significantly influenced. When no base is used, glycolaldehyde is the main product from EG oxidation over Pt catalyst (selectivity ~69.4 %, **Table 10**). At progressively higher base concentrations, the glycolaldehyde selectivity gradually decreases with more glycolic acid formation due to the increased oxidation rate. When the reaction rate is close to its maximum at optimum NaOH concentration, more carbon balance deficit (based on liquid phase product analysis) was observed which is attributed to CO₂/CO₃²⁻ formation as a result of C-C cleavage (SI, **Figure A - 8**). Further increase in the base amount results in less CO₂ formation, higher glycolic acid selectivity, and more formic acid as by-product. The formation of formic acid was not

observed under neutral conditions or lower base concentrations. This phenomenon can be explained by the reaction mechanism demonstrated in the SI (Scheme S3). When excess NaOH is used, -OH from the base occupies the active site that creates steric hindrance to deter CO₂ formation from C-C cleavage and decreases the oxidation rate due to its competitive adsorption with the -OH groups from the EG.

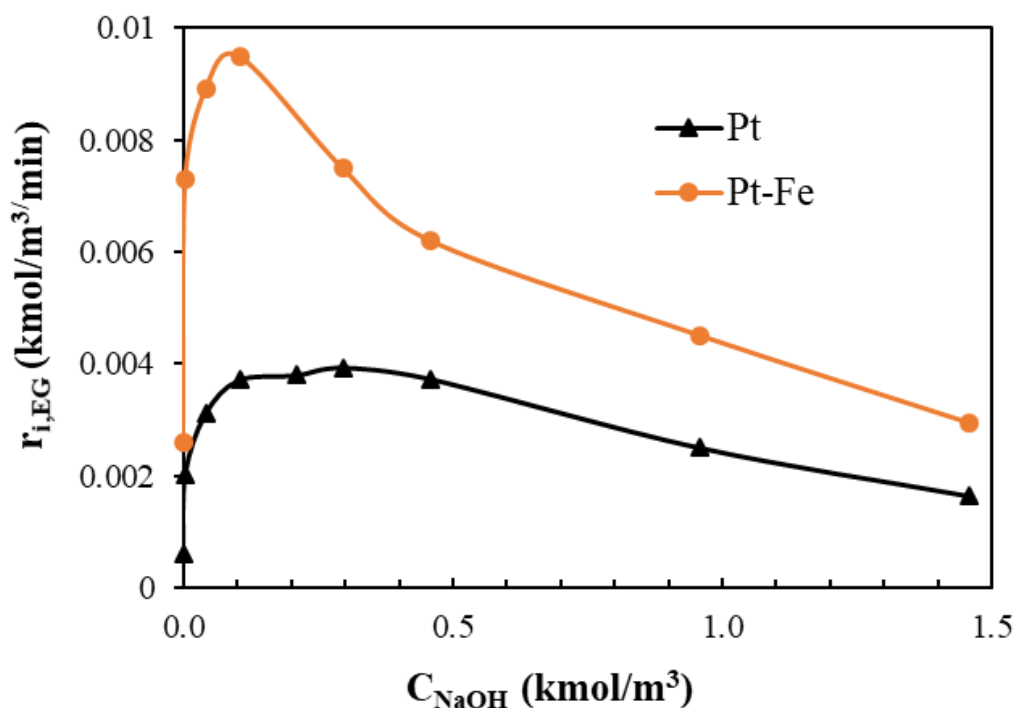


Figure 21. Base effect on Initial Reaction Rate for EG oxidation with Pt Catalyst. Reaction conditions: initial EG conc. = 0.295 kmol/m³, 70 °C, P_{O2} = 30 bar, catalyst loading (Pt/CeO₂) = 2 kg/m³, initial reaction rate ($r_{i,\text{EG}}$) is calculated based on the data of EG conversion $\leq 15\%$

Table 9. Base Effect on Product Selectivity for Pt Catalyst

C_{NaOH} (kmol/m ³)	Conversion%, EG	Selectivity%			CB
		Glycolaldehyde	Glycolic Acid	Formic Acid	
0.00	7.1	69.4	30.6	-	1.00
0.00	10.8	48.2	28.1	-	0.97
0.04	26.7	22.2	29.7	-	0.87
0.10	39.0	8.3	38.8	-	0.79
0.21	51.0	2.5	55.0	-	0.79
0.30	54.4	2.7	46.7	3.9	0.74
0.46	49.0	-	70.2	2.6	0.87
0.96	33.7	-	72.3	2.3	0.91
1.46	23.5	-	73.3	1.7	0.94

In addition to NaOH, some “mild” bases were also examined for potential promotional effect in EG oxidation. The concentration-time profiles of EG and the main by-products are shown in **Figure 22** for these experiments. Compared to the case of no base addition, NaHCO₃ or Na₂CO₃ also accelerate the oxidation reaction initially but only for a short duration. After approximately 20 minutes, the reaction rate slows down rapidly and nearly stops. Therefore, a poisoning effect is caused by the introduction of HCO₃⁻ and CO₃²⁻ ions in this reaction system. This explains the “deactivation period” in **Error! Reference source not found.** (4 to 12 hours) when no further oxidation can be observed. The poisoning effect of CO₃²⁻ species is attributed to the CO₂ produced from the C-C cleavage of EG that dissolves in the alkaline water solution. The product distribution patterns with NaHCO₃ and Na₂CO₃ are similar to that observed at neutral condition: glycolaldehyde and glycolic acid are the main products with no formic acid detected.

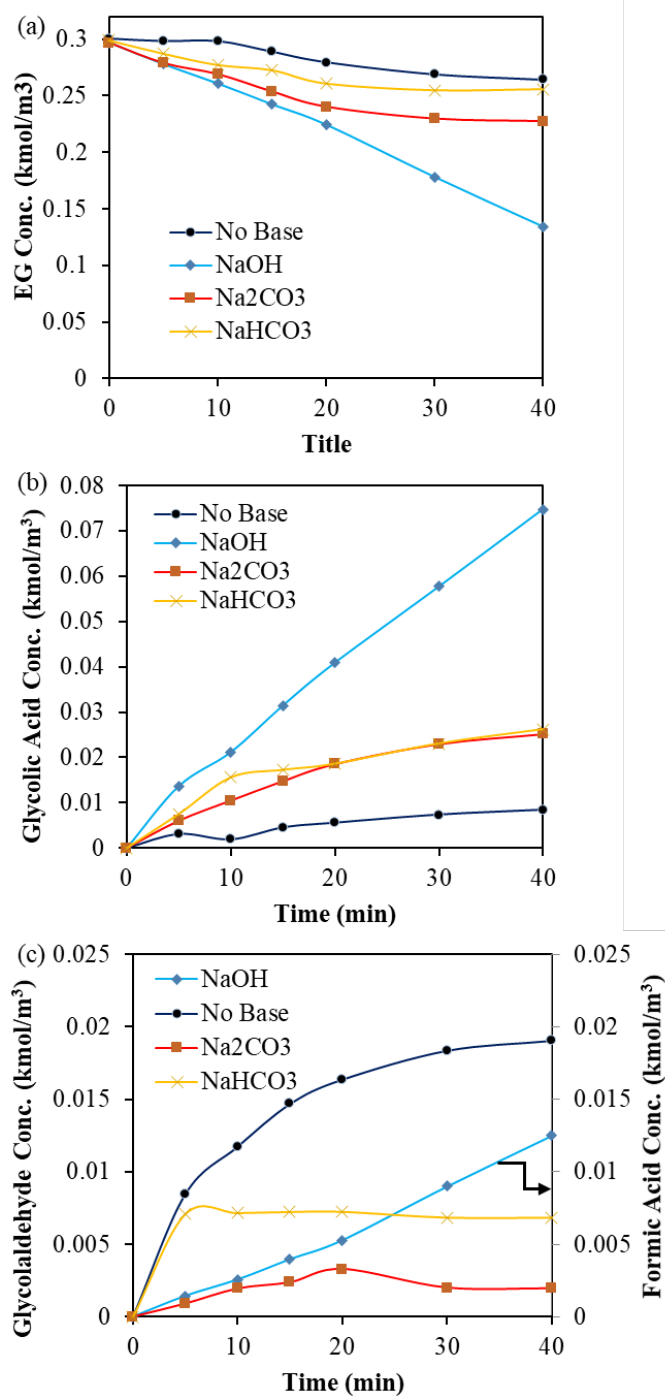


Figure 22. Concentration-time Profiles of EG oxidation using different base with Pt catalyst. Reaction conditions: initial EG conc.= 0.295 kmol/m³, base-to-EG molar ratio=1:1, 70 °C, P_{O2} = 30 bar, catalyst loading (Pt/CeO₂) = 2 kg/m³

3.4 Conclusion

From the screening of bimetallics, we found that the interpolation principle theory can not be used to explain the bimetallic effect for this reaction. Pt-Fe is the only successful example in showing an improved activity while other bimetallics such as Pd-Fe, Au-Fe, Ag-Fe showed comparable catalytic performance to the monometallics. The TOF on Pt-Fe catalyst (19.1 sec^{-1}) is approximately 17 times higher than that observed on Pt catalyst ($\text{TOF}=1.11 \text{ sec}^{-1}$) in the presence of a base promoter at 70°C and ambient pressure of O_2 . 100% conversion of EG and 62% glycolic selectivity was obtained at the end of reaction in 4 hours. Unlike Pt catalyst, the alloyed Pt-Fe structure enables efficient electron transfer from Fe to Pt that favors dissociative O_2 adsorption on the catalyst surface and its participation in the EG oxidation reaction. This conclusion is supported by the observed differences in the O_2 orders on the two catalysts. While the NaOH base promotes EG oxidation on both Pt and bimetallic Pt-Fe catalysts at lower concentrations, it inhibits the EG oxidation rates at sufficiently higher concentrations. Further, the amount of base also influences the product selectivity favoring glycolic acid at high NaOH concentrations. In the presence of excess amount of base, however, the O_2 and OH species also compete for active sites resulting in the observed rate inhibition and changes in product selectivity.

Chapter 4: Oxidation of Glucose using Mono and Bimetallic Catalysts in Base Free Conditions

4.1 Introduction

Carbohydrates have recently attracted significant interest as a renewable feedstock alternative to petroleum for making a wide range of industrial chemicals. Glucose is one such option that is produced in large quantities through photosynthesis. As mentioned in the literature survey on glucose oxidation (Chapter 1.4,1) , the direct formation of glucaric acid from glucose is very difficult, mainly due to the catalyst's low activity for the secondary oxidation. Two strategies have been used together to achieve higher yield of glucaric acid: (1) tuning the nanostructure of monometallic catalysts by adding a second metal; (2) use alkali as promoters or create basic sites on the catalyst surface to accelerate the oxidation rate.

In the previous work, the alloyed Pt-Cu catalyst shows a seven-fold higher oxidation rate compared to the Pt catalyst and leads to glucaric acid production in the final products.[86] In addition, structure-activity studies on Pt-Cu has been established that the alloyed Pt-Cu exhibits better activity over the core-shell structured Pt-Cu catalysts. By the kinetics studies, it was found that the activation energy barriers for secondary oxidation reaction was decreased for the bimetallic Pt-Cu catalyst. Unfortunately, the activation energies for the C-C cleavage reactions were also enhanced so that the overall yield for glucaric acid is only around 27% due to the formation of a large number of C₂-C₃ products. In addition to the Pt-Cu catalysts, other bimetallics such as the Pt-Pd [107] and Au-Bi [165] have also been reported to produce glucaric acid from direct oxidation of glucose in the aqueous phase.

However, the above-mentioned works were all conducted in the presence of base promoters (NaOH or KOH). This poses a technical difficulty and extra cost in separating the glucaric acid from its salt. In addition, Vlachos and colleagues recently investigated the influence of acidity and basicity of reaction medium on the product distribution of glucose oxidation using the Pt/C catalyst.[117] It was found that glucaric acid tends to decompose under alkaline conditions that the presence of NaOH facilitates the glucaric acid degradation on Pt metal although it can promote the overall oxidation rate. This explains the situation that most of the current bimetallic catalyst such as Pt-Pd and Pt-Cu catalysts showed higher activity but poor glucaric acid selectivity due to the formation of light carboxylic acids. [86, 107] Wojcieszak and co-workers recently reported a Cs-doped Au/CeO₂ catalyst that shows enhanced oxidation activity under base-free conditions due to the surface local basicity (Cs-OH surface species).[166] But the main product is glucuronic acid (~76% selectivity) that still requires another step of oxidation to form the glucaric acid. Currently, the suitable catalyst for the direct oxidation of glucose to glucaric acid under base-free conditions is still scarce.

In this Chapter, the effects of catalyst support, synthesis methods, reducing agents and mono/bimetallic catalysts on glucose oxidation activity and selectivity are investigated along with TEM and XRD characterization to gain insights into structure/activity relationships. The effects of experimental conditions such as O₂ pressure, glucose concentration and temperature are also optimized to achieve a higher yield of glucaric acid production from the glucose oxidation under base-free conditions.

4.2 Experimental and Methodology

4.2.1 Materials

All the powder supports were procured from commercial suppliers: TiO₂-a (ACROS Organics, 98+%, anatase), TiO₂-r (ACROS Organics, 98+%, rutile), SiO₂ (Sigma-aldrich, 12nm, 175-225 m²/g), Nb₂O₅ (Sigma-aldrich, 99.9%), Al₂O₃ (Sigma-aldrich, gamma phase), CeO₂ (Sigma-aldrich, 99%, <50 nm and <5 μm), NH₄-ZSM-5 zeolite (Alfa-aesar, ammonium type, SiO₂:Al₂O₃=23:1, 425 m²/g). The NH₄-ZSM-5 was calcined at 400 °C for 6 hours before catalyst preparation to obtain HZSM-5. D-glucose (Sigma-aldrich, >99.5%, GC grade), N, N-dimethylformamide (Alfa Aesar, DMF, HPLC grade, >99.9%). Pt(acac)₂ (Sigma-aldrich, 97%), H₂PtCl₆·6H₂O (Sigma-aldrich, ≥37.5% Pt basis), Cu(NO₃)₂·2.5H₂O (Sigma-aldrich)

4.2.2 Catalyst Preparation

A range of mono- and bimetallic catalysts were prepared using various synthesis methods as described below.

(1) Solvothermal Method: The monometallic Pt/TiO₂ (solvothermal) was prepared by a facile one-pot method as described in our previous publications.[84] A certain amount of metal precursor Pt(acac)₂ and TiO₂ powder (targeted Pt loading = 5 wt%) were mixed with 20 ml DMF first in a 45 mL autoclave. The mixture was purged with N₂ and heated up to 200 °C under 10 bar N₂ atmosphere. After 12 hours of vigorous stirring, the autoclave was cooled to room temperature. The catalyst was washed with ethanol/water (volume ratio = 2:1) solution several times before transferring to a vacuum oven to dry overnight at 60 °C. DMF acts as both the solvent and the reducing agent during the catalyst preparation.

(2) Impregnation Method: The precursor ($\text{H}_2\text{PtCl}_6 \cdot 6\text{H}_2\text{O}$) aqueous solution was added dropwise to the powder supports following a conventional incipient wetness impregnation method. The moisturized catalysts were dried at $90\text{ }^\circ\text{C}$ and calcined at $500\text{ }^\circ\text{C}$ for a certain amount of time.

(3) Wet Chemistry Method (WC-1): TiO_2 or another type of support was added to an aqueous solution of Pt precursor ($\text{H}_2\text{PtCl}_6 \cdot 6\text{H}_2\text{O}$) and stirred for an hour. An aqueous solution of the reducing agent Me_2AB (dimethyl ammonium-borane, 0.16 g in 100 ml H_2O) was dropwise added to the precursor slurry at a rate of one drop per second at room temperature and stirred vigorously overnight. The catalyst powder was centrifuged, dried at $90\text{ }^\circ\text{C}$ and calcined at $500\text{ }^\circ\text{C}$ for a certain amount of time to remove the organic materials on the metal surface.

(4) Wet Chemistry Method (WC-2): Similar to the WC-1 method, the metal precursors ($\text{H}_2\text{PtCl}_6 \cdot 6\text{H}_2\text{O}$ and $\text{Cu}(\text{NO}_3)_2 \cdot 2.5\text{H}_2\text{O}$) were mixed with TiO_2 in water and stirred for an hour. Then, an aqueous solution of the reducing agent (0.026 mol/L, 100 mL)- Me_2AB (dimethyl ammonia-borane), AB (ammonia borane) or NaBH_4 (sodium borohydride) was added dropwise to the aqueous mixture at room temperature and stirred overnight. The centrifuged catalyst powders were washed with ethanol/water (2:1 in volume) solution, dried at $60\text{ }^\circ\text{C}$ overnight before use.

4.2.3 Catalyst Characterization

The actual bulk metal composition was determined by inductively coupled plasma (ICP-OES, Horiba J-Y 2000). Transmission electron microscopy (TEM) was performed using the FEI Tecnai F20 XT instrument according to the following procedure: the TEM samples were prepared by suspending the catalyst powder in anhydrous ethanol and agitated with ultrasonic. Then, 10 μL of ethanol suspension was placed onto a nickel grid with the lacey carbon film (from Ted Pella Inc.) and air dried for TEM examination. The particle size distribution statistics was established

on the basis of measuring 160 nanoparticles using the software-Image J. Energy-dispersive X-ray spectroscopy (EDX) was used to obtain elemental mapping for the bimetallic Pt-Cu nanocrystals.

X-ray powder diffraction analysis was carried out on a Bruker D8 powder diffractometer with a copper target (Cu $K\alpha$ radiation) operating at 40 kV and a current of 40mA to analyze the crystal structure. The diffraction angle 2θ was scanned between 5° and 105° , at a rate of $0.01^\circ/\text{min}$.

The surface chemical state was determined by X-ray photoelectron spectroscopy (XPS) using the PHI 5000 Versa Probe II with monochromatic Al $K\alpha$ radiation. The binding energies were calibrated with respect to the signal for C 1s (binding energy of 284.5 eV). The data analysis was done using the software – CasaXPS.

4.2.4 Activity Test

Catalytic performance tests were conducted in a multiple slurry reactor system with magnetic stirring and continuous temperature/pressure control (Parr, 5000 Multiple Reactor System, **Figure A - 10**). The safety check for the experimental conditions was performed, as shown in the Appendix. The reactor system consists of a parallel array of six 45 mL autoclave reactors that are equipped with independent temperature and pressure controllers. In a typical oxidation experiment, an aqueous glucose solution (2.5 mol/L, 20 ml) was charged in the autoclave with a measured amount of catalyst (0.4 g). No alkali was added to meet the requirement of the initial neutral condition. After a fixed-time batch run, the reactor was cooled to room temperature and depressurized. The product-catalyst slurry was centrifuged to collect the clear liquid products. The liquid samples were analyzed by a high-performance liquid chromatography (HPLC) (Shimadzu Model LC-10A) equipped with 0.005 N aqueous H_2SO_4 as mobile phase at a flow rate of 0.5 ml/min and dual detectors of the refractive index detector (RID) and the UV/visible detector. The

molecular structures of glucose and the main oxidation products are illustrated in the Appendix as **Figure A - 9**. An example of the HPLC results is also shown as **Figure A - 13**. The conversion of glucose and selectivity of products were calculated using the following formulas:

where, $C_{i,g}$, $C_{f,g}$, $C_{c,g}$ represent the number of carbons in the initial glucose, final glucose and converted glucose respectively, in the unit of mol; $C_{f,p}$ represents the carbon numbers in the final product, in the unit of mol; $N_{c,g}$ is the mole of converted glucose and $N_{surface\ metal}$ is the mole of Pt exposed on the catalyst surface.

$$\begin{aligned}
 Conversion &= \frac{C_{i,g} - C_{f,g}}{C_{i,g}} \\
 Selectivity &= \frac{C_{f,p}}{C_{c,g}} \\
 N_{surface\ metal} &= \frac{catalyst\ weight \cdot bulk\ metal\ content(\%)}{metal\ molecular\ mass} \cdot metal\ dispersion\ (\%) \\
 Carbon\ balance &= \frac{\sum C_{f,p} + C_{f,g}}{C_{i,g}} \\
 Initial\ TOF &= \frac{N_{c,g}}{N_{surface\ metal} \cdot Time}
 \end{aligned}$$

The carbon balances are based only on liquid phase products. In cases where the carbon balances are significantly lower, the deficit is due to CO₂ formation, which was qualitatively confirmed by sampling the gas phase at the end of a run but not quantitatively accounted for.

4.3 Results and Discussions

4.3.1 Screening of Mono Pt Catalysts

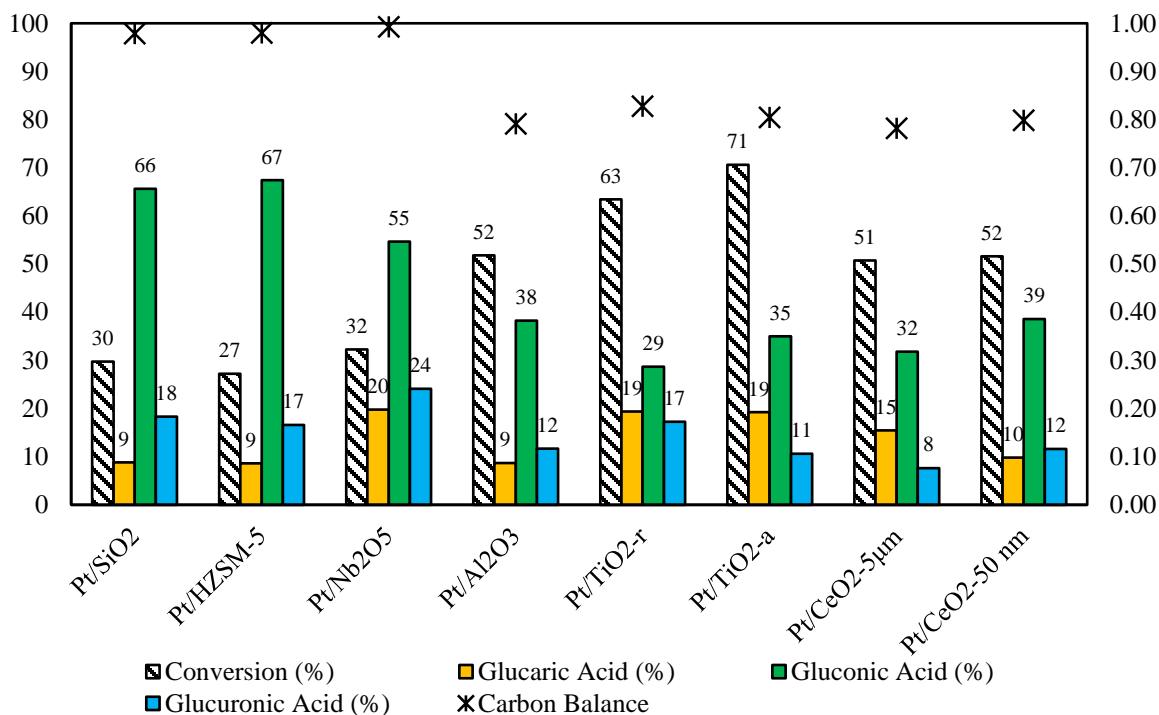


Figure 23. Conversion of glucose (%) and selectivity of products (%). Reaction conditions: time=12 h, 15 bar O₂, initial pH=7, 80 °C, initial glucose concentration = 0.278 mol/L.

A screening of several supported monometallic Pt catalysts was performed as a first step mainly to understand the support effect. The Pt catalysts deposited on various oxide supports were prepared by a wet chemistry method (WC-1) as described in the experimental section. The physical properties including surface area, particle size and Pt metal contents of these catalysts are presented in the Table 11. The Pt content of all the catalysts is nearly the same (~5 wt%). The glucose oxidation results are as shown in **Figure 23**, indicating significant difference in the performance of the various Pt/support catalysts, whose textural characteristics are summarized in the Table 11.

The glucose conversion as well as product distribution of Pt/CeO₂-5 μ m and Pt/CeO₂-50 nm catalysts were very similar. Therefore, the support particle size does not appear to influence either glucose conversion or glucaric acid selectivity. The glucaric acid selectivity with Nb₂O₅ (20%), TiO₂-r (19%) and TiO₂-a (19%) supported Pt catalysts are the highest among the studied support materials, even though they are non-porous materials (Table 11)

In contrast, the high surface area supports, SiO₂ and ZSM-5, do not lead to higher glucose conversion or glucaric acid selectivity. Therefore, the significant performance variation when using different supports may be explained as a result of metal-support interaction effect. Considering the higher glucose conversion with Pt/TiO₂-a (71%) catalyst compared with Pt/Nb₂O₅ (32%) and Pt/TiO₂-r (63%), the anatase structured TiO₂ was selected as the support to perform the next-step of catalyst optimization.

It is known that H₂/CO/O₂ chemisorption behavior is significantly altered when a metal is supported on TiO₂ compared to non-transitional metal oxides, such as SiO₂, Al₂O₃, and MgO as supports.[167, 168] It is also reported that the Pt/TiO₂ exhibits improved catalytic activity towards oxygen reduction reaction (ORR), hydrogen oxidation, and water gas shift reaction (WGS) due to the interaction between Pt and TiO₂. [169, 170] It has been found experimentally that the binding energy (BE) of Pt 4f electrons down-shifts significantly for TiO₂ supported Pt catalyst.[170] This suggests that an increased electron density on Pt can facilitate lattice strain and charge transfer towards better catalytic activity.

Table 10. Physical properties of the monometallic Pt catalysts

Catalyst ^a	Pt (wt%) ^b	Surface Area (m ² /g) ^c	Particle Size ^c
Pt/SiO ₂	5.49	175-225	12 nm
Pt/HZSM-5	4.37	425	-
Pt/Nb ₂ O ₅	5.18	-	44 μ m
Pt/Al ₂ O ₃	5.30	>40	<50 nm
Pt/TiO ₂ -r	4.84	50	<100 nm
Pt/TiO ₂ -a	5.65	45-55	<25 nm
Pt/CeO ₂ -5 μ m	4.93	-	<5 μ m
Pt/CeO ₂ -50 nm	5.18	30	<50 nm

^aAll the catalysts are synthesized by the WC-1 method.

^bThe Pt composition is determined by ICP-OES.

^cThe surface area and particle size of metal oxide supports.

4.3.1 Effect of Synthesis Methods for Mono and Bimetallic Catalysts

Table 11. Synthesis method and bimetallic effects on glucose oxidation^a

No.	Base/ Neutral	Catalyst Synthesis Method ^b	Pt (wt%) ^c	Cu (wt%) ^c	Conversion (%)	Selectivity (%)			C ₂ -C ₃ Products ^d	Carbon Balance
						Glucaric	Gluconic	Guluronic		
						Acid	Acid	Acid		
1	Neutral	Solvothermal	4.23	-	19	12	74	17	5	1.01
2	Neutral	Impregnation	3.77	-	22	7	82	9	0	0.99
3	Neutral	WC-1	5.59	-	71	19	35	11	7	0.80
4	Neutral	WC-1	5.76	1.40	73	35	22	20	9	0.91
5	Neutral	WC-2 (NaBH ₄)	5.08	3.30	85	44	25	22	3	0.94
6	Base	WC-2, (NaBH ₄)	5.08	3.30	100	12	29	6	- ^e	- ^e

^aReaction conditions: time = 12 h, 15 bar O₂, 80 °C, initial glucose concentration = 0.278 mol/L. #1-5 tests were performed at initial neutral condition, #6 was performed with NaOH (0.556 mol/L)

^bAll the catalysts are supported on the TiO₂-a.

^cPt and Cu metal contents are determined by the ICP-OES.

^dThe C₂-C₃ products include oxalic acid, tartronic acid, glyoxal, glyceric acid, glycolic acid and acetic acid.

^eThe side products of test #6 cannot be determined entirely. Hence the C₂-C₃ product selectivity and carbon balance data are not shown.

Three different synthesis methods were examined to prepare the monometallic Pt catalysts. The test results are shown as entries 1~3 in **Table 12**. The monometallic Pt catalysts prepared by solvothermal and impregnation methods showed similar glucose conversion (~20%), with

gluconic acid as the primary product (selectivity >70%). The mono-Pt catalyst prepared by the wet chemistry method (WC-1) showed significantly higher glucose conversion (71%) with a glucaric acid selectivity of 19%. Considerable amount of CO₂ was observed as a byproduct leading to drop in liquid phase carbon balance. CO₂ formation was confirmed qualitatively by bubbling the gas phase in the reactor after the reaction through aqueous NaOH solution, followed by CaCl₂ treatment. The white precipitate formation (CaCO₃) confirms the existence of CO₂ in the product gas (Appendix, **Figure A - 12**).

The TEM images of Pt catalysts prepared by different methods are shown in the

Figure 25. The Pt nanocrystals prepared by the solvothermal and impregnation methods both exhibit polyhedral shapes surrounded by several flat facets. The Pt nanocrystals prepared by the wet chemistry method (WC-1) demonstrates a ‘near spherical’ shape with no exposure of clear flat planes. The Ostwald ripening phenomenon was observed showing that small round particles were merged and finally grown into larger particles. This near-spherical shape is formed due to the non-anisotropy during nanocrystal growth in a capping agent free environment.[171]

The average particle size of these three nanocrystals are $\sim 18.8 \pm 8.6$ nm (solvothermal), $\sim 15 \pm 6.8$ nm (impregnation) and $\sim 11.6 \pm 4.8$ nm (wet chemistry) respectively. The activity of the three catalysts shows size dependency to a certain extent. However, the significantly higher glucose conversion with Pt catalyst by WC-1 method shows that the catalytic oxidation of glucose is a shape/morphology-controlled process. Generally, the exterior surface of a sphere can be interpreted as consisting of numerous (100) and (111) facets combined with considerable corner and edge sites.[172] Therefore, the Pt catalyst by WC-1 method has more corner/edge sites but less flat surface sites, comparable to the polyhedral shaped Pt catalysts prepared by the impregnation or solvothermal method. Experimental/theoretical studies on comparing the activity

of catalysts with different types of sites (flat surface site, kink site, step site and corner site) could be meaningful to provide further insights for the reaction mechanism in the future.

Test #4 in **Table 12** shows the catalytic performance of bimetallic Pt-Cu catalyst prepared by the WC-1 method. Comparing these results with the mono-Pt catalyst (#3), it is observed that while the bimetallic catalyst did not promote the glucose conversion significantly (71% to 73%), it improves the glucaric acid selectivity from 19% to 35% and the glucuronic acid selectivity from 11% to 20%, implying an acceleration of the secondary oxidation rate (gluconic to glucaric acid). Another interesting observation with bimetallic catalyst was suppression of CO₂ formation. Such an effect of Pt-Cu has been reported in a previous publication on glucose oxidation under alkaline condition.[86] Here, the bimetallic effect was observed to still exist for the base-free conditions. Alloying of Cu and Pt (as illustrated in the characterization section) can change the electronic density of Pt influencing adsorption of glucose and its derivatives. In addition, the second metal's spatial effects may also control C-C cleavage to reduce CO₂ formation.

Furthermore, by modifying the WC-1 method to the WC-2 as described in the experimental section, the glucaric acid selectivity was enhanced from 35% to 44%, while the glucose conversion increases from 73% to 85% under neutral conditions. Testing the same catalyst under alkaline conditions, the glucose was consumed completely (conversion=100%, test #6 in **Table 12**). However, several side products are formed in addition to the three carboxylic acids with a decrease in the glucaric acid selectivity to 12% indicating significant C-C cleavage under basic condition. It was reported that tartronic acid and oxalic acid selectivity was as high as 30% and 15% respectively under alkaline conditions using the bimetallic Pt-Cu or Pt-Pd catalysts.[86, 107] However, the selectivity of C₂-C₃ products decreased to less than 10% for the Pt or PtCu catalysts studied in this work under neutral conditions. In this situation, the alkali promoter

accelerates not only the glucose oxidation, but also increases the rate of C-C cleavage reactions to form small molecules and over-oxidation to form CO₂.

It's noteworthy that we were unable to prepare stable 5% Pt or 5% Pt-Pd supported on TiO₂ by the wet chemistry method (WC-2) using NaBH₄. The metal particles were washed off from the support during the washing-centrifugation procedure (Appendix, **Figure A - 11**). A plausible mechanism to explain this observation could be as follows. It has been reported that the bimetallic particle size is highly dependent on the second alloying metal.[173] Pt-Cu alloying is known to result in a decrease in the size of Pt nanocrystals (Pt~4.7 nm to PtCu~3.2 nm;[173] Pt~15 nm to PtCu~3.3 nm[174]). On the contrary, Pt-Pd alloy nanoparticle usually has either the same [175] or even a larger size [107, 176] compared to the monometallic Pt particle. The smaller particle size of Pt-Cu results in a larger surface area; thus, the Pt-Cu nanoparticle can attract more ions/cations in the solution to carry more electrical charge. In this situation, the Coulombic force could be enhanced to facilitate the stable attachment of nanoparticle on TiO₂. Also, smaller particles usually have higher surface energy which will also help in their immobilization on TiO₂ to reach a thermodynamically stable state.

4.3.2 Bimetallic Catalysts

Table 12. Effect of the Pt:Cu atomic ratio in precursor on glucose oxidation^a

No.	Precursor Pt:Cu Atomic Ratio ^b	Pt (wt%) ^c	Cu (wt%) ^c	Conversion (%)	Selectivity (%)				Carbon Balance
					Glucaric	Gluconic	Glucuronic	C ₂ -C ₃	
					Acid	Acid	Acid	Products ^d	
1	1:3	5.08	3.30	85	44	25	22	3	0.94
2	1:2	4.30	3.06	84	47	21	20	7	0.96
3	1:1	5.17	2.08	81	48	20	14	8	0.95

^aReaction conditions: time=12 h, 15 bar O₂, initial pH = 7, 80 °C, initial glucose concentration = 0.278 mol/L.

^bAll the catalysts are synthesized by the WC-2 method using NaBH₄ as reducing agent.

^cPt and Cu metal contents are determined by the ICP-OES.

^dThe C₂-C₃ products include oxalic acid, tartronic acid, glyoxal, glyceric acid, glycolic acid and acetic acid.

To explore the possibility of further improving the glucaric acid yield, we altered the catalyst preparation by tuning the Pt to Cu metal ratio and changing the reducing agent. The experimental results of changing the composition of Pt:Cu precursors (from 1:1 to 1:3) are shown in **Table 13**. It can be seen that the Cu content in the bimetallic catalysts increases to a limited extent (from 2.1% to 3.3%), rather than the expected 3-fold increase. This result indicates that the additional Cu species are not likely to be alloyed with Pt and removed from the catalyst surface during the catalyst washing procedure. Comparing their catalytic performances in the oxidation reaction, it is found that the catalyst with higher Cu content shows slightly higher glucose conversion but the lowest glucaric acid selectivity. However, the reaction results of three catalysts in **Table 13** are similar. Hence, the effect of reducing agent was studied using the formulation in which the molar Pt/Cu ratio in the synthesis mixture is 1.

Table 13. Reducing agent effect on glucose oxidation^a

No.	Reducing Agent ^b	Pt ^c (wt%)	Cu ^c (wt%)	Conversion (%)	Selectivity (%)				Carbon Balance
					Glucaric	Gluconic	Glucuronic	C ₂ -C ₃	
					Acid	Acid	Acid	Products ^d	
1	Me ₂ AB	5.17	2.08	85	45	14	14	5	0.81
2	AB	5.74	2.08	85	43	15	14	5	0.80
3	NaBH ₄	4.13	1.70	92	60	20	12	7	0.99

^aReaction conditions: time=12 h, 15 bar O₂, initial pH=7, 90 °C, initial glucose concentration = 0.278 mol/L.

^bAll the catalysts are synthesized by the WC-2 method.

^cPt and Cu metal compositions are determined by the ICP-OES.

^dThe C₂-C₃ products include oxalic acid, tartronic acid, glyoxal, glyceric acid, glycolic acid and acetic acid.

NaBH₄ is generally considered to be a strong reducing agent that facilitates a fast reduction of the metal precursors. To moderate the reduction rate, two other weak reductants were used and compared with NaBH₄. As can be seen from the reaction results in the **Table 14**, the catalyst prepared by using NaBH₄ shows the highest glucose conversion (92%) and glucaric acid selectivity (60%). The pH value drops from seven to around two after reaction. Moreover, the catalysts prepared by using weak reducing agents (Me₂AB and AB) demonstrate significant CO₂ formation leading to drop in liquid phase carbon balance closure to around 0.8. The difference in using Me₂AB and AB are almost negligible.

Figure 26 shows the TEM results of Pt-Cu/TiO₂ prepared by WC-2 method using AB and Me₂AB as reductants respectively. Using AB as reducing agent, a nano-rod structure of around 2.9

nm width and 9.3 nm length has been synthesized. The two ends of the nano-rod are semi-spherical shaped. The coalescence of Pt-Cu crystallites leads to this nano-rod structure. Some nano-rods coalesce further to form branched structures or large nanoclusters. The Pt-Cu catalyst reduced by Me₂AB demonstrates spherical nanostructure (nano-ball) with a diameter of 8.4±2.7 nm. Its particle aggregation degree is the lowest of all three catalysts showing that most of the nano-balls are dispersed uniformly on the surface of TiO₂. It can be seen that changing reducing agent not only tunes the particle size, but also controls the morphology. But overall, the wet chemistry method (reduction process) produces nanocrystals with no flat outer facets.

As a result of optimization, the Pt-Cu/TiO₂-a catalyst synthesized by the wet chemistry method (WC-2) using NaBH₄ as a reducing agent is selected as the best catalyst to study the effect of reaction conditions. Characterization of this catalyst using XRD and HR-TEM are shown in the following section.

4.3.3 Characterization of Bimetallic Pt-Cu Catalyst.

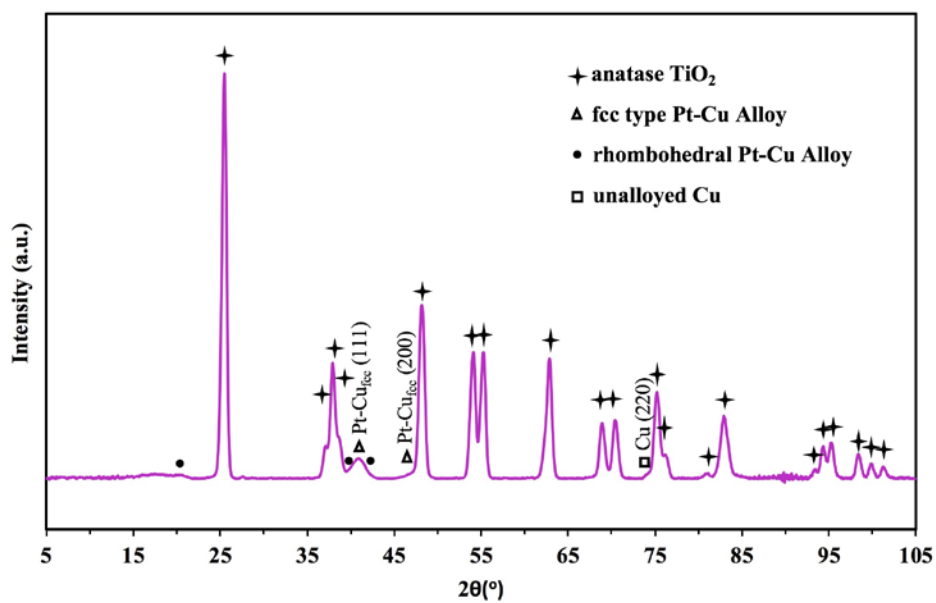


Figure 24. XRD pattern of 5% Pt-Cu (1:1)/ TiO_2 -a (WC-2, NaBH_4)

Table 14. Theoretical XRD calculations for Pt-Cu alloy structure

Crystal structure: fcc type of Pt-Cu alloy				
Calculated lattice constant - $a = 0.380048$ nm (Pt-Cu molar ratio = 6:4)				
$\lambda = 0.154$ nm				
h	k	l	d spacing	2θ
1	0	0	0.380	23.4
1	1	0	0.269	33.3
1	1	1	0.219	41.1
2	0	0	0.190	47.8
2	2	0	0.134	70.0
3	1	1	0.115	84.5
2	2	2	0.110	89.2
4	0	0	0.095	108.3

To gain insights on the phase information of the PtCu bimetallic nanoparticles, XRD was performed on 5% Pt-Cu/TiO₂-a (WC-2, NaBH₄). Due to the low metal loading, most of the reflections presented in the XRD pattern are anatase TiO₂ diffraction peaks (JCPDS No. 21-1272, symbolized by the ‘star’ signal in **Figure 24**). In comparison with the standard XRD patterns of platinum and copper species, no diffraction peaks regarding PtO₂, CuO and Cu₂O were observed. The XRD diffraction peaks at 41° and 47° corresponded to the (111) and (200) lattice planes of a disordered fcc Pt-Cu alloy crystal structure with a space group of Fm3m.[177-179] Note that the diffraction peak at 41° is very broad, likely reflecting the inclusion of multiple small peaks. The

plausible peaks at 38.5° , 42.1° , and the small bump at 20.7° may indicate the presence of a small amount of rhombohedral Pt-Cu alloy crystallite (with the space group of $R\bar{3}m$).^[177] The XRD reflections of the fcc Pt-Cu phase located in between the corresponding diffraction peaks of pure fcc Pt (JCPDS No. 04-0802) and Cu (JCPDS No. 04-0836) crystal planes, demonstrated the alloy formation by placing Cu atoms into the Pt lattice. By theoretical calculations as shown in the **Table 15**, the lattice constant of Pt-Cu alloy is estimated around 0.38 nm, which falls in between the lattice constants for pure Pt (0.3923 nm) and Cu (0.3615 nm), consistent with Vegard's law on the linear dependence of an alloy's lattice parameter. The peak at 74° signifies the existence of pure fcc copper phase that was not fully alloyed with Pt.

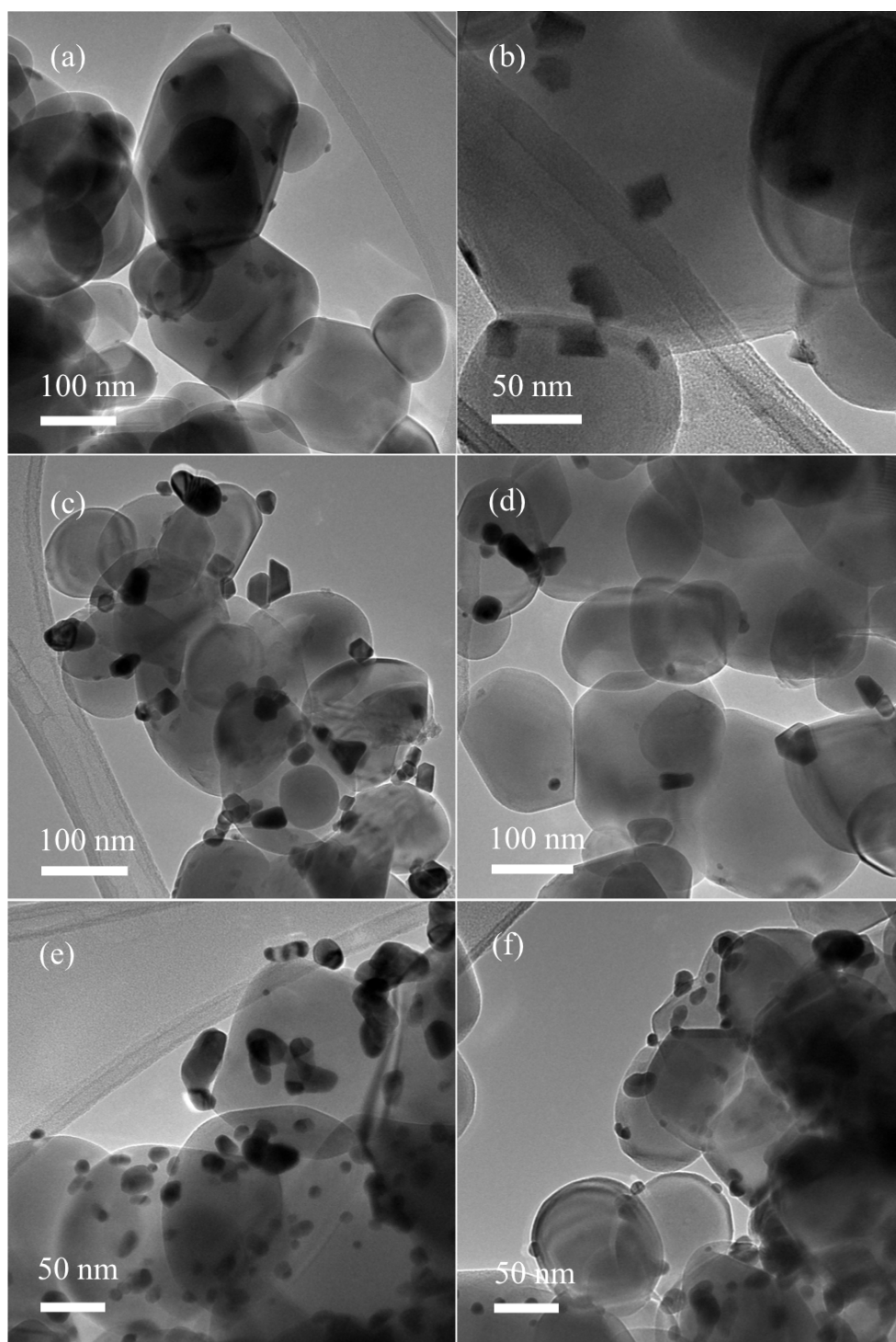


Figure 25. TEM images of Pt-Cu/TiO₂ catalysts by different synthesis methods: (a, b) impregnation; (c, d) solvothermal; (e, f) wet chemistry method (WC-1)

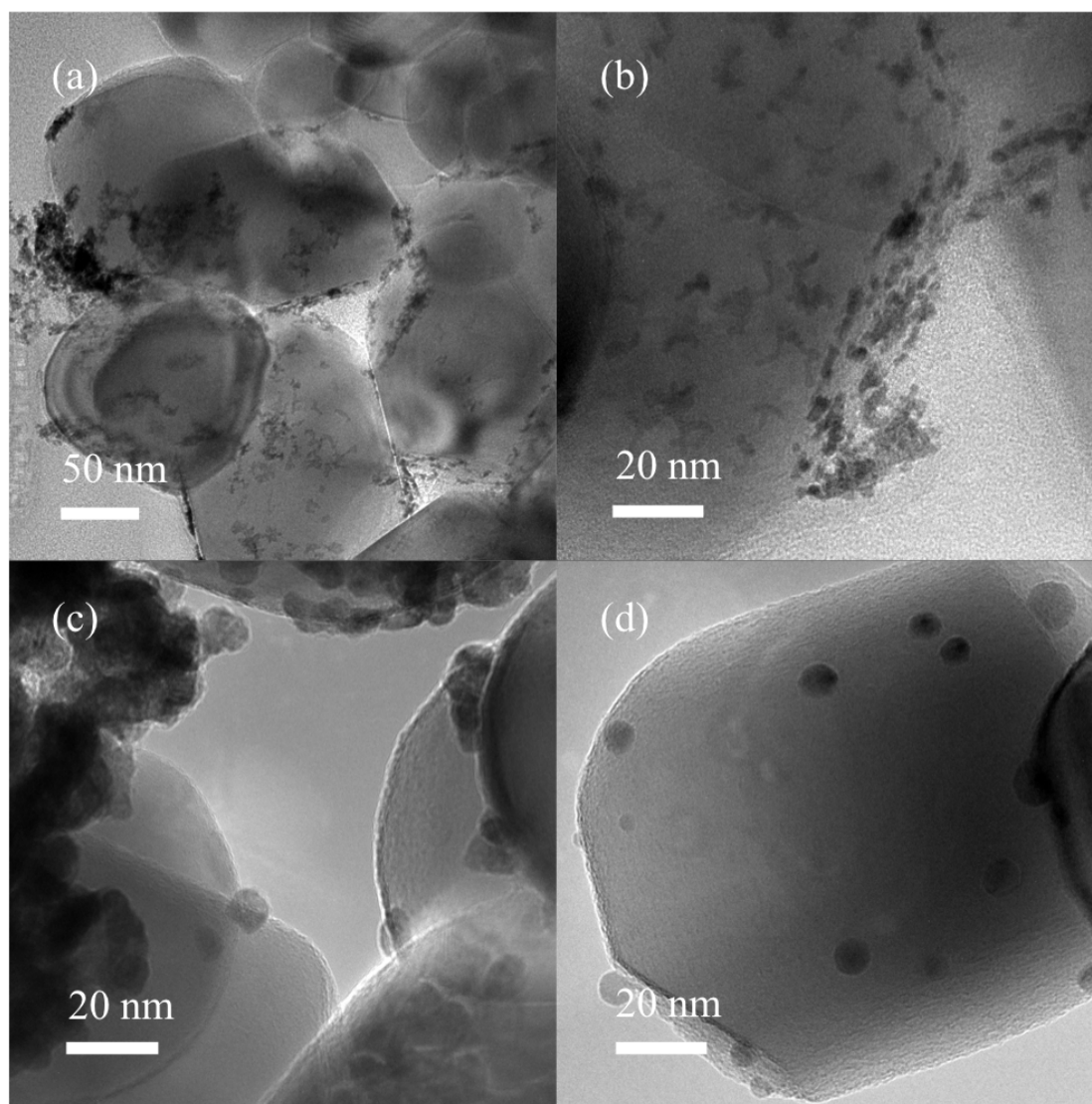


Figure 26. TEM images of Pt-Cu/TiO₂ catalysts by wet chemistry method (WC-2) using different reducing agents: (a, b) AB; (c, d) Me₂AB

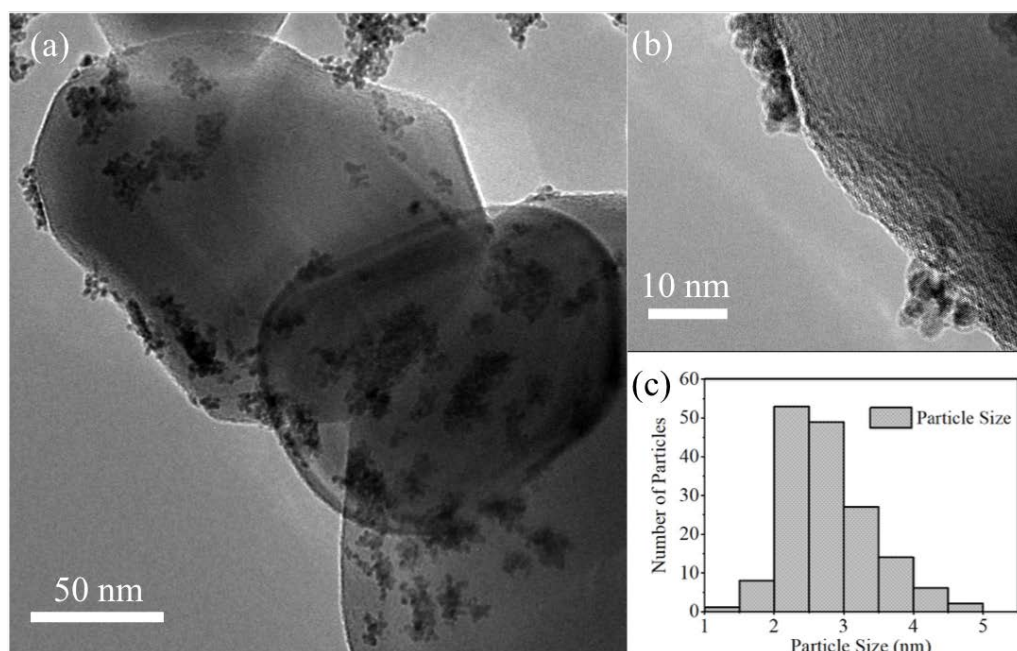


Figure 27. TEM image and particle size distribution of 5% Pt-Cu /TiO₂-a (WC-2, NaBH₄)

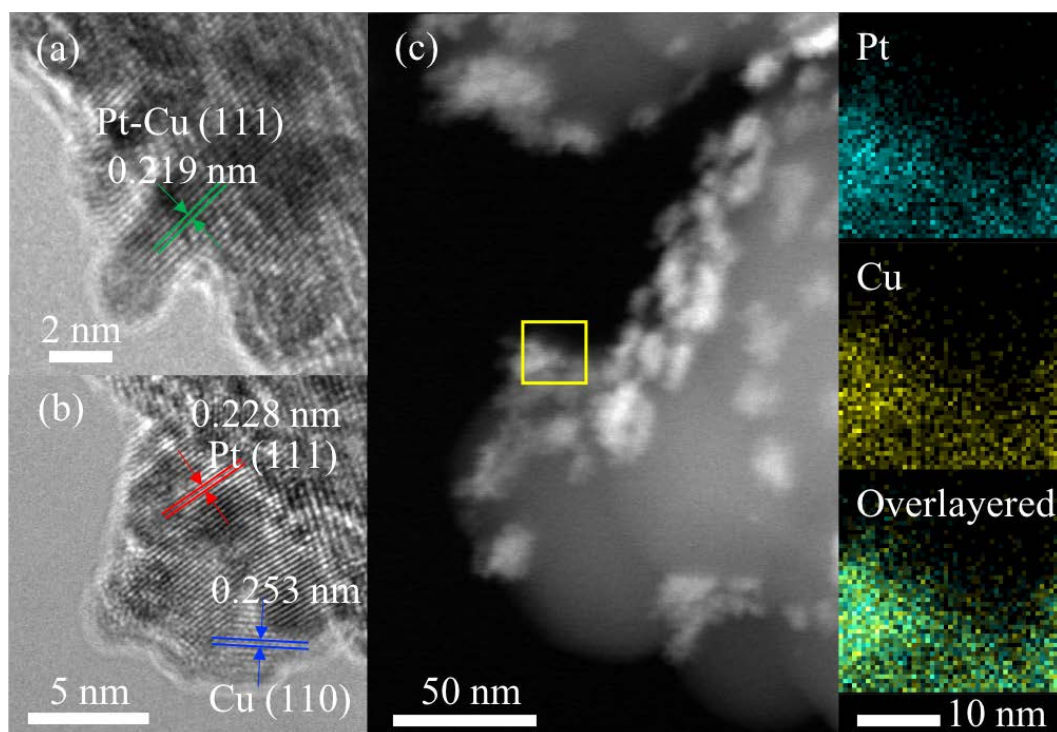


Figure 28. HRTEM and EDX images of 5% Pt-Cu/TiO₂-a (WC-2, NaBH₄)

Figure 27 shows the typical TEM images of the PtCu/TiO₂-a catalyst with different magnifications. The TiO₂ surface is covered by nanoclusters consisting of a number of small Pt-Cu nanocrystals. The size distribution of these small nanocrystals shows a narrow range of particle size around 2.8 ± 0.6 nm on average. As shown in the higher resolution picture - **Figure 28** (b), the nanocrystals are spherical-like particles without a clear/sharp boundary. Within each nanocluster, the lattice planes are randomly orientated between domains as observed in HRTEM image in **Figure 28** (b). The nanocluster formation can be described as a result of nucleation burst due to the fast reduction by NaBH₄ and the absence of stabilizing surfactant. This follows crystal growth until reaching a final particle size and coalescence to form the nanoclusters. The Ostwald ripening mechanism is not observed here because the small nanocrystals still maintain homogeneous shape/size, and they are not merged into noticeable larger crystals in each nanocluster. The small dimension of these nanocrystals is beneficial to expose a high metal surface area, to provide enough reactive sites for the oxidation reaction. However, this advantage was attenuated by their agglomeration into the nanoclusters to some extent.

The Pt and Cu elements are uniformly distributed throughout the nanocrystal, as observed from the EDX elemental mapping results in **Figure 28** (c). **Figure 28** (a) presents the HRTEM of the Pt-Cu alloy particle that owns a lattice spacing of 0.219 nm, matching closely to the calculated lattice spacing of fcc Pt-Cu (111) plane based on the XRD results. The alloy structure of Pt-Cu is confirmed in this situation. Meanwhile, we also observed monometallic Pt and Cu nanocrystals that are not alloyed during nanocrystal growth, as illustrated in **Figure 28** (b). The lattice spacing 0.228 nm and 0.253 nm are corresponding to the fcc Pt (111) and fcc Cu (110) planes respectively. This observation explains the appearance of the Cu peak in the XRD pattern.

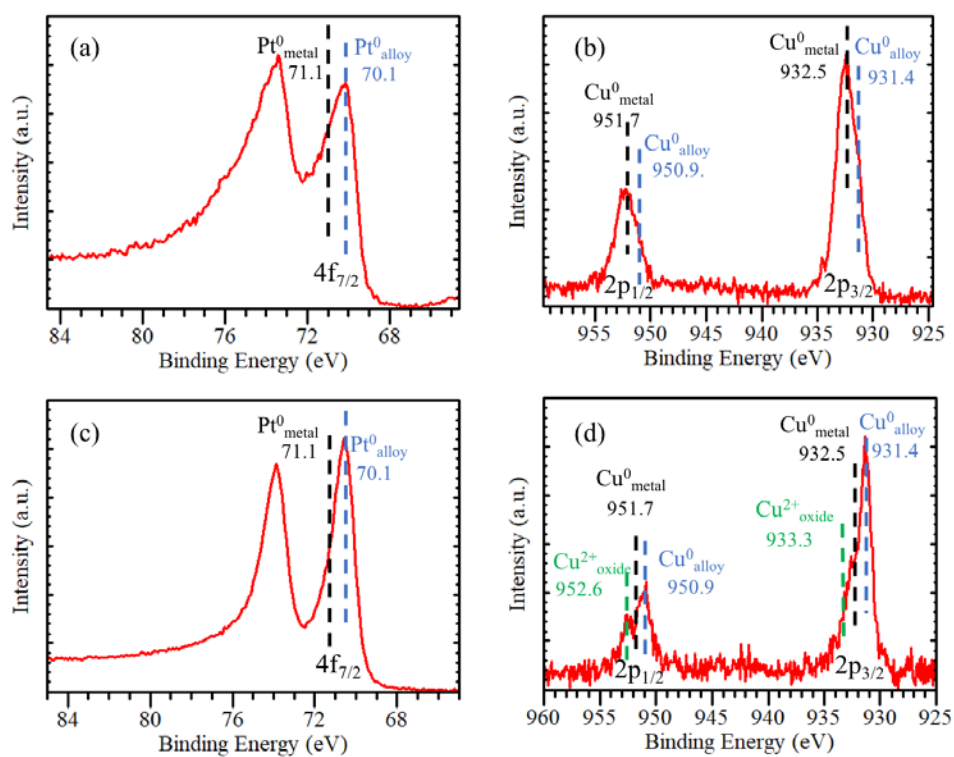


Figure 29. Pt 4f and Cu 2p XPS spectra of new (a-b) and used (c-d) Pt-Cu/TiO₂ catalyst

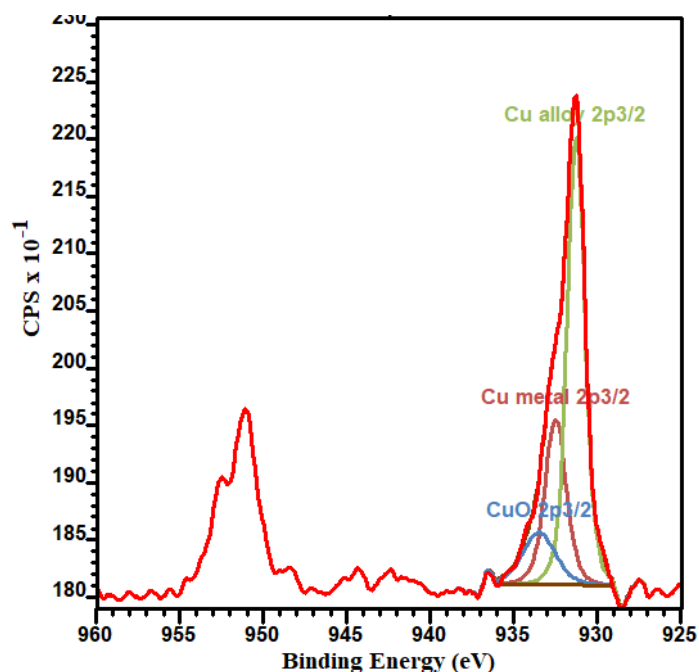


Figure 30. Cu 2p XPS curve fitting results of Pt-Cu/TiO₂ catalyst after reaction

Table 15. Quantification results of Cu 2p XPS curve fitting using CasaXPS

Name	BE Position (eV)	Peak Fitting Area	% Atom Conc.
Cu ⁰ metal 2p _{3/2}	932.50	246.101	26.73
Cu ⁰ alloy 2p _{3/2}	931.27	555.133	60.31
Cu ²⁺ 2p _{3/2}	933.48	119.37	12.96

XPS analysis was performed to investigate the chemical state of Pt and Cu in the optimized Pt-Cu/TiO₂ catalyst. The C 1s peak at 284.5 eV was used as a reference for energy calibration. The XPS spectra of Pt 4f for the Pt-Cu/TiO₂ sample before and after oxidation reaction are presented in **Figure 29** (a) and (c) respectively. The Pt 4f_{7/2} peak can be fitted into two peaks. The metallic Pt⁰ 4f_{7/2} peak is at 71.1 eV. In addition, a dominant peak at 70.1 eV was observed for both the new

and used Pt-Cu/TiO₂ catalysts. This negative shift is consistent with reported value for the alloyed Pt-Cu (negative shift of about 0.6 eV [180]), and also our XRD and TEM results for the formation of Pt-Cu alloy. The chemical state of Pt shows no significant change before or after the oxidation reaction.

The XPS spectra of Cu 2p of the new and used catalysts are shown in **Figure 29** (b) and (d). The Cu 2p_{3/2} for the new catalyst is at 932.5 eV, corresponding to metallic Cu. A shoulder peak of 931.3 eV was observed due to the formation of Pt-Cu alloy, consistent with alloyed Cu 2p spectra reported in literature.[180] For the used catalyst, the Cu 2p features are obviously different from those of the new catalyst. The peak intensity of metallic Cu 2p_{3/2} (at 932.5 eV) was decreased while a new shoulder peak appears at 933.5 eV, which reveals the formation of Cu²⁺ (CuO). Simultaneously, a significant Cu 2p_{1/2} shoulder peak corresponding to Cu²⁺ species appears at 952.6 eV for the used catalyst, which was not distinguished for the new catalyst. However, the alloyed Cu⁰ peaks can still be observed at 950.9 eV (2p_{1/2}) and 931.4 eV (2p_{3/2}). This reveals that the alloyed Cu cannot be oxidized under the reaction condition, but the unalloyed Cu species were partially oxidized to form CuO on the catalyst surface. This is a plausible reason to explain the activity decrease shown in catalyst recycle test (**Figure 31**). The atomic ratio of Cu²⁺ in total Cu species is about 13%, calculated from peak areas by curve fitting software (**Table 16**). Additionally, the Cu 3p_{3/2} peak is at approximately 75 eV, which overlaps with the Pt 4f peak. The partial oxidation of unalloyed Cu species was observed to influence the peak shape at 75 eV.

4.3.3 Effect of Reaction Conditions

Table 16. Glucose oxidation results at different temperatures using 5% Pt-Cu/TiO₂-a^a

T (°C)	Conversion (%)	Selectivity (%)				Carbon Balance
		Glucaric	Gluconic	Guluronic	C ₂ -C ₃	
		Acid	Acid	Acid	products ^b	
80	74	42	18	20	6	0.90
85	86	47	21	15	6	0.91
90	92	60	20	12	7	0.99
95	93	45	18	10	7	0.82
100	98	39	9	6	5	0.61
105	100	26	3	0	3	0.33 ^c

^aThe catalyst is repared by WC-2 method using NaBH₄ as reducing agent. Reaction conditions: time = 12 h, 15 bar O₂, initial pH = 7, initial glucose concentration = 0.278 mol/L.

^bThe C₂-C₃ products include oxalic acid, tartronic acid, glyoxal, glyceric acid, glycolic acid and acetic acid.

^cThe carbon balance loss was caused by CO₂ formation which is quantitatively confirmed by gas chromatography (GC), explained in the Appendix (**Table A - 2**)

The glucose conversion and product distribution data at different temperatures using the optimized Pt-Cu/TiO₂-a (WC-2, NaBH₄) catalyst are presented in **Table 17**. The glucose conversion increases with increase in temperature as expected. 100% conversion was obtained at 105 °C. The glucaric acid and gluconic acid selectivity first increased and then decreased with temperature. The highest glucaric acid selectivity of 60% was obtained at 90 °C, with glucose conversion of 92%, with gluconic selectivity of 20%, and glucuronic acid selectivity of 12%. At

95 °C and higher temperatures, the liquid phase carbon balance dropped significantly due to CO₂ formation.

Table 17. Glucose oxidation results at different O₂ pressures using 5% Pt-Cu/TiO₂^a

P _{O2} (bar)	Conversion (%)	Selectivity (%)				Carbon Balance
		Glucaric	Gluconic	Glucuronic	C ₂ -C ₃	
		Acid	Acid	Acid	Products ^b	
15	92	60	20	12	7	0.99
30	100	58	10	8	6	0.86
45	100	49	8	7	4	0.69

^aThe catalyst is repared by WC-2 method using NaBH₄ as reducing agent. Reaction conditions: time=12 h, 15 bar O₂, initial pH=7, initial glucose concentration = 0.278 mol/L, T=90 °C.

^bThe C₂-C₃ products include oxalic acid, tartronic acid, glyoxal, glyceric acid, glycolic acid and acetic acid.

Table 18. Glucose oxidation results at different initial glucose concentrations using 5% Pt-Cu/TiO₂^a

Conc. (mol/L)	Conversion (%)	Selectivity (%)				Carbon Balance
		Glucaric	Gluconic	Glucuronic	C ₂ -C ₃	
		Acid	Acid	Acid	Products ^b	
0.139	100	39	4	0	5	0.48
0.278	92	60	20	12	7	0.99
0.556	60	34	23	26	9	0.96

^aThe catalyst is repared by WC-2 method using NaBH₄ as reducing agent. Reaction conditions: time=12 h, 15 bar O₂, initial pH=7, T=90 °C.

^bThe C₂-C₃ products include oxalic acid, tartronic acid, glyoxal, glyceric acid, glycolic acid and acetic acid.

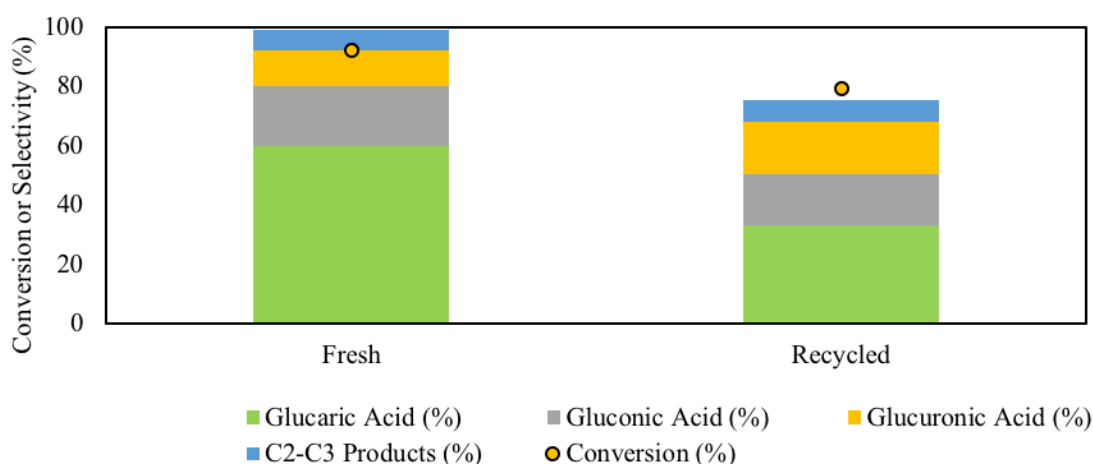


Figure 31. Recycle test results of Pt-Cu/TiO₂ catalyst; Reaction conditions: 15 bar O₂, initial pH=7, T=90 °C, initial glucose concentration = 0.278 mol/L, catalyst Pt-Cu/TiO₂-a prepared by WC-2

The study of O₂ pressure and initial glucose concentration was also performed, The results are presented in **Table 18** and **Table 19**. Glucose was completely converted at higher pressures (30 bar and 45 bar), however, the C₆ products selectivity dropped with increasing O₂ pressure due to the CO₂ formation and C-C cleavage products. At higher initial glucose concentration (0.556 mol/L), the glucose conversion decreased to 60% (see **Table 19**) without significant CO₂ formation. At lower initial glucose concentration (0.139 mol/L), the glucose was completely converted as expected. Glucaric acid is nearly the only C₆ product indicating that almost all the gluconic acid and glucuronic acid intermediates are converted to glucaric acid. However, after glucose is converted, significant formation of CO₂ was observed (liquid phase carbon balance drops to 0.48).

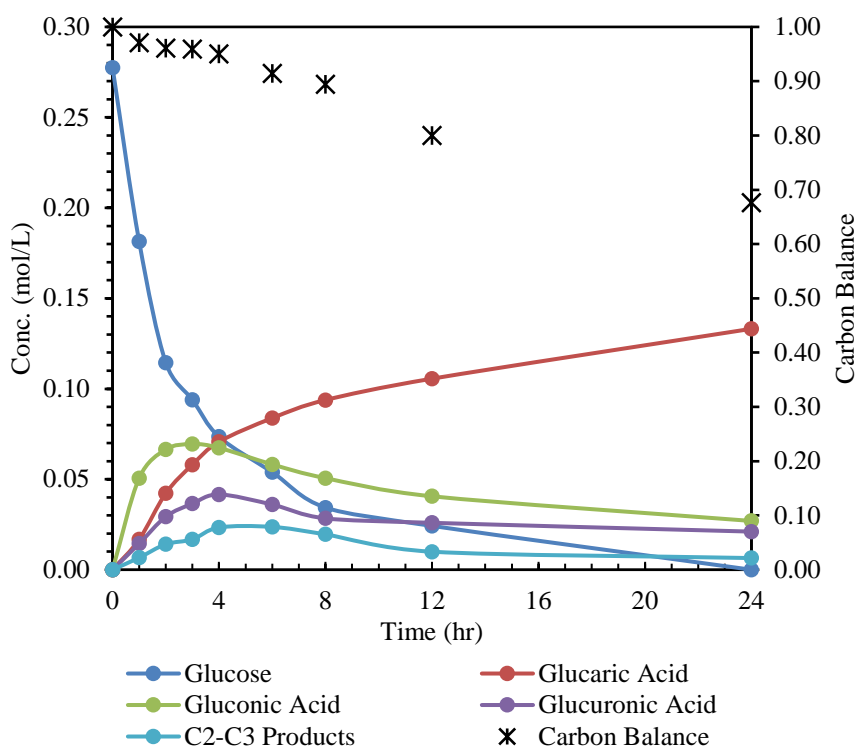


Figure 32. Concentration-time profile of glucose oxidation under neutral condition using the semi-batch reactor. Reaction conditions: 15 bar O₂, initial pH=7, T=90 °C, initial glucose concentration = 0.278 mol/L, catalyst Pt-Cu/TiO₂-a prepared by WC-2 method using NaBH₄ as reducing agent. The C₂-C₃ products include oxalic acid, tartronic acid, glyoxal, glyceric acid, glycolic acid and acetic acid.

In order to understand the product distribution at various conversion levels, concentration-time profiles were also determined using the bimetallic Pt-Cu/TiO₂-a catalyst in a semi-batch reactor at 90 °C and 15 bar. The results are shown in **Figure 32**. As can be seen, glucose conversion is relatively fast at the beginning with an initial turnover frequency (TOF) of 46.4 h⁻¹(based on glucose conversion).

An important observation is that glucaric acid is formed from the start of the reaction unlike the base promoted oxidation.[107] Derrien et al. observed similar trend that glucaric acid forms at the start of glucose oxidation using the Au-Pt bimetallic catalyst.[114] This suggests that under neutral conditions, glucose inhibition is not significant providing adequate sites for oxidation of

the gluconic and glucuronic acid intermediates to glucaric acid. The glucaric acid selectivity was observed to increase with time. However, after 12 h, significant CO₂ formation was observed due to over-oxidation of substrates leading to a drop in the liquid phase carbon balance.

4.4 Conclusion

Glucose oxidation under neutral conditions was performed using different mono- and bimetallic Pt catalysts. Catalyst optimization was conducted to study the effects of support, synthesis method, secondary metal, and reducing agent, with the findings summarized as follows: (1) diameter and surface area of the supports are not key factors influencing the catalytic performance; strong metal-support interaction is observed between Pt and TiO₂ to explain the increase in glucose conversion and glucaric acid selectivity compared to the Pt supported on other oxides as supports; (2) the wet chemistry method is found to be beneficial to glucaric acid production than the solvothermal method or the impregnation method (3) the mono- Pt and bimetallic Pt-Cu catalysts showed similar glucose conversion but significant difference in product distributions with higher selectivity for glucaric acid with bimetallic catalyst; (4) the synthesized Pt-Cu/TiO₂-a catalyst using a strong reducing agent NaBH₄ shows a higher glucaric acid selectivity compared to other Pt-Cu catalysts prepared by the same method but using weak reductants (Me₂AB or AB).

Characterization of the bimetallic catalyst showed that the optimized Pt-Cu catalyst has an alloyed structure and a nanocluster shape containing small round Pt-Cu particles (~2.8 nm diameter). A series of oxidation experiments using this catalyst were performed under various reaction conditions (temperature, pressure, and initial glucose concentrations). Our findings reveal that significantly less C-C cleavage products are formed under base-free conditions. compared to

the alkaline conditions. Additionally, it was found that glucaric acid selectivity increases with the temperature, but large amount of CO₂ was formed at temperatures > 90 °C. Using lower or higher initial glucose concentrations, the glucose conversion was increased or decreased as expected, but with decreased glucaric acid selectivity under both situations. At higher O₂ pressures, the liquid phase carbon balances dropped significantly due to the CO₂ formation by over-oxidation. In addition, the time-concentration profiles obtained from a semi-batch experiment showed that glucaric acid formation occurs from start of the reaction, unlike inhibition by glucose in the alkali promoted oxidations reported previously.[106, 107]

Chapter 5: Synthesis of Monodispersed Pt-Cu Cubes, Octahedrons, Tetrahedrons on TiO₂ for Glucose Oxidation: Facet Dependent Catalytic Activity and Selectivity

5.1 Introduction

During the last few decades, nanoscience has made significant advances in the synthesis of Pt based nanocrystals (NCs) with desired shape and size due to potential applications in catalysis. For instance, Pt cube [181, 182], cuboctahedrons [183], octahedron/tetrahedron [184], rod [185], wire [186], and Pt-based alloys with various shapes [187, 188] have been successfully synthesized. It has been unveiled that the exposed facet of a NC affects its catalytic properties significantly. As an example, Pt cubes enclosed by (100) facets demonstrates higher selectivity to cyclohexane in the hydrogenation of benzene, compared to Pt cuboctahedrons enclosed by a mixture of (100) and (111) facets.[183] In another case, Pd cube demonstrates higher activity compared to the Pd octahedron enclosed by (111) facet for electrooxidation of formic acid.[189] In other examples, facet-dependent catalysis has also been reported to influence the activity or selectivity for the hexacyanoferrate (III)/thiosulfate redox reaction,[190] isomerization of olefins [191], water gas shift (GWS) reaction,[192] oxygen reduction reaction (ORR) [193] and photocatalytic reactions.[194]

Despite the rapid development of nanotechnology and their successful demonstration in heterogeneous catalysis, the industrial application of these NCs with tailored structures is still a

challenge. The reported synthesis methods require the use of proper capping agents to direct the growth of a specific crystal facet, but the washing-separation step (to remove the capping agent or template) creates high energy cost during centrifugation and produces large amount of nonpolar solvent wastes. Part of the NCs are usually sacrificed due to the inefficient separation that not only influences the yield of the metal NCs but also causes hazardous risks for the waste solvent treatment. Meanwhile, the recycling and separation of these NCs for a liquid-phase reaction will be extremely difficult and costly due to their nano-scale size. For the purpose of industrial applications, a heterogeneous catalyst must be easy to be prepare and recycle. Currently, impregnation is most widely used industrial method to prepare the supported noble metal catalysts due to its convenience and economic feature. In this method, the active metals are deposited on an inert support material to improve the physical properties of nanoparticles, such as metal distribution and thermal/mechanical stability to minimize the metal loss in a continuously operated reactor. However, the shape of synthesized nanoparticles is usually irregular that makes the identification of such existing surface of an industrial catalyst extremely challenging.[195] In addition, the metal particles are hard to be shape-tuned for the improvements in catalytic performances.

To build a bridge between fundamental studies and industrial applications, it is of essential to achieve shape selective NCs deposited on a physical support by a facile and extendible method. Herein, by using a solvothermal method coupled with selection of suitable solvent, capping agent and template, we demonstrate synthesis of TiO_2 supported Pt-based NCs with cubic, octahedra and stellar tetrahedra shapes. The cubes are enclosed by six (100) facets and the octahedrons are enclosed by eight (111) facets. The stellar tetrahedrons are grouped by two tetrahedrons but still enclosed by also only the (111) type of facets (**Figure 33**). These three “low index” facets are

vitaly important since they are atomical-scale flat and relatively free of defects. In addition, the NCs with high index facets (hkl) can be theoretically considered as a group of (111), (100), and (110) flat facets coupled with a number of steps, edges, kinks and corners within the structure.[196]

For the application purpose, we studied the catalytic performance of these synthesized NCs in the aqueous phase glucose oxidation under base-free conditions. To our knowledge, the shape dependency of catalysts for this reaction has not been studied previously. The oxidation of glucose to glucaric acid is recognized as an environmentally friendly alternative to the conventional petrochemical routes. However, the secondary oxidation step (gluconic acid to glucaric acid) is found as a slow step that limits the production of glucaric acid. Strong alkali such as NaOH or KOH were reported as promoters to oxidation reactions but pose separation difficulties in obtaining the acids from their alkaline salts.[197] So far, only a few studies have achieved glucaric acid selectivity under the base-free conditions using Pt based catalysts.[108, 197-199] In the last chapter, the support effect and bimetallic effect has been studied. As a result, Pt-Cu bimetallic catalyst supported on TiO₂ demonstrated the highest glucose conversion (92%) and glucaric acid selectivity (60%) under the base-free oxidation conditions. Correspondingly, the shape effect Pt-Cu catalyst is discussed for the aqueous phase oxidation of glucose-to-glucaric acid in this chapter.

5.2 Experimental and Methodology

5.2.1 Materials

All the chemicals were procured from the commercial suppliers without addition treatment before use. Polyvinylpyrrolidone (PVP, Sigma-aldrich, MW=40,000 g/mol), potassium bromide (KBr, Sigma-aldrich, FT-IR grade), potassium tetrachloroplatinate (II) and copper (II) chloride

dihydrate (K_2PtCl_4 and $\text{CuCl}_2 \cdot 2\text{H}_2\text{O}$, ACROS Organics, 99%, extra pure). 0.1 N hydrochloric acid (HCl) water solution (CHATA Chemical, HPLC grade), hexadecyltrimethylammonium bromide (CTAB, Sigmaaldrich, $\geq 99\%$), TiO_2 -a (ACROS Organics, 98+%, anatase), platinum (III) acetylacetonates ($\text{Pt}(\text{acac})_2$, Sigma-aldrich, 97%), copper (II) acetylacetonates ($\text{Cu}(\text{acac})_2$, Sigma-aldrich, 97%), formaldehyde solution (fisher scientific, 37 wt % in H_2O , Baker AnalyzedTM), D-glucose (Sigma-aldrich, >99.5%, GC grade), N, N-dimethylformamide (Alfa Aesar, DMF, HPLC grade, >99.9%), sodium iodide (ACS reagent, $\geq 99.5\%$)

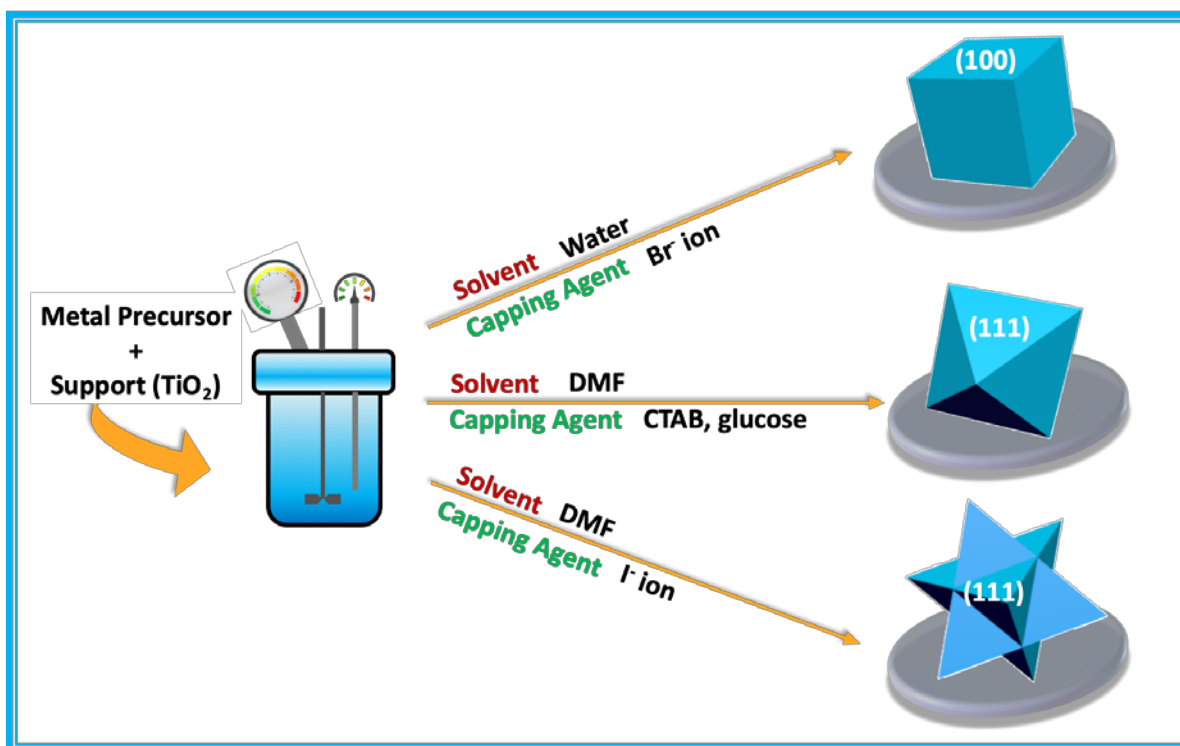


Figure 33. Scheme of one-pot synthesis of shape controlled nanocrystals

5.2.2 Synthesis of TiO₂ supported Pt and Pt-Cu Cubes

In a typical synthesis, 1.5 g of Polyvinylpyrrolidone (PVP, Sigma-aldrich, MW=40,000 g/mol) and 16 g of potassium bromide (KBr, Sigma-aldrich, FT-IR grade) were dissolved in 100mL deionized water. Proper amount of the metal precursors - K₂PtCl₄ and CuCl₂·2H₂O was added simultaneously to the solution under stirring for the preparation of the Pt-Cu catalyst. In the preparation of Pt cubes, only K₂PtCl₄ was used. The pH value of the precursor solution was adjusted using 0.1 N hydrochloric acid (HCl) solution. 1.76 g of TiO₂ powder was then added to the precursor solution and the total volume of solution was adjusted to 225 mL. The homogeneous slurry was stirred at room temperature for at least 30 minutes and then transferred to a 300 mL autoclave reactor with mechanical stirring and precise temperature/pressure control. The autoclave was sealed and heated at 160 °C for 4 hours under stirring (600 rpm) and 10 bar N₂ atmosphere. After cooling down, the upper clear liquid containing KBr and PVP was removed. The grey catalyst powder was further washed by water/ethanol (v/v = 1:2) solution for 7 times and dried in vacuum oven at 60 °C overnight.

5.2.3 Synthesis of TiO₂ supported PtCu octahedron

For this synthesis, 0.76 g of CTAB, 1.89 g glucose, and 21 mL formaldehyde solution were dissolved in 150 mL DMF. Proper amounts of Pt(acac)₂ and Cu(acac)₂ were added simultaneously into the DMF solution and stirred for about 30 minutes. 2.5 g of TiO₂ powder was then added to the precursor solution under stirring and then transferred to a 300 mL autoclave reactor. The autoclave was sealed and heated at 180 °C for 12 hours under stirring (600 rpm) and 10 bar N₂ atmosphere. Decomposition of formaldehyde generates CO as a reducing agent. After cooling

down, the upper clear liquid was removed. The grey catalyst powder was further washed by water/ethanol (v/v = 1:2) solution for 7 times and dried in vacuum oven at 60 °C overnight.

5.2.4 Synthesis of TiO₂ supported PtCu stella octangula

In this case, 0.2 g Pt(acac)₂, 0.13 g Cu(acac)₂ and 0.38 g NaI were added to 225 mL DMF and stirred until dissolved. 1.9 g of TiO₂ powder was added to the DMF solution and stirred for about 30 minutes. The slurry was then transferred to the 300 mL autoclave reactor. The autoclave was sealed and heated at 130 °C for 16 h with 600 rpm stirring under 10 bar N₂ atmosphere. The autoclave reactor was then naturally cooled down, contents washed and dried under the same conditions as described in the above sections.

5.2.5 Catalyst Characterization

Transmission electron microscopy (TEM) imaging and energy-dispersive X-ray spectroscopy (EDX) elemental mapping were acquired on a FEI Tecnai F20 XT instrument at the University of Kansas. The particle size distribution was determined based on a measurement of more than 120 nanoparticles for each catalyst using the software ImageJ.

Powder X-ray diffraction (XRD) analysis was done on a Bruker D8 powder diffractometer with a cooper target (Cu K α radiation) operating at 40 kV and a current of 40 mA to obtain the crystal structure information for Pt and Pt nanoparticles. A scanning rate of 0.01° min⁻¹ was used, and the diffraction angle (2 θ) was scanned within a range from 5° to 105°.

5.2.6 Oxidation Reaction

The catalytic performances of Pt and Pt-Cu catalysts were evaluated for the oxidation of glucose under base-free conditions in a semi-batch slurry stirred reactor system. In this reactor system, an autoclave reactor coupled with 100 mL vessel (Parr), magnetic stirring and precise temperature/pressure control is connected to a O₂ reservoir to maintain constant oxygen pressure during an experiment. In a typical oxidation experiment, an aqueous glucose solution (2.5 mol/L, 60 mL) was charged into the autoclave with the measured amounts of catalysts (1.2 g). No alkali was added to meet the requirement of base-free conditions. During a reaction, around 0.5~1 mL of liquid is sampled and analyzes during the high-performance liquid chromatography (HPLC). The glucose conversion (%), product selectivity (%) and turn-over frequency (TOF) values are calculated according to the formula as provided in the Supporting Information. (SI)

5.3 Results and Discussions

5.3.1 Morphology and Structures

A scheme of the synthesis methods is illustrated as **Figure 33** and the TEM images are shown as **Figure 34**. The synthesized nanoparticles are highly shape selective and mono-dispersed. The average sizes of Pt and Pt-Cu cubes are 8.7 ± 1.3 nm and 4.7 ± 0.8 nm respectively (**Table 20**). Comparing to non-supported cubes synthesized at the same conditions (Appendix IV, **Figure A - 15**), the particle size of cubes is not changed significantly. Therefore, the presence of TiO₂ support does not appear to disturb the facet-controlled synthesis; instead, it anchors the Pt nanocrystals at the early age of formation.

Here, Br^- ion is used as the shape directing agent for the formation of (100) facets in Pt and Pt-Cu cubes. PVP40 is used as the stabilizer to obtain the homogeneous deposition of NCs on the TiO_2 . We have found that the molecular weight of PVP affects the morphology of the nanocubes significantly. The Pt-Cu cubes using PVP29 (MW=29,000, **Figure A - 16**) has less unity in size and shape compared to those synthesized by the same method but using PVP40 (**Figure 34**). It's worthy to mention that PVP cannot be removed completely by regular ethanol/water washing procedure. The attached PVP on the surface can create steric effects that block the access to reactant molecules (glucose) to the active sites on the catalyst hence decreases the oxidation rates.

Therefore, we utilized a reported PVP-removal method that does not require thermal treatment step to remove the PVP residues before the oxidation experiments.[200] In this method, NaBH_4 is used to produce hydride to displace the PVP adsorbed on the metal surface, then tert-butylamine (TBA) is used to dissolve the PVP to avoid its re-adsorption. It has been experimentally proved to remove the surface PVP species completely by FTIR and Raman spectra. [200] The catalytic performance of PtCu cubes before and after PVP-removal are shown in the Appendix IV as **Table A - 3** and **Figure 45** (b) respectively. It can be seen that glucose conversion is negligible before PVP-removal (8.4% at 12h) with the formation of gluconic acid as the only product. In contrast, the PVP-free Pt-Cu cube shows the conversion of 72.6% at the same experimental conditions.

The Pt-Cu octahedrons and stella tetrahedrons have average sizes of 22.5 ± 4.3 nm and 15.2 ± 3.9 nm respectively. CTAB and I^- are both reported to be used as shape directing agents for the formation of the (111) facets in Pt-based alloys. However, it is interesting to see that the use of I^- resulted in the formation of two interpenetrating tetrahedra (*stella octangula*) NCs that is not reported for Pt-Cu alloys previously. The EDX (Figure 3a) analysis shows that all the synthesized

Pt-Cu nanoparticles belong to alloy structure. In previous literature, stellar structured NCs of Au, Cu-Ni MOF particles have been reported.[91, 201] However, these reported stellar nanoparticles are usually synthesized by a two-step seed mediated method with a particle size of larger than 80 nm or even sub-micrometer level. It is rare to see the formation of sub-20nm sized stellar nanoparticles in a simple one-step route.

Figure 38 shows the X-ray diffraction (XRD) patterns of the Pt and Pt-Cu nanoparticles. The peak at 43° representing unalloyed Cu species in the bimetallic catalysts and the peaks representing Cu_2O and CuO species were not observed. The diffraction peak at 40° corresponds to the (111) lattice plane in the monometallic Pt catalyst then the peak shifts to higher degrees in the bimetallics due to the alloy formation. According to the XRD calculations demonstrated in the last chapter (Page 95), all the bimetallic Pt-Cu shown in this part of work belong to the random fcc type of alloy. As demonstrated in the **Figure 38**, the atoms in this type of crystal lattice could be Pt or Cu randomly distributed. To determine the chemical states of Pt and Cu in the nanocrystals, XPS analysis was performed the results of which are shown in **Figure 39**. Only the metallic state of Pt species was found in all the catalysts. In addition, the binding energy of Pt^0 4f peak was shifted from 71.2 eV to around 70.2 eV in the Pt-Cu bimetallics. Two different types of peaks (at 951.2 eV and 952.5 eV) were observed that correspond to unalloyed Cu^0 2p and alloyed Cu^0 2p peaks respectively. Besides these metallic Cu species, no Cu oxide was detected which matches with the findings from the XRD results.

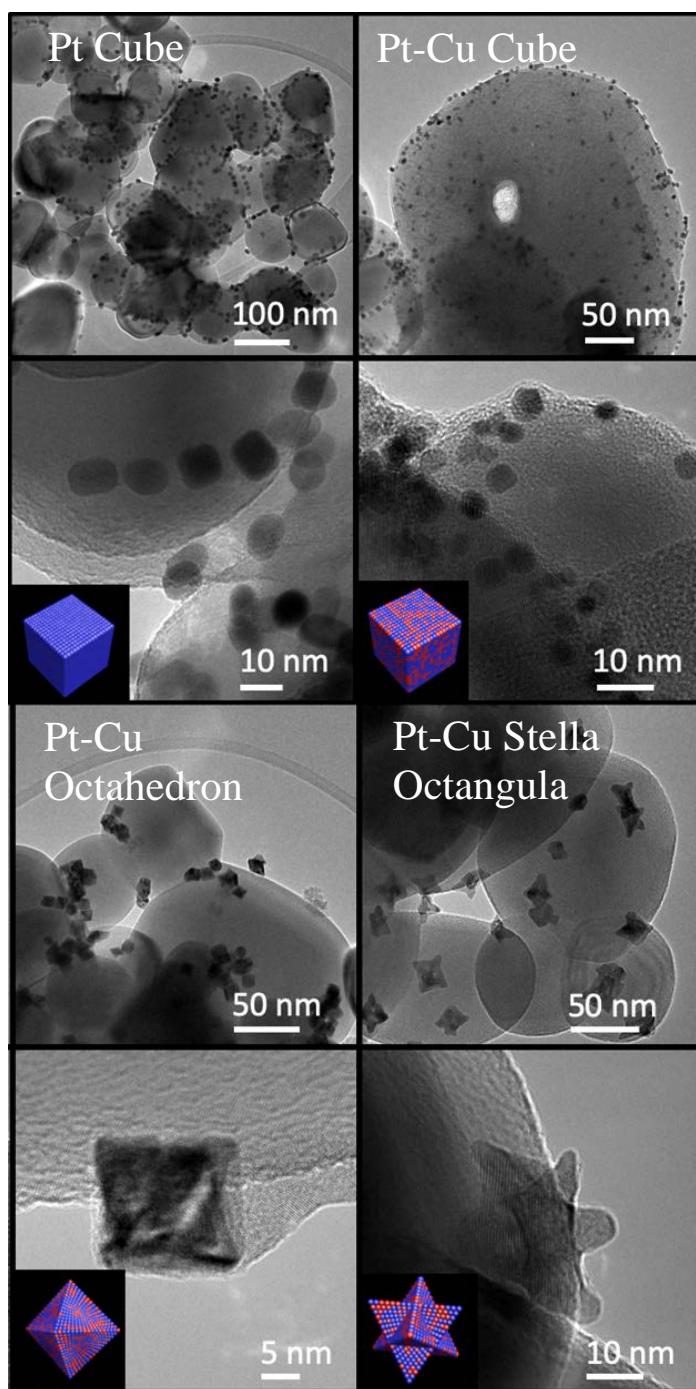


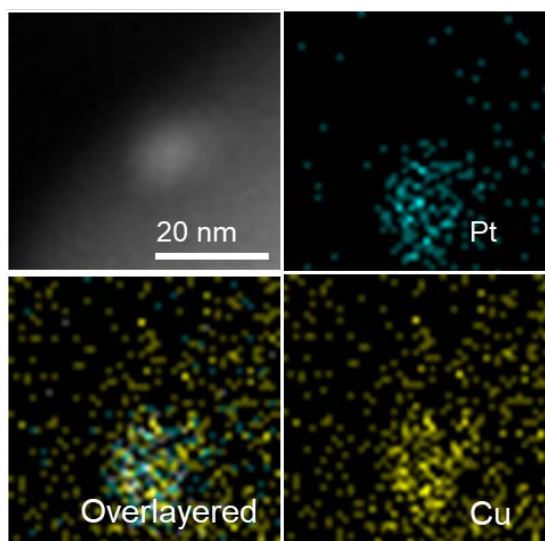
Figure 34. TEM images of shape-controlled Pt and Pt-Cu nanoparticles on TiO_2 support

Table 19. Metal composition and particle size of the Pt and Pt-Cu nanoparticles

	Particle Size (nm)	Pt (wt%) ^a	Cu (wt%) ^a	FE ^b
Pt _C	8.7 ± 1.3	2.79		0.032
Pt-Cu _C	4.7 ± 0.8	3.10	0.37	0.059
Pt-Cu _{OH}	22.5 ± 4.3	3.98	1.32	0.012
Pt-Cu _{SO}	15.2 ± 3.9	1.48	0.96	0.018

^ametal loading (wt%) was obtained from the ICP analysis; Pt_C: Pt cube; Pt-Cu_C: Pt-Cu Cube; Pt-Cu_{OH}: Pt-Cu Octahedron; Pt-Cu_{SO} Stella Octangula;

^bmetal dispersion number (FE) calculations are based on an empirical correlation [140]: if metal particles have small size (nanoparticle size < 24 × atom diameter), $FE = \frac{2.64}{(\frac{nanoparticle\ size}{atom\ diameter})^{0.81}}$; if metal particles are large (nanoparticle size > 24 × atom diameter), $FE = \frac{5.01}{(\frac{nanoparticle\ size}{atom\ diameter})}$

**Figure 35.** STEM/EDX images of Pt-Cu cube

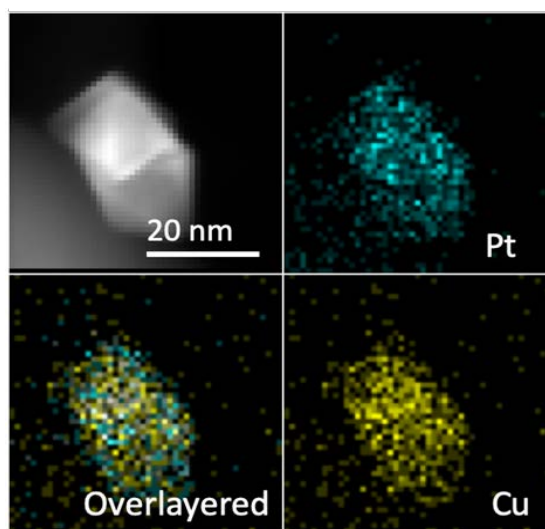


Figure 36. STEM/EDX images of Pt-Cu octahedron

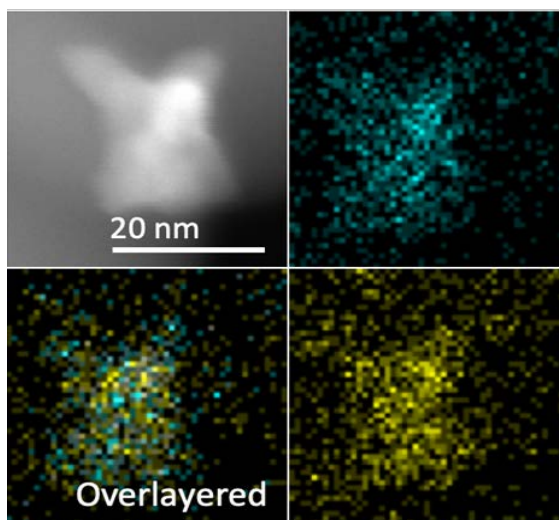


Figure 37. STEM/EDX images of Pt-Cu stella octangula

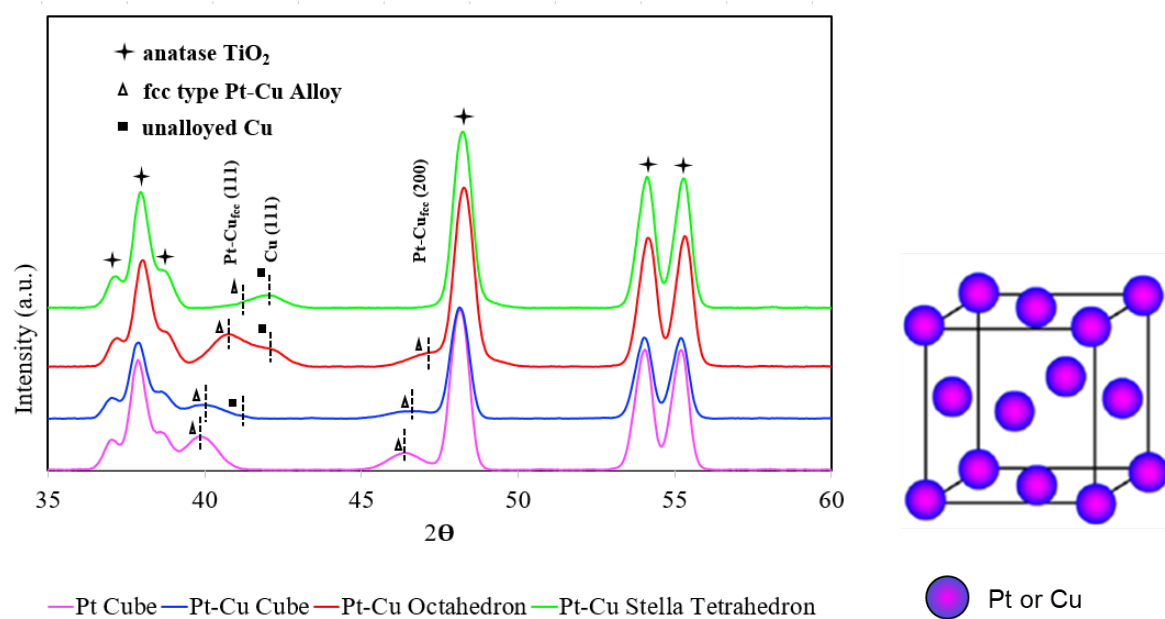


Figure 38. XRD patterns of Pt and Pt-Cu nanocrystals and crystal structure of Pt-Cu alloy

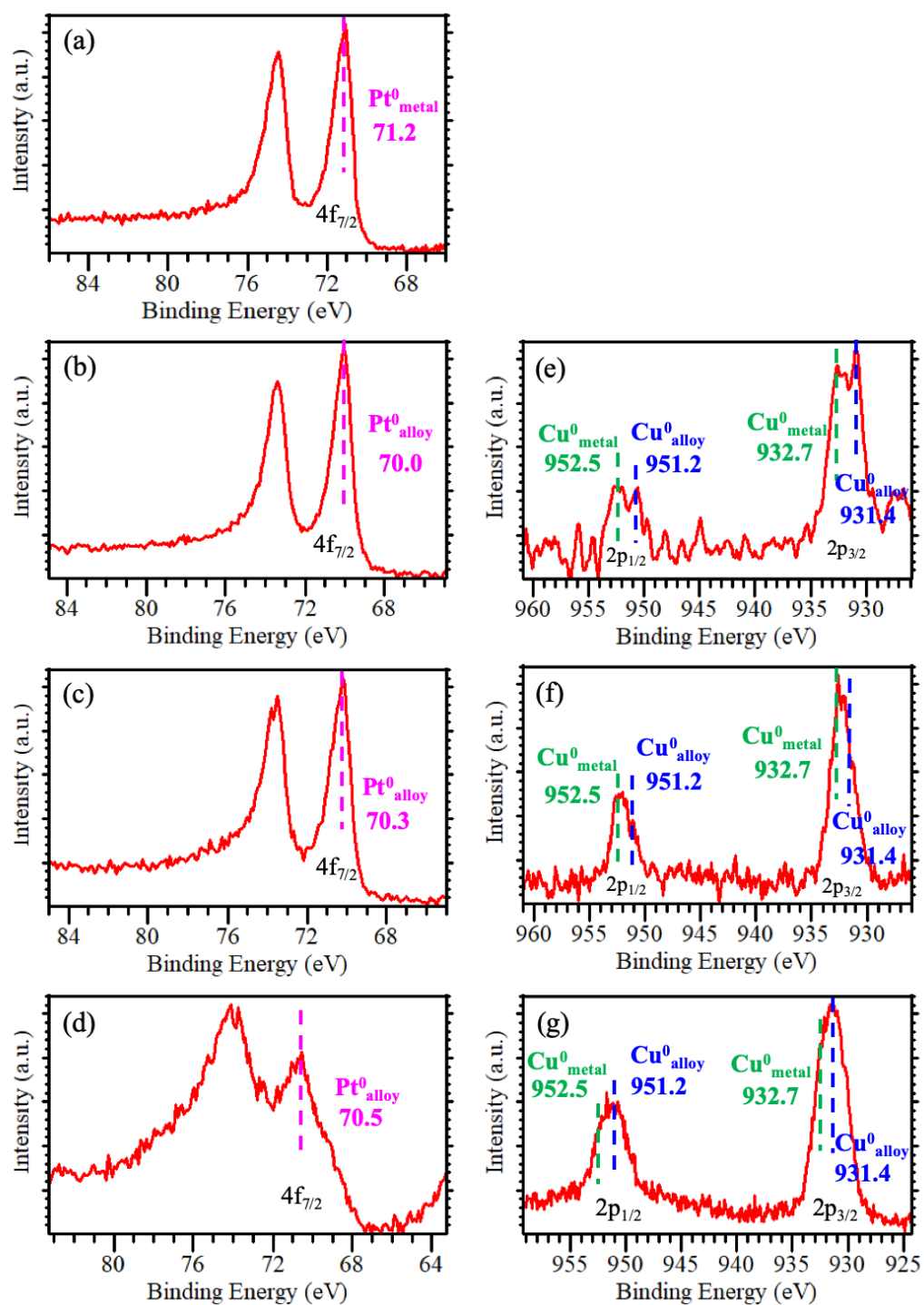


Figure 39. XPS of Pt and Pt-Cu nanoparticles

5.3.2 Evaluation of Catalytic Performance

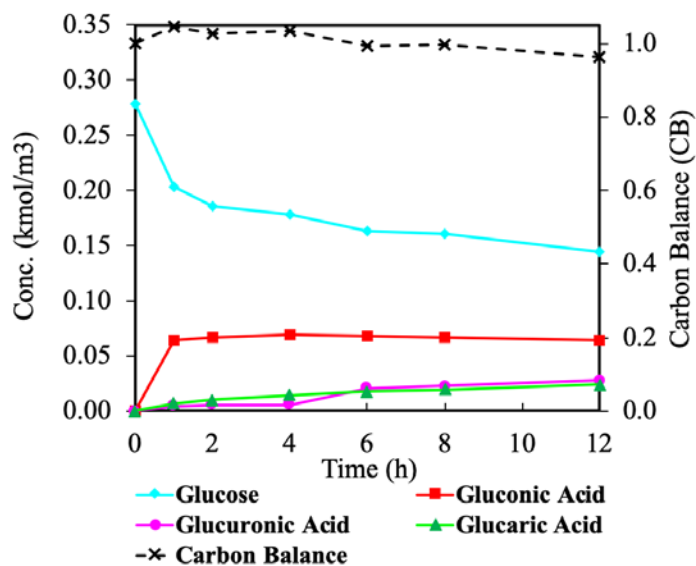


Figure 40. Concentration-time profile of glucose oxidation on Pt cube catalyst

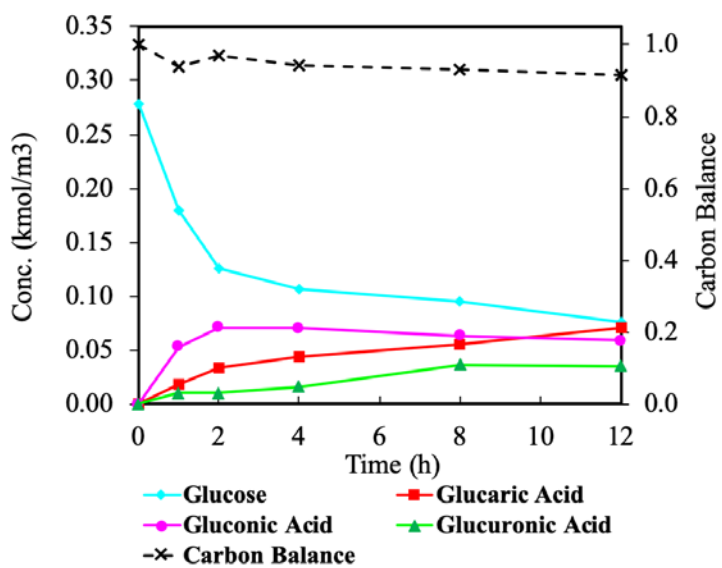


Figure 41. Concentration-time profile of glucose oxidation on Pt-Cu cube catalyst

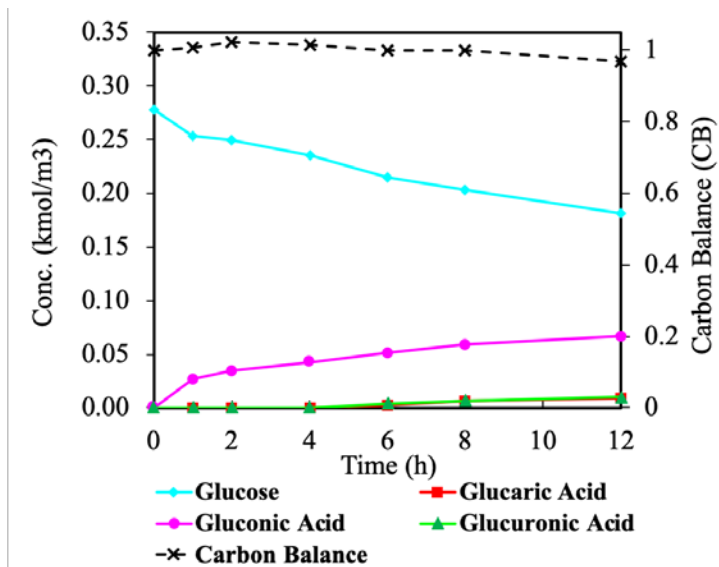


Figure 42. Concentration-time profile of glucose oxidation on Pt-Cu octahedron catalyst

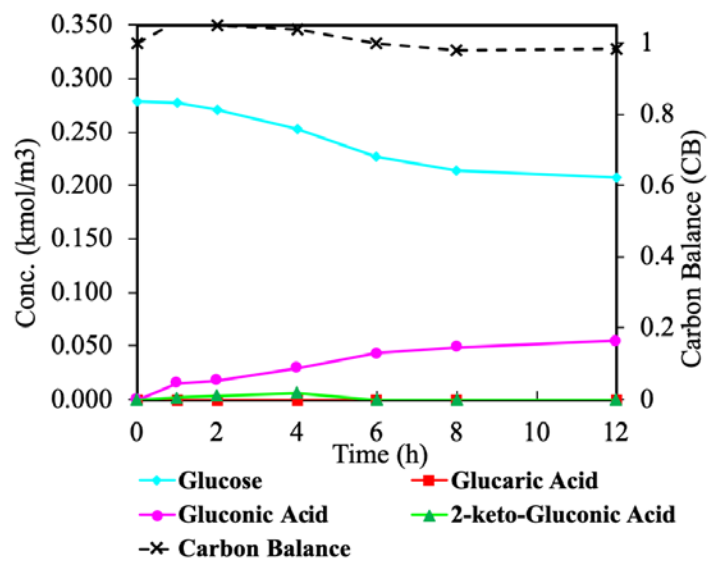


Figure 43. Concentration-time profile of glucose oxidation on Pt-Cu stella octangula catalyst

The concentration-time profiles of testing four different catalysts in aqueous phase glucose oxidation are shown in **Figure 40**, **Figure 41**, **Figure 42** and **Figure 43** respectively. In addition, the summaries of product selectivity at 12 hours and the catalyst activity based on glucose conversion ($\text{TOF}_{\text{glucose}}$) and glucaric acid ($\text{TOF}_{\text{glucaric}}$) formation are presented in **Figure 44** and **Figure 45**. In general, for all the tested catalysts the products are limited to C_6 products (gluconic acid, glucuronic acid and glucaric acid). This indicates that the C-C cleavage reactions are largely suppressed and also the C_2 - C_4 byproducts formation is almost negligible. Therefore, one may conclude that the (100) and (111) plane facets are the active sites preferred for the oxidation rather than other reactions.

The Pt metal loading in Pt cube (Pt_C) and Pt-Cu cube (Pt-Cu_C) is similar (~ 3 wt%, **Table 20**). However, the average particle size of Pt-Cu is about half of the average particle size of Pt cube. The size effect of the bimetallic catalyst creates a better Pt dispersion on the TiO_2 compared to the monometallic catalyst. Therefore, the initial oxidation rate of Pt-Cu is higher than that with monometallic Pt catalyst, as shown in **Figure 40** and **Figure 41**. After excluding the size effect, the overall activity of bimetallic cube ($\text{TOF}_{\text{glucose}}$) is one-third lower than that of the monometallic. However, the activity for glucaric acid formation ($\text{TOF}_{\text{glucaric}}$) of Pt-Cu cube is 113 h^{-1} while the $\text{TOF}_{\text{glucaric}}$ of Pt cube is only about 12 h^{-1} . In other words, a significant bimetallic effect was observed in promoting the selective formation of glucaric acid. This conclusion is also reflected in the final product selectivity. The glucaric acid selectivity at 12 h was increased from 21% to 37% due to the bimetallic effect with gluconic acid selectivity decreasing from 52% to 34%. This phenomenon indicates that Cu in the bimetallic catalyst decreases the rate of first oxidation step (glucose to gluconic acid) though creating more Pt active sites by size effect. Nevertheless, the

presence of Cu promotes the secondary oxidation steps (oxidation of gluconic acid or glucuronic acid to glucaric acid). A plausible mechanism to explain this phenomenon is: Due to the alloy formation, the charge transfer from Pt to Cu creates a moderate surface that is suitable for competitive adsorption of both hydroxyl group (in gluconic acid) and aldehyde group (in glucose). Therefore, the formed gluconic acid can stay on the surface for further oxidation rather than leaving the active site quickly. On the contrary, the monometallic Pt surface can only support the strong adsorption of aldehyde group but not provide a strong-enough adsorption for the primary hydroxyl group in the gluconic acid, suppressing the secondary oxidation step.

As for the shape effect, we can see that the catalytic performance of the two nanoparticles with (111) facets – Pt-Cu_{OH} and Pt-Cu_{SO} are very similar. Compared to the Pt-Cu cube, the TOF values of these two catalysts are significantly lower. In addition, the formation of secondary oxidation products (glucaric acid and glucuronic acid) is almost negligible, as can be seen from **Figure 44** and **Figure 45**. This observation indicates that the (111) facet of Pt-Cu does not favor adsorption and oxidation of primary hydroxyl groups (-OH) in gluconic acid. At the same time, (100) facet is preferred for the production of glucaric acid due to its strong adsorption for both aldehyde group and the primary hydroxyl group in the glucose molecule.

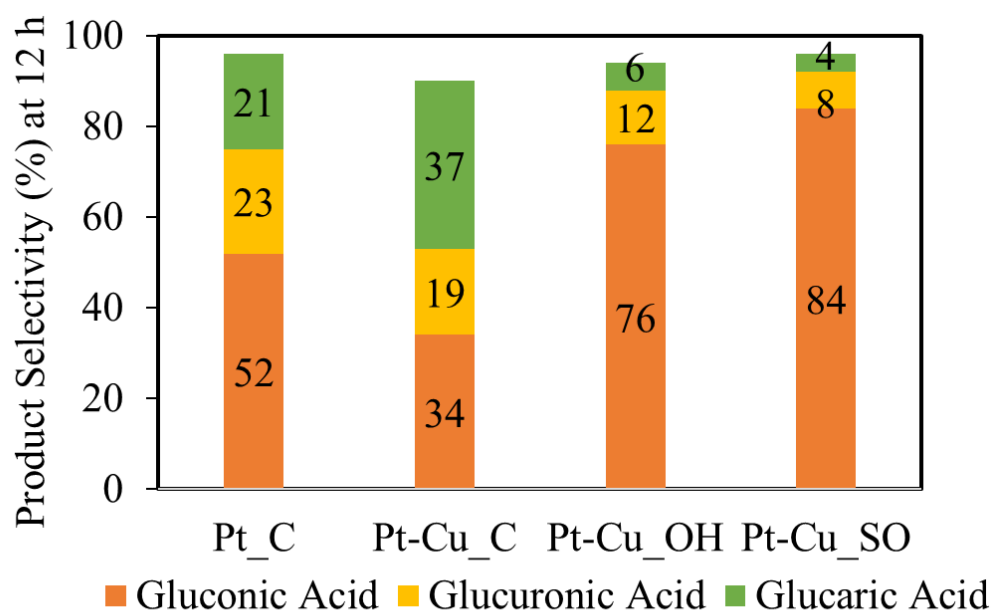


Figure 44. Selectivity of main products from glucose oxidation on Pt and Pt-Cu catalysts

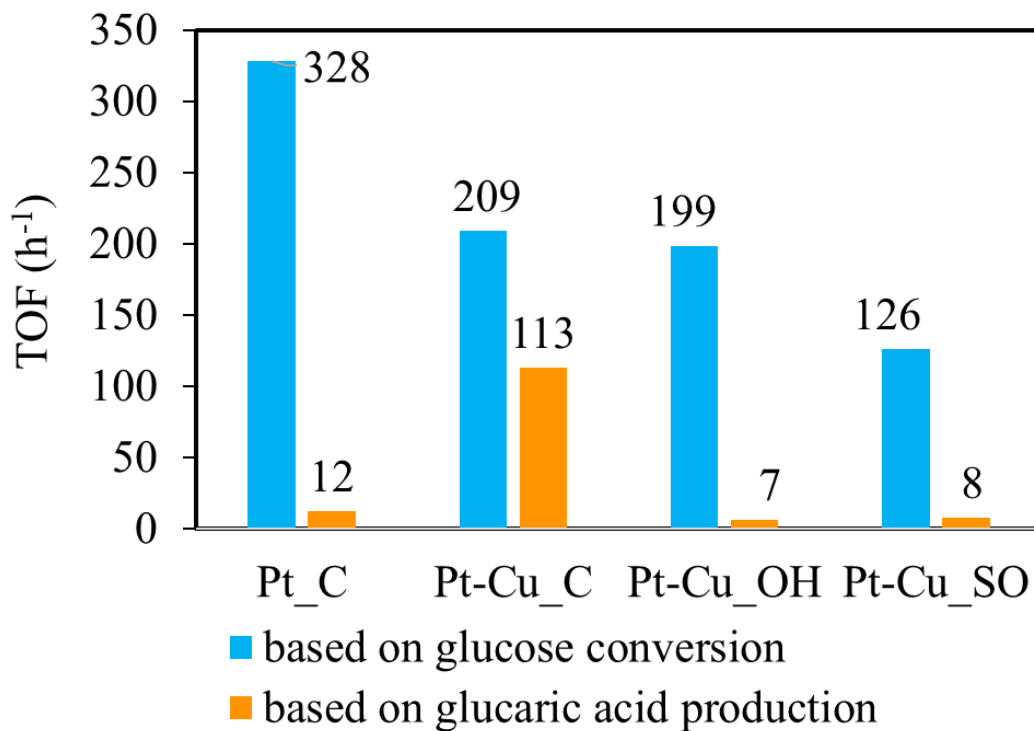


Figure 45. Activity of Pt and Pt-Cu nanocatalyst on glucose oxidation

5.4 Conclusion

The TiO₂ supported Pt and Pt-Cu nanocrystals with different exposed facets, such as nano-cubes with (100) facets, nano-octahedra and nano-stella octangula with (111) facets, were synthesized successfully by a facile one-pot synthesis strategy. The organic capping agents on the particle surface were then removed by a room-temperature method to preserve the morphology of Pt nanocrystals. Several important conclusions can be drawn from this work based on the results presented in this chapter:

- (1) The C-C cleavage reaction is largely suppressed by tuning the exposed facets in the Pt nanoparticles. The low index facets such as (111) and (100) of Pt catalysts are not active enough to catalyze the C-C cleavage reactions.
- (2) The two nanoparticles enclosed with (111) facets exhibited a quite similar catalytic performance: they showed a weaker performance towards glucose oxidation than the Pt-Cu cubes that exposed 100 facets, especially in the formation of glucaric acid.
- (3) The bimetallic effect of Pt-Cu cube is demonstrated by generating a size effect to facilitate Pt metal dispersion in the catalyst. The different adsorption states and strength for glucose and gluconic acid, which originated from the electronic effect of introducing 3d transitional metal (Cu) to Pt, explains the enhanced activities for the selective production of glucaric acid.

Chapter 6: Conclusions and Recommendations for Future Work

6.1 Conclusions

6.1.1 Oxidation of Ethylene Glycol

A highly active Pt-Fe catalyst was developed in this work for aqueous phase oxidation of ethylene glycol to glycolic acid, based on the screening of eight different monometallics and four different bimetallic formulations. The TOF on Pt-Fe catalyst (19.1 sec^{-1}) is approximately 17 times higher than that observed on Pt catalyst ($\text{TOF}=1.11 \text{ sec}^{-1}$) in the presence of a base promoter at 70°C and ambient pressure of O_2 . 100% conversion of EG and 62% glycolic acid selectivity was obtained at the end of reaction in 4 hours. The reaction mechanism of EG oxidation was studied with an emphasis of revealing the bimetallic effect and the base effect. It was found that the presence of a base and bimetallic catalyst affects the reaction orders for O_2 . On the monometallic Pt surface, O_2 participates in the reaction following a $-\text{OH}$ mediated mechanism that the additional O in the glycolic acid comes from water rather than from O_2 gas. However, the alloyed Pt-Fe structure enables efficient electron transfer from Fe to Pt that favors dissociative O_2 adsorption on the catalyst surface and its participation in the EG oxidation reaction. The NaOH base promotes EG oxidation on both Pt and bimetallic Pt-Fe catalysts at lower concentrations but it inhibits the EG oxidation rates at sufficiently higher concentrations. Further, the amount of base also influences the product selectivity favoring glycolic acid at higher NaOH concentrations. In the presence of excess amount of base, the O_2 and OH species compete for the active sites resulting in the observed rate inhibition and changes in product selectivity.

6.1.2 Oxidation of Glucose

The first part of this work screened the support, metal species and catalyst synthesis conditions for producing glucaric acid selectively from the oxidation of glucose in base-free aqueous solutions. Among the tested combinations, the Pt–Cu/TiO₂ bimetallic catalyst showed ~60% glucaric acid selectivity in one-step glucose oxidation under base-free conditions at 90 °C and 15 bar O₂. The catalyst consists of Pt metal particles (~2.8 nm diameter on average) with a dominant presence of the alloyed Pt–Cu phase, as confirmed by X-ray diffraction and transmission electron microscopy analysis.

The second part of the study on glucose oxidation established an expandable approach for the facile one-pot synthesis of facet-controlled nanoparticles supported on metal oxide: from cubic to stellated interpenetrating polyhedral structures. In addition, this is the first time to obtain the Pt–Cu stellated octangular nanostructure with uniform and small particle size (< 20nm). Experimentally, it is proved that bimetallic effect (Pt–Cu) and crystal facet (100) are the keys to promote the glucaric acid formation in the base-free liquid phase oxidation of glucose. In addition, the Pt–Cu cube demonstrated the highest activity (113 h⁻¹) to date for producing glucaric acid under base-free conditions.

6.2 Recommendations

Based on the findings of this work, the following studies are suggested to continue research on this topic.

- (1) Although enhanced activity has been observed by using a Pt-Fe bimetallic catalyst, significant C-C cleavage phenomenon was also observed. The formed CO_2 reacted with NaOH in the solution to form CO_3^{2-} which has a poisoning effect on the catalyst. Therefore, proper strategies such as add another metal promoter should be considered to modify the Pt-Fe surface to depress the C-C cleavage/decarboxylation reactions.
- (2) Synthesis of nanocatalyst deposited on solid base supports should be considered to further improve the activity of glucose oxidation under neutral conditions.
- (3) Bimetallic effect and shape-dependent effect studies can be conveniently performed using the catalysts synthesized in this work but testing the oxidation of other sugars and polyols, for example, glycerol, xylitol, mannitol and sorbitol would be useful to make more generalized conclusions.
- (4) Conducting DFT calculations to analyze the electronic structure of the mono and bimetallic Pt-Cu surfaces - (100) or (111), and the adsorption energies on the alloyed catalysts. The existence of correlation between the adsorption energy and the d-band center of the alloy catalysts should be examined to check the proposed hypotheses in explaining the activity change on different facets.
- (5) Performing the parametric studies and kinetic modelling on glucose oxidation using the shape-controlled catalysts to fully understand the reaction mechanisms of different facets.

(6) Synthesis of novel bimetallic structures are still expected for more applications on the oxidation of sugars and polyols. In this work, we have utilized the size effect, facet control, and bimetallic effect to promote the oxidation by tuning the metal dispersion, exposed facets and d-band center control. In the future, the core-shell structure and hollow/frame structured nanoparticles should be considered for better surface energy control with the aid of the lattice mismatch and the increased surface-to-volume ratio.

Notations

$C_{c,EG}$ = the number of carbons regarding converted EG during the reaction

$C_{f,EG}$ = the final number of carbons regarding EG in the reaction solution

$C_{f,p}$ = the number of total carbons in the final products

$C_{i,EG}$ = the initial number of carbons regarding EG in the reaction solution

$C_{c,g}$ = the number of carbons regarding converted glucose during the reaction

$C_{f,g}$ = the final number of carbons regarding glucose in the reaction solution

$C_{i,g}$ = the initial number of carbons regarding glucose in the reaction solution

$C_{glucose}$ = glucose concentration in the reactant solution, kmol/m³

CB = carbon balance

d_p = diameter of the catalyst particle, m

De = effective diffusivity, m²/h

Ea = activation energy, eV

FE = metal dispersion number

k_{g-l} = gas-liquid mass transfer coefficient, m/h

k_{l-s} = liquid-solid mass transfer coefficient, m/h

$N_{c,EG}$ = the mole of converted EG during the reaction

$N_{c,g}$ = the mole of converted glucose during the reaction

$N_{surface\ metal}$ = the mole of Pt exposed on the catalyst surface

$P_{glucose}^{vap}$ = vapor pressure of D-glucose, Pa

P_{oxygen} = pressure of O₂ under experimental conditions, Pa

P_{water}^{vap} = vapor pressure of water, Pa

$R_{oxidation}$ = initial reaction rate of glucose oxidation, kmol/m³·h

$r_{i,EG}$ = initial reaction rate regarding EG conversion, kmol/m³·min

S = selectivity, %

TOF = turn-over frequency, h⁻¹

X = conversion, %

$x_{glucose}$ = mole fraction of glucose in the liquid phase

$y_{glucose}$ = mole fraction of glucose in the gas phase

$\gamma_{glucose}$ = volatility of glucose

ρ_p = density of the catalyst particle, kg/m³

ω_{cat} = catalyst loading, kg/m³

References

1. *Bioenergy Technologies Office Multi-year Program Plan*, U.S.D.o. Energy, Editor. 2016.
2. Teixeira, T.R., et al., *Forest biomass power plant installation scenarios*. Biomass and Bioenergy, 2018. **108**: p. 35-47.
3. *WBA Global Bioenergy Statistics 2018*. 2018, World Bioenergy Association.
4. Birol, F. *Renewables Market Analysis and Forecast from 2018 to 2023*. 2018; Available from: <https://www.iea.org/renewables2018/>.
5. Isa, K.M., T.A.T. Abdullah, and U.F.M. Ali, *Hydrogen donor solvents in liquefaction of biomass: A review*. Renewable and Sustainable Energy Reviews, 2018. **81**: p. 1259-1268.
6. Demirbas, A., *Biorefineries for Biomass Upgrading Facilities*. Green Energy and Technology. 2010: Springer.
7. Lambert, M., *Biogas: a significant contribution to decarbonising gas markets*. Energy Insight, 2017. **15**.
8. *Biomethane-status and factors affecting market development and trade*. 2014, IEA Bioenergy.
9. Garside, M., *Ethanol Fuel Production in Top Countries 2018*. 2018, Statista.
10. Wang, T., *Global biodiesel production by country 2018*. 2018.
11. Wan, H., R.V. Chaudhari, and B. Subramaniam, *Catalytic hydroprocessing of p-cresol: metal, solvent and mass-transfer effects*. Topics in Catalysis, 2012. **55**(3-4): p. 129-139.

12. Bob Flach, S.L., Karin Bendz, Bettina Dahlbacka, Dietmar Achilles, *EU-27 Biofuels Annual Report*. 2010, United States Department of Agriculture (USDA).
13. Duffy, P., XXV.—*On the constitution of stearine*. Quarterly Journal of the Chemical Society of London, 1853. **5**(4): p. 303-316.
14. Greg Pahl, B.M., *Biodiesel: Growing a New Energy Economy, 2nd Edition*. 2008.
15. Demirbas, A., *Political, economic and environmental impacts of biofuels: A review*. Applied energy, 2009. **86**: p. S108-S117.
16. Sheehan, J., et al., *An overview of biodiesel and petroleum diesel life cycles*. 2000, National Renewable Energy Lab., Golden, CO (US).
17. *Biodiesel*. Available from: <https://www.fueleconomy.gov/feg/biodiesel.shtml>.
18. *A comprehensive analysis of biodiesel impacts on exhaust emissions*. 2002, Environmental Protection Agency of U.S.
19. Borås, U.o., *New method makes bioethanol from waste -- in existing plants*, in *ScienceDaily*. 2017.
20. Economics, B.E., *BP Energy Outlook 2018 Edition*. 2018, Technical Report). [https://www. bp. com/content/dam/bp/en/corporate/pdf](https://www.bp.com/content/dam/bp/en/corporate/pdf....)
21. Perlack, R.D., *Biomass as feedstock for a bioenergy and bioproducts industry: the technical feasibility of a billion-ton annual supply*. 2005: Oak Ridge National Laboratory.
22. Dodds, D.R. and R.A. Gross, *Chemicals from biomass*. Science, 2007. **318**(5854): p. 1250-1251.
23. Sheldon, R.A., *Green and sustainable manufacture of chemicals from biomass: state of the art*. Green Chemistry, 2014. **16**(3): p. 950-963.

24. Bidy, M., C. Scarlata, and C. Kinchin, *Chemical from Biomass: A Market Assessment of Bioproducts with Near-term Potential (Technical Report NREL/TP-5100-65509)*. 2016.
25. Werpy, T. and G. Petersen, *Top value added chemicals from biomass: volume I-- results of screening for potential candidates from sugars and synthesis gas*. 2004, National Renewable Energy Lab., Golden, CO (US).
26. Holladay, J.E., et al., *Top value-added chemicals from biomass-Volume II—Results of screening for potential candidates from biorefinery lignin*. 2007, Pacific Northwest National Lab.(PNNL), Richland, WA (United States).
27. Zakzeski, J., et al., *The catalytic valorization of lignin for the production of renewable chemicals*. Chemical reviews, 2010. **110**(6): p. 3552-3599.
28. Goldstein, I.S., *Chemicals from cellulose*, in *Organic chemicals from biomass*. 2018, CRC Press. p. 101-124.
29. Nandiwale, K.Y., et al., *Zirconium-incorporated mesoporous silicates show remarkable lignin depolymerization activity*. ACS Sustainable Chemistry & Engineering, 2017. **5**(8): p. 7155-7164.
30. Yang, F., M.A. Hanna, and R. Sun, *Value-added uses for crude glycerol--a byproduct of biodiesel production*. Biotechnology for biofuels, 2012. **5**(1): p. 13.
31. Dodekatos, G., S. Schünemann, and H. Tüysüz, *Recent advances in thermo-, photo-, and electrocatalytic glycerol oxidation*. ACS Catalysis, 2018. **8**(7): p. 6301-6333.
32. He, J., et al., *New catalytic strategies for α , ω -diols production from lignocellulosic biomass*. Faraday discussions, 2017. **202**: p. 247-267.

33. He, J., et al., *Synthesis of 1, 6-Hexanediol from Cellulose Derived Tetrahydrofuran-Dimethanol with Pt-WO_x/TiO₂ Catalysts*. ACS Catalysis, 2018. **8**(2): p. 1427-1439.
34. Xiao, B., et al., *Synthesis of 1, 6-hexanediol from HMF over double-layered catalysts of Pd/SiO₂+ Ir-ReO_x/SiO₂ in a fixed-bed reactor*. Green Chemistry, 2016. **18**(7): p. 2175-2184.
35. Fang, Z. and X. Qi, *Production of Platform Chemicals from Sustainable Resources*. 2017: Springer.
36. van Putten, R.-J., et al., *Hydroxymethylfurfural, a versatile platform chemical made from renewable resources*. Chemical reviews, 2013. **113**(3): p. 1499-1597.
37. Fiorentino, G., M. Ripa, and S. Ulgiati, *Chemicals from biomass: technological versus environmental feasibility. A review*. Biofuels, Bioproducts and Biorefining, 2017. **11**(1): p. 195-214.
38. Saygin, D., et al., *Assessment of the technical and economic potentials of biomass use for the production of steam, chemicals and polymers*. Renewable and Sustainable Energy Reviews, 2014. **40**: p. 1153-1167.
39. Mountford, P., *Green Chemistry in the Pharmaceutical Industry*. Dunn, PJ, 2010: p. 145-160.
40. Constable, D.J., A.D. Curzons, and V.L. Cunningham, *Metrics to 'green' chemistry—which are the best?* Green Chemistry, 2002. **4**(6): p. 521-527.
41. Guerrero-Pérez, M.O. and M.A. Banares, *Metrics of acrylonitrile: From biomass vs. petrochemical route*. Catalysis Today, 2015. **239**: p. 25-30.
42. Juodeikiene, G., et al., *Green metrics for sustainability of biobased lactic acid from starchy biomass vs chemical synthesis*. Catalysis Today, 2015. **239**: p. 11-16.

43. Sanders, J.P. and R.A. Sheldon, *Comparison of the sustainability metrics of the petrochemical and biomass-based routes to methionine*. Catalysis today, 2015. **239**: p. 44-49.
44. Morais, A.R., et al., *Chemical and biological-based isoprene production: Green metrics*. Catalysis Today, 2015. **239**: p. 38-43.
45. Uytendaele, M., W. Van Hecke, and K. Vanbroekhoven, *Sustainability metrics of 1-butanol*. Catalysis today, 2015. **239**: p. 7-10.
46. Marinas, A., et al., *Sustainability metrics for a fossil-and renewable-based route for 1, 2-propanediol production: A comparison*. Catalysis Today, 2015. **239**: p. 31-37.
47. Cespi, D., et al., *Butadiene from biomass, a life cycle perspective to address sustainability in the chemical industry*. Green Chemistry, 2016. **18**(6): p. 1625-1638.
48. Eerhart, A., A. Faaij, and M.K. Patel, *Replacing fossil based PET with biobased PEF; process analysis, energy and GHG balance*. Energy & environmental science, 2012. **5**(4): p. 6407-6422.
49. Belboom, S. and A. Leonard, *Does biobased polymer achieve better environmental impacts than fossil polymer? Comparison of fossil HDPE and biobased HDPE produced from sugar beet and wheat*. Biomass and bioenergy, 2016. **85**: p. 159-167.
50. Tsiropoulos, I., et al., *Life cycle impact assessment of bio-based plastics from sugarcane ethanol*. Journal of Cleaner Production, 2015. **90**: p. 114-127.
51. Chen, L., R.E. Pelton, and T.M. Smith, *Comparative life cycle assessment of fossil and bio-based polyethylene terephthalate (PET) bottles*. Journal of Cleaner Production, 2016. **137**: p. 667-676.

52. Cok, B., et al., *Succinic acid production derived from carbohydrates: An energy and greenhouse gas assessment of a platform chemical toward a bio-based economy*. Biofuels, Bioproducts and Biorefining, 2014. **8**(1): p. 16-29.
53. Ruppert, A.M., K. Weinberg, and R. Palkovits, *Hydrogenolysis goes bio: from carbohydrates and sugar alcohols to platform chemicals*. Angewandte Chemie International Edition, 2012. **51**(11): p. 2564-2601.
54. Murata, K., I. Takahara, and M. Inaba, *Propane formation by aqueous-phase reforming of glycerol over Pt/H-ZSM5 catalysts*. Reaction Kinetics and Catalysis Letters, 2008. **93**(1): p. 59-66.
55. Wawrzetz, A., et al., *Towards understanding the bifunctional hydrodeoxygenation and aqueous phase reforming of glycerol*. Journal of Catalysis, 2010. **269**(2): p. 411-420.
56. Huber, G.W., R.D. Cortright, and J.A. Dumesic, *Renewable alkanes by aqueous-phase reforming of biomass-derived oxygenates*. Angewandte Chemie International Edition, 2004. **43**(12): p. 1549-1551.
57. Li, N., G.A. Tompsett, and G.W. Huber, *Renewable high-octane gasoline by aqueous-phase hydrodeoxygenation of C5 and C6 carbohydrates over Pt/zirconium phosphate catalysts*. ChemSusChem, 2010. **3**(10): p. 1154-1157.
58. Chen, K., et al., *One-Pot Conversion of Sugar and Sugar Polyols to n-Alkanes without C-C Dissociation over the Ir-ReOx/SiO₂ Catalyst Combined with H-ZSM-5*. ChemSusChem, 2013. **6**(4): p. 613-621.
59. Zhang, Q., et al., *Highly Selective Sorbitol Hydrogenolysis to Liquid Alkanes over Ni/HZSM-5 Catalysts Modified with Pure Silica MCM-41*. ChemCatChem, 2012. **4**(8): p. 1084-1087.

60. Jin, X., et al., *Nanostructured Metal Catalysts for Selective Hydrogenation and Oxidation of Cellulosic Biomass to Chemicals*. The Chemical Record, 2018.
61. Ten Dam, J. and U. Hanefeld, *Renewable chemicals: dehydroxylation of glycerol and polyols*. ChemSusChem, 2011. **4**(8): p. 1017-1034.
62. Oh, J., S. Dash, and H. Lee, *Selective conversion of glycerol to 1, 3-propanediol using Pt-sulfated zirconia*. Green Chemistry, 2011. **13**(8): p. 2004-2007.
63. Nimlos, M.R., et al., *Mechanisms of glycerol dehydration*. The Journal of Physical Chemistry A, 2006. **110**(18): p. 6145-6156.
64. Qin, L.-Z., M.-J. Song, and C.-L. Chen, *Aqueous-phase deoxygenation of glycerol to 1, 3-propanediol over Pt/WO₃/ZrO₂ catalysts in a fixed-bed reactor*. Green chemistry, 2010. **12**(8): p. 1466-1472.
65. Longjie, L., et al., *Mesoporous WO₃ supported Pt catalyst for hydrogenolysis of glycerol to 1, 3-propanediol*. Chinese Journal of Catalysis, 2012. **33**(7-8): p. 1257-1261.
66. Kurosaka, T., et al., *Production of 1, 3-propanediol by hydrogenolysis of glycerol catalyzed by Pt/WO₃/ZrO₂*. Catalysis Communications, 2008. **9**(6): p. 1360-1363.
67. Wang, J., et al., *Hydrogenolysis of Glycerol to 1, 3-propanediol under Low Hydrogen Pressure over WO_x-Supported Single/Pseudo-Single Atom Pt Catalyst*. ChemSusChem, 2016. **9**(8): p. 784-790.
68. Martin, A., et al., *Glycerol hydrogenolysis into propanediols using in situ generated hydrogen—A critical review*. European journal of lipid science and technology, 2013. **115**(1): p. 9-27.

69. Roy, D., B. Subramaniam, and R.V. Chaudhari, *Aqueous phase hydrogenolysis of glycerol to 1, 2-propanediol without external hydrogen addition*. Catalysis Today, 2010. **156**(1-2): p. 31-37.
70. Shabaker, J., G. Huber, and J. Dumesic, *Aqueous-phase reforming of oxygenated hydrocarbons over Sn-modified Ni catalysts*. Journal of Catalysis, 2004. **222**(1): p. 180-191.
71. Jiang, T., et al., *Investigation on the xylitol aqueous-phase reforming performance for pentane production over Pt/HZSM-5 and Ni/HZSM-5 catalysts*. Applied energy, 2012. **90**(1): p. 51-57.
72. Johnstone, R.A., A.H. Wilby, and I.D. Entwistle, *Heterogeneous catalytic transfer hydrogenation and its relation to other methods for reduction of organic compounds*. Chemical Reviews, 1985. **85**(2): p. 129-170.
73. Aramendía, M.a.A., et al., *Liquid-phase heterogeneous catalytic transfer hydrogenation of citral on basic catalysts*. Journal of Molecular Catalysis A: Chemical, 2001. **171**(1-2): p. 153-158.
74. Mallat, T. and A. Baiker, *Oxidation of alcohols with molecular oxygen on platinum metal catalysts in aqueous solutions*. Catalysis Today, 1994. **19**(2): p. 247-283.
75. Prati, L. and M. Rossi, *Chemoselective catalytic oxidation of polyols with dioxygen on gold supported catalysts*, in *Studies in Surface Science and Catalysis*. 1997, Elsevier. p. 509-516.
76. Della Pina, C., et al., *Selective oxidation using gold*. Chemical Society Reviews, 2008. **37**(9): p. 2077-2095.
77. Cattaneo, S., et al., *Gold Catalysts for the Selective Oxidation of Biomass-Derived Products*. ChemCatChem, 2019. **11**(1): p. 309-323.

78. Comotti, M., et al., *The catalytic activity of “naked” gold particles*. Angewandte Chemie International Edition, 2004. **43**(43): p. 5812-5815.
79. Megías-Sayago, C., et al., *Influence of gold particle size in Au/C catalysts for base-free oxidation of glucose*. Catalysis Today, 2018. **306**: p. 183-190.
80. Dimitratos, N., et al., *Effect of particle size on monometallic and bimetallic (Au, Pd)/C on the liquid phase oxidation of glycerol*. Catalysis Letters, 2006. **108**(3-4): p. 147-153.
81. Dimitratos, N., et al., *Effect of the preparation method of supported Au nanoparticles in the liquid phase oxidation of glycerol*. Applied Catalysis A: General, 2016. **514**: p. 267-275.
82. Cai, J., et al., *Gold nanoclusters confined in a supercage of Y zeolite for aerobic oxidation of HMF under mild conditions*. Chemistry—A European Journal, 2013. **19**(42): p. 14215-14223.
83. Dimitratos, N., et al., *Synergetic effect of platinum or palladium on gold catalyst in the selective oxidation of D-sorbitol*. Catalysis letters, 2005. **99**(3-4): p. 181-185.
84. Jin, X., et al., *Phase Transformed PtFe Nanocomposites Show Enhanced Catalytic Performances in Oxidation of Glycerol to Tartronic Acid*. Industrial & Engineering Chemistry Research, 2017. **56**(45): p. 13157-13164.
85. Jin, X., et al., *Lattice distortion induced electronic coupling results in exceptional enhancement in the activity of bimetallic PtMn nanocatalysts*. Applied Catalysis A: General, 2017. **534**: p. 46-57.
86. Jin, X., et al., *Exceptional performance of bimetallic Pt₁Cu₃/TiO₂ nanocatalysts for oxidation of gluconic acid and glucose with O₂ to glucaric acid*. Journal of Catalysis, 2015. **330**: p. 323-329.

87. Jin, X., et al., *Anisotropic growth of PtFe nanoclusters induced by lattice-mismatch: Efficient catalysts for oxidation of biopolyols to carboxylic acid derivatives*. Journal of Catalysis, 2016. **337**: p. 272-283.
88. Zhang, H. and N. Toshima, *Crown Jewel-structured Au/Pd nanoclusters as novel catalysts for aerobic glucose oxidation*. Journal of nanoscience and nanotechnology, 2013. **13**(8): p. 5405-5412.
89. Amaniampong, P.N., et al., *Unraveling the mechanism of the oxidation of glycerol to dicarboxylic acids over a sonochemically synthesized copper oxide catalyst*. Green chemistry, 2018. **20**(12): p. 2730-2741.
90. Singh, O.V. and R. Kumar, *Biotechnological production of gluconic acid: future implications*. Applied microbiology and biotechnology, 2007. **75**(4): p. 713-722.
91. Shankar, S., et al., *Metal-organic microstructures: from rectangular to stellated and interpenetrating polyhedra*. Journal of the American Chemical Society, 2014. **137**(1): p. 226-231.
92. Wenkin, M., et al., *Influence of metallic precursors on the properties of carbon-supported bismuth-promoted palladium catalysts for the selective oxidation of glucose to gluconic acid*. Applied Catalysis A: General, 1996. **148**(1): p. 181-199.
93. De Wit, G., et al., *Catalytic dehydrogenation of reducing sugars in alkaline solution*. Carbohydrate Research, 1981. **91**(2): p. 125-138.
94. Comotti, M., C. Della Pina, and M. Rossi, *Mono-and bimetallic catalysts for glucose oxidation*. Journal of Molecular Catalysis A: Chemical, 2006. **251**(1): p. 89-92.
95. Biella, S., L. Prati, and M. Rossi, *Selective oxidation of D-glucose on gold catalyst*. Journal of Catalysis, 2002. **206**(2): p. 242-247.

96. Bepalov, V. and V. Aleksandrov, [*Anticarcinogenic effect of potassium salts of glucaric and glucuronic acid in induced models of cervical and esophageal tumors*]. *Voprosy onkologii*, 2011. **58**(4): p. 537-540.
97. Simone, C.B., et al., *Cancer, lifestyle modification and glucarate*. *Journal of Orthomolecular Medicine*, 2001. **16**(2): p. 83-90.
98. Zóltaszek, R., et al., [*The biological role of D-glucaric acid and its derivatives: potential use in medicine*]. *Postepy higieny i medycyny doswiadczalnej* (Online), 2007. **62**: p. 451-462.
99. Walaszek, Z., et al., *Metabolism, uptake, and excretion of a D-glucaric acid salt and its potential use in cancer prevention*. *Cancer detection and prevention*, 1996. **21**(2): p. 178-190.
100. Hanausek, M., Z. Walaszek, and T.J. Slaga, *Detoxifying cancer causing agents to prevent cancer*. *Integrative Cancer Therapies*, 2003. **2**(2): p. 139-144.
101. Werpy, T., et al., *Top value added chemicals from biomass. Volume 1-Results of screening for potential candidates from sugars and synthesis gas*. 2004, DTIC Document.
102. Mustakas, G., R. Slotter, and R. Zipf, *Pilot plant potassium acid saccharate by nitric acid oxidation of dextrose*. *Industrial & Engineering Chemistry*, 1954. **46**(3): p. 427-434.
103. Smith, T.N., et al., *Modifications in the nitric acid oxidation of D-glucose*. *Carbohydrate research*, 2012. **350**: p. 6-13.
104. Thaburet, J.-F., et al., *TEMPO-mediated oxidation of maltodextrins and D-glucose: effect of pH on the selectivity and sequestering ability of the resulting polycarboxylates*. *Carbohydrate Research*, 2001. **330**(1): p. 21-29.

105. Dirkx, J.M., H.S. van der Baan, and J.M. van den Broen, *The preparation of D-glucaric acid by the oxidation of D-gluconic acid catalysed by platinum on carbon*. Carbohydrate Research, 1977. **59**(1): p. 63-72.
106. Besson, M., et al., *Oxidation of glucose and gluconate on Pt, Pt Bi, and Pt Au catalysts*. Recueil des Travaux Chimiques des Pays-Bas, 1996. **115**(4): p. 217-221.
107. Jin, X., et al., *Synergistic Effects of Bimetallic PtPd/TiO₂ Nanocatalysts in Oxidation of Glucose to Glucaric Acid: Structure Dependent Activity and Selectivity*. Industrial & Engineering Chemistry Research, 2016. **55**(11): p. 2932-2945.
108. Megías-Sayago, C., et al., *Gold catalysts screening in base-free aerobic oxidation of glucose to gluconic acid*. Catalysis today, 2017. **279**: p. 148-154.
109. Cao, Y., et al., *Base-free oxidation of glucose to gluconic acid using supported gold catalysts*. Catalysis Science & Technology, 2015. **6**(1): p. 107-117.
110. Qi, P., et al., *Catalysis and reactivation of ordered mesoporous carbon-supported gold nanoparticles for the base-free oxidation of glucose to gluconic acid*. ACS Catalysis, 2015. **5**(4): p. 2659-2670.
111. Wang, Y., et al., *Insights into the stability of gold nanoparticles supported on metal oxides for the base-free oxidation of glucose to gluconic acid*. Green Chemistry, 2014. **16**(2): p. 719-726.
112. Rautiainen, S., et al., *Microwave-assisted base-free oxidation of glucose on gold nanoparticle catalysts*. Catalysis Communications, 2016. **74**: p. 115-118.
113. Wojcieszak, R., et al., *Advances in Base-Free Oxidation of Bio-Based Compounds on Supported Gold Catalysts*. Catalysts, 2017. **7**(11): p. 352.

114. Derrien, E., et al., *Aerobic oxidation of glucose to glucaric acid under alkaline-free conditions: Au-based bimetallic catalysts and effect of residues in a hemicellulose hydrolysate*. Industrial & Engineering Chemistry Research, 2017.
115. Thomas R. Boussie, E.L.D., Zachary M. Fresco, Vincent J. Murphy, James Shoemaker, Raymond Archer, Hong Jiang *Production of Adipic Acid and Derivatives from Carbohydrate-Containing Materials*. 2010, RENNOVIA Inc USA.
116. Vincent J. Murphy, J.S., Guang Zhu, Raymond Archer, George Frederick Salem, Eric L. Dias *Oxidation Catalysts*. 2011, RENNOVIA Inc USA.
117. Lee, J., B. Saha, and D.G. Vlachos, *Pt catalysts for efficient aerobic oxidation of glucose to glucaric acid in water*. Green Chemistry, 2016.
118. Smits, P., et al., *Lead modified platinum on carbon catalyst for the selective oxidation of (2-) hydroxycarbonic acids, and especially polyhydroxycarbonic acids to their 2-keto derivatives*. Applied catalysis, 1987. **33**(1): p. 83-96.
119. Sun, J. and H. Liu, *Selective hydrogenolysis of biomass-derived xylitol to ethylene glycol and propylene glycol on supported Ru catalysts*. Green Chemistry, 2011. **13**(1): p. 135-142.
120. Shmotin, V., et al., *Effect of iodine-containing promoter on the catalytic activity of silver in the course of ethylene glycol oxidation*. Russian journal of applied chemistry, 2006. **79**(9): p. 1458-1462.
121. Mamontov, G.V., et al., *Influence of phosphate addition on activity of Ag and Cu catalysts for partial oxidation of alcohols*. Catalysis today, 2013. **203**: p. 122-126.
122. Vodyankina, O.V., et al., *Selective oxidation of alcohols over Ag-containing Si₃N₄ catalysts*. Catalysis today, 2013. **203**: p. 127-132.

123. Case, J.M., *Gold catalysts prepared by ion exchange for use in ethylene glycol oxidation: An exploratory study*. 2009, University of Cape Town.
124. Griffin, M.B., et al., *The selective oxidation of ethylene glycol and 1, 2-propanediol on Au, Pd, and Au–Pd bimetallic catalysts*. *Journal of catalysis*, 2013. **307**: p. 111-120.
125. Mitsui-Chemicals, *JP,3748588,B*. 1995: Japan.
126. Berndt, H., et al., *Oxygen adsorption on Au/Al₂O₃ catalysts and relation to the catalytic oxidation of ethylene glycol to glycolic acid*. *Applied Catalysis A: General*, 2003. **244**(1): p. 169-179.
127. Prati, L. and M. Rossi, *Gold on carbon as a new catalyst for selective liquid phase oxidation of diols*. *Journal of Catalysis*, 1998. **176**(2): p. 552-560.
128. Bianchi, C.L., et al., *Gold on carbon: influence of support properties on catalyst activity in liquid-phase oxidation*. *Catalysis letters*, 2003. **85**(1-2): p. 91-96.
129. Porta, F., et al., *New Au (0) sols as precursors for heterogeneous liquid-phase oxidation catalysts*. *Journal of Catalysis*, 2002. **211**(2): p. 464-469.
130. Porta, F. and M. Rossi, *Gold nanostructured materials for the selective liquid phase catalytic oxidation*. *Journal of Molecular Catalysis A: Chemical*, 2003. **204**: p. 553-559.
131. Porta, F., et al., *Metal sols as a useful tool for heterogeneous gold catalyst preparation: reinvestigation of a liquid phase oxidation*. *Catalysis Today*, 2000. **61**(1-4): p. 165-172.
132. John, L.D., *Process for manufacture of glycolic acid*. 1939, Google Patents.
133. Kataoka, M., et al., *Glycolic acid production using ethylene glycol-oxidizing microorganisms*. *Bioscience, biotechnology, and biochemistry*, 2001. **65**(10): p. 2265-2270.

134. Matsumoto, T., et al., *CO 2-free power generation on an iron group nanoalloy catalyst via selective oxidation of ethylene glycol to oxalic acid in alkaline media*. Scientific reports, 2014. **4**: p. 5620.
135. Xia, T., et al., *Enhanced catalytic activities of NiPt truncated octahedral nanoparticles toward ethylene glycol oxidation and oxygen reduction in alkaline electrolyte*. ACS applied materials & interfaces, 2016. **8**(17): p. 10841-10849.
136. Berndt, H., et al., *Oxygen adsorption on Au/Al₂O₃ catalysts and relation to the catalytic oxidation of ethylene glycol to glycolic acid*. Applied Catalysis A: General, 2003. **244**(1): p. 169-179.
137. Van Haasterecht, T., et al., *Transformations of polyols to organic acids and hydrogen in aqueous alkaline media*. Catalysis Science & Technology, 2014. **4**(8): p. 2353-2366.
138. KHAN, M.I.A., et al., *Liquid-phase Oxidation of Ethylene Glycol on a Pt/C Catalyst. II. Kinetic Studies*. Chemical and Pharmaceutical Bulletin, 1983. **31**(6): p. 1827-1832.
139. Jin, X., et al., *Oxidation of Glycerol to Dicarboxylic Acids Using Cobalt Catalysts*. ACS Catalysis, 2016. **6**(7): p. 4576-4583.
140. Borodziński, A. and M. Bonarowska, *Relation between crystallite size and dispersion on supported metal catalysts*. Langmuir, 1997. **13**(21): p. 5613-5620.
141. Vojvodic, A., et al., *Exploring the limits: A low-pressure, low-temperature Haber–Bosch process*. Chemical Physics Letters, 2014. **598**: p. 108-112.
142. Dahl, S., et al., *Electronic factors in catalysis: the volcano curve and the effect of promotion in catalytic ammonia synthesis*. Applied Catalysis A: General, 2001. **222**(1-2): p. 19-29.

143. Yuan, Z.-F., et al., *NaOH alone can be a homogeneous catalyst for selective aerobic oxidation of alcohols in water*. Journal of Catalysis, 2017. **353**: p. 37-43.
144. Ouali, A., et al., *NaOH-Promoted Hydrogen Transfer: Does NaOH or Traces of Transition Metals Catalyze the Reaction?* ChemCatChem, 2009. **1**(4): p. 504-509.
145. Kwon, Y., et al., *Electrocatalytic oxidation of alcohols on gold in alkaline media: base or gold catalysis?* Journal of the American Chemical Society, 2011. **133**(18): p. 6914-6917.
146. Yentekakis, I., et al., *In situ controlled promotion of catalyst surfaces via NEMCA: the effect of Na on the Pt-catalyzed CO oxidation*. Journal of Catalysis, 1994. **146**(1): p. 292-305.
147. Harkness, I.R. and R.M. Lambert, *Chemisorption and reactivity of nitric oxide on Na-dosed platinum {111}*. Journal of the Chemical Society, Faraday Transactions, 1997. **93**(7): p. 1425-1429.
148. Ide, M.S. and R.J. Davis, *The important role of hydroxyl on oxidation catalysis by gold nanoparticles*. Accounts of chemical research, 2013. **47**(3): p. 825-833.
149. Zope, B.N., et al., *Reactivity of the gold/water interface during selective oxidation catalysis*. Science, 2010. **330**(6000): p. 74-78.
150. Chang, C.-R., et al., *A water-promoted mechanism of alcohol oxidation on a Au (111) surface: understanding the catalytic behavior of bulk gold*. Acs Catalysis, 2013. **3**(8): p. 1693-1699.
151. Alonso, D.M., S.G. Wettstein, and J.A. Dumesic, *Bimetallic catalysts for upgrading of biomass to fuels and chemicals*. Chemical Society Reviews, 2012. **41**(24): p. 8075-8098.

152. Jacobsen, C.J., et al., *Catalyst design by interpolation in the periodic table: bimetallic ammonia synthesis catalysts*. Journal of the American Chemical Society, 2001. **123**(34): p. 8404-8405.
153. Ravel, B. and M. Newville, *ATHENA, ARTEMIS, HEPHAESTUS: data analysis for X-ray absorption spectroscopy using IFEFFIT*. Journal of synchrotron radiation, 2005. **12**(4): p. 537-541.
154. Ketchie, W.C., M. Murayama, and R.J. Davis, *Promotional effect of hydroxyl on the aqueous phase oxidation of carbon monoxide and glycerol over supported Au catalysts*. Topics in Catalysis, 2007. **44**(1-2): p. 307-317.
155. Ramachandran, P. and R. Chaudhari, *Three-phase catalytic reactors*. Vol. 2. 1983: Gordon & Breach Science Pub.
156. Mears, D.E., *Tests for transport limitations in experimental catalytic reactors*. Industrial & Engineering Chemistry Process Design and Development, 1971. **10**(4): p. 541-547.
157. Wang, J.-P., *FePt magnetic nanoparticles and their assembly for future magnetic media*. Proceedings of the IEEE, 2008. **96**(11): p. 1847-1863.
158. Kotobuki, M., et al., *XAFS Characterization of Pt-Fe/zeolite Catalysts for Preferential Oxidation of CO in Hydrogen Fuel Gases*. Catalysis Letters, 2005. **103**(3): p. 263-269.
159. Vannice, M.A. and R.L. Garten, *The synthesis of hydrocarbons from CO and H₂ over well-characterized supported PtFe catalysts*. Journal of Molecular Catalysis, 1976. **1**(3): p. 201-222.
160. Xu, H., et al., *Highly active Pt-Fe bicomponent catalysts for CO oxidation in the presence and absence of H₂*. Energy & Environmental Science, 2012. **5**(4): p. 6313-6320.

161. Nørskov, J.K., et al., *Towards the computational design of solid catalysts*. Nature chemistry, 2009. **1**(1): p. 37.
162. Stamenkovic, V., et al., *Changing the activity of electrocatalysts for oxygen reduction by tuning the surface electronic structure*. Angewandte Chemie, 2006. **118**(18): p. 2963-2967.
163. Su, H.-Y., et al., *Structure evolution of Pt-3d transition metal alloys under reductive and oxidizing conditions and effect on the CO oxidation: a first-principles study*. Catalysis today, 2011. **165**(1): p. 89-95.
164. Kotobuki, M., et al., *Reaction mechanism of preferential oxidation of carbon monoxide on Pt, Fe, and Pt-Fe/mordenite catalysts*. Journal of Catalysis, 2005. **236**(2): p. 262-269.
165. Solmi, S., et al., *Oxidation of d-Glucose to Glucaric Acid Using Au/C Catalysts*. ChemCatChem, 2017. **9**(14): p. 2797-2806.
166. Wojcieszak, R., et al., *Selective oxidation of glucose to glucuronic acid by cesium-promoted gold nanoparticle catalyst*. Journal of Molecular Catalysis A: Chemical, 2016. **422**: p. 35-42.
167. Tauster, S., S. Fung, and R.L. Garten, *Strong metal-support interactions. Group 8 noble metals supported on titanium dioxide*. Journal of the American Chemical Society, 1978. **100**(1): p. 170-175.
168. Dulub, O., W. Hebenstreit, and U. Diebold, *Imaging cluster surfaces with atomic resolution: the strong metal-support interaction state of Pt supported on TiO₂ (110)*. Physical Review Letters, 2000. **84**(16): p. 3646.

169. Bruix, A., et al., *A New Type of Strong Metal–Support Interaction and the Production of H₂ through the Transformation of Water on Pt/CeO₂ (111) and Pt/CeO_x/TiO₂ (110) Catalysts*. Journal of the American Chemical Society, 2012. **134**(21): p. 8968-8974.
170. Lewera, A., et al., *Metal–support interactions between nanosized Pt and metal oxides (WO₃ and TiO₂) studied using X-ray photoelectron spectroscopy*. The Journal of Physical Chemistry C, 2011. **115**(41): p. 20153-20159.
171. Lisiecki, I., *Size, shape, and structural control of metallic nanocrystals*. 2005, ACS Publications.
172. Zeng, X.-M., et al., *High-index-faceted platinum nanoparticles: insights into structural and thermal stabilities and shape evolution from atomistic simulations*. Journal of Materials Chemistry A, 2014. **2**(29): p. 11480-11489.
173. Khan, I.A., et al., *Fabrication of highly stable and efficient PtCu alloy nanoparticles on highly porous carbon for direct methanol fuel cells*. ACS applied materials & interfaces, 2016. **8**(32): p. 20793-20801.
174. Zhou, S., et al., *Pt–Cu core–shell and alloy nanoparticles for heterogeneous NO_x reduction: anomalous stability and reactivity of a core–shell nanostructure*. Angewandte Chemie International Edition, 2005. **44**(29): p. 4539-4543.
175. Lopes, T., E. Antolini, and E. Gonzalez, *Carbon supported Pt–Pd alloy as an ethanol tolerant oxygen reduction electrocatalyst for direct ethanol fuel cells*. international journal of hydrogen energy, 2008. **33**(20): p. 5563-5570.
176. Lee, Y.-W., et al., *Octahedral Pt-Pd alloy catalysts with enhanced oxygen reduction activity and stability in proton exchange membrane fuel cells*. RSC Advances, 2012. **2**(3): p. 1119-1125.

177. Oezaslan, M., F. Hasché, and P. Strasser, *PtCu₃, PtCu and Pt₃Cu alloy nanoparticle electrocatalysts for oxygen reduction reaction in alkaline and acidic media*. Journal of The Electrochemical Society, 2012. **159**(4): p. B444-B454.
178. Liao, Y., et al., *Composition-tunable PtCu alloy nanowires and electrocatalytic synergy for methanol oxidation reaction*. The Journal of Physical Chemistry C, 2016. **120**(19): p. 10476-10484.
179. Oezaslan, M., F. Hasché, and P. Strasser, *In situ observation of bimetallic alloy nanoparticle formation and growth using high-temperature XRD*. Chemistry of Materials, 2011. **23**(8): p. 2159-2165.
180. Huang, J., et al., *The effect of the support on the surface composition of PtCu alloy nanocatalysts: In situ XPS and HS-LEIS studies*. Chinese Journal of Catalysis, 2017. **38**(7): p. 1229-1236.
181. Kang, Y. and C.B. Murray, *Synthesis and electrocatalytic properties of cubic Mn–Pt nanocrystals (nanocubes)*. Journal of the American Chemical Society, 2010. **132**(22): p. 7568-7569.
182. Ye, H., et al., *Polyvinylpyrrolidone (PVP)-Capped Pt nanocubes with superior peroxidase-Like activity*. ChemNanoMat, 2017. **3**(1): p. 33-38.
183. Bratlie, K.M., et al., *Platinum nanoparticle shape effects on benzene hydrogenation selectivity*. Nano letters, 2007. **7**(10): p. 3097-3101.
184. Kang, Y., et al., *Shape-controlled synthesis of Pt nanocrystals: the role of metal carbonyls*. ACS nano, 2012. **7**(1): p. 645-653.

185. Li, C., T. Sato, and Y. Yamauchi, *Electrochemical synthesis of one-dimensional mesoporous Pt nanorods using the assembly of surfactant micelles in confined space*. Angewandte Chemie International Edition, 2013. **52**(31): p. 8050-8053.
186. Zhu, C., S. Guo, and S. Dong, *PdM (M= Pt, Au) Bimetallic Alloy Nanowires with Enhanced Electrocatalytic Activity for Electro-oxidation of Small Molecules*. Advanced Materials, 2012. **24**(17): p. 2326-2331.
187. Li, C., et al., *Composition-driven shape evolution to Cu-rich PtCu octahedral alloy nanocrystals as superior bifunctional catalysts for methanol oxidation and oxygen reduction reaction*. Nanoscale, 2018. **10**(10): p. 4670-4674.
188. Lu, B.-A., et al., *Octahedral PtCu alloy nanocrystals with high performance for oxygen reduction reaction and their enhanced stability by trace Au*. Nano Energy, 2017. **33**: p. 65-71.
189. Jin, M., et al., *Palladium nanocrystals enclosed by {100} and {111} facets in controlled proportions and their catalytic activities for formic acid oxidation*. Energy & Environmental Science, 2012. **5**(4): p. 6352-6357.
190. Narayanan, R. and M.A. El-Sayed, *Shape-dependent catalytic activity of platinum nanoparticles in colloidal solution*. Nano letters, 2004. **4**(7): p. 1343-1348.
191. Lee, I., et al., *Synthesis of heterogeneous catalysts with well shaped platinum particles to control reaction selectivity*. Proceedings of the National Academy of Sciences, 2008. **105**(40): p. 15241-15246.
192. Si, R. and M. Flytzani-Stephanopoulos, *Shape and crystal-plane effects of nanoscale ceria on the activity of Au-CeO₂ catalysts for the water-gas shift reaction*. Angewandte Chemie International Edition, 2008. **47**(15): p. 2884-2887.

193. Wang, C., et al., *A general approach to the size-and shape-controlled synthesis of platinum nanoparticles and their catalytic reduction of oxygen*. Angewandte Chemie International Edition, 2008. **47**(19): p. 3588-3591.
194. Yu, J., et al., *Enhanced photocatalytic CO₂-reduction activity of anatase TiO₂ by coexposed {001} and {101} facets*. Journal of the American Chemical Society, 2014. **136**(25): p. 8839-8842.
195. Cao, S., et al., *Size-and shape-dependent catalytic performances of oxidation and reduction reactions on nanocatalysts*. Chemical Society Reviews, 2016. **45**(17): p. 4747-4765.
196. Science, A.A.f.t.A.o., *Platinum Nanocrystals with High-Index Facets*. Science, 2007. **316**(5825): p. 657-657.
197. Shi, H., et al., *Oxidation of Glucose using Mono and Bimetallic Catalysts in Base Free Conditions*. Organic Process Research & Development, 2018.
198. Derrien, E., et al., *Aerobic Oxidation of Glucose to Glucaric Acid under Alkaline-Free Conditions: Au-Based Bimetallic Catalysts and the Effect of Residues in a Hemicellulose Hydrolysate*. Industrial & Engineering Chemistry Research, 2017. **56**(45): p. 13175-13189.
199. Lee, J., B. Saha, and D.G. Vlachos, *Pt catalysts for efficient aerobic oxidation of glucose to glucaric acid in water*. Green Chemistry, 2016. **18**(13): p. 3815-3822.
200. Luo, M., et al., *Facile removal of polyvinylpyrrolidone (PVP) adsorbates from Pt alloy nanoparticles*. Journal of Materials Chemistry A, 2015. **3**(6): p. 2770-2775.
201. Kumar, P.S., et al., *High-yield synthesis and optical response of gold nanostars*. Nanotechnology, 2007. **19**(1): p. 015606.

202. Kresse, G. and J. Furthmüller, *Efficiency of ab-initio total energy calculations for metals and semiconductors using a plane-wave basis set*. Computational materials science, 1996. **6**(1): p. 15-50.
203. Vanderbilt, D., *Soft self-consistent pseudopotentials in a generalized eigenvalue formalism*. Physical Review B, 1990. **41**(11): p. 7892.
204. Monkhorst, H.J. and J.D. Pack, *Special points for Brillouin-zone integrations*. Physical review B, 1976. **13**(12): p. 5188.
205. Hammer, B., L.B. Hansen, and J.K. Nørskov, *Improved adsorption energetics within density-functional theory using revised Perdew-Burke-Ernzerhof functionals*. Physical Review B, 1999. **59**(11): p. 7413.
206. Wang, S., et al., *Universal transition state scaling relations for (de) hydrogenation over transition metals*. Physical Chemistry Chemical Physics, 2011. **13**(46): p. 20760-20765.
207. Grabow, L.C., et al., *Descriptor-based analysis applied to HCN synthesis from NH₃ and CH₄*. Angewandte Chemie International Edition, 2011. **50**(20): p. 4601-4605.
208. Medford, A.J., et al., *CatMAP: a software package for descriptor-based microkinetic mapping of catalytic trends*. Catalysis Letters, 2015. **145**(3): p. 794-807.
209. NIST, *NIST Computational Chemistry Comparison and Benchmark Database*. 2016.
210. Hammer, B., *Coverage dependence of N₂ dissociation at an N, O, or H precovered Ru (0001) surface investigated with density functional theory*. Physical Review B, 2001. **63**(20): p. 205423.

211. Mhadeshwar, A., et al., *The Role of Adsorbate–Adsorbate Interactions in the Rate Controlling Step and the Most Abundant Reaction Intermediate of NH₃ Decomposition on Ru*. Catalysis Letters, 2004. **96**(1-2): p. 13-22.
212. Lausche, A.C., et al., *On the effect of coverage-dependent adsorbate–adsorbate interactions for CO methanation on transition metal surfaces*. Journal of catalysis, 2013. **307**: p. 275-282.
213. Xu, Y., et al., *In silico search for novel methane steam reforming catalysts*. New Journal of Physics, 2013. **15**(12): p. 125021.
214. Schumann, J., et al., *Selectivity of synthesis gas conversion to C₂+ oxygenates on fcc (111) transition-metal surfaces*. ACS Catalysis, 2018. **8**(4): p. 3447-3453.
215. Jalid, F., et al., *Understanding trends in hydrodeoxygenation reactivity of metal and bimetallic alloy catalysts from ethanol reaction on stepped surface*. Journal of catalysis, 2017. **353**: p. 265-273.
216. Khan, T.S., F. Jalid, and M.A. Haider, *First-principle microkinetic modeling of ethanol dehydrogenation on metal catalyst surfaces in non-oxidative environment: design of bimetallic alloys*. Topics in Catalysis, 2018. **61**(18-19): p. 1820-1831.
217. Carrettin, S., et al., *Oxidation of glycerol using supported Pt, Pd and Au catalysts*. Physical Chemistry Chemical Physics, 2003. **5**(6): p. 1329-1336.
218. Hibbitts, D. and M. Neurock, *Promotional effects of chemisorbed oxygen and hydroxide in the activation of C–H and O–H bonds over transition metal surfaces*. Surface Science, 2016. **650**: p. 210-220.
219. Demirel-Gülen, S., M. Lucas, and P. Claus, *Liquid phase oxidation of glycerol over carbon supported gold catalysts*. Catalysis Today, 2005. **102**: p. 166-172.

220. Kim, T.S., et al., *Water activated by atomic oxygen on Au (111) to oxidize CO at low temperatures*. Journal of the American Chemical Society, 2006. **128**(19): p. 6282-6283.
221. Jones, G., *Origin of catalytic activity in sponge Ni catalysts for hydrogenation of carbonyl compounds*. Catalysis, Structure & Reactivity, 2015. **1**(2): p. 78-87.
222. Oja, V. and E. Suuberg, *Vapor pressures and enthalpies of sublimation of D-glucose, D-xylose, cellobiose, and levoglucosan*. Journal of Chemical & Engineering Data, 1999. **44**(1): p. 26-29.

Appendix

Appendix I Supplementary Information for Chapter 2

Methodology of Density Functional Theory Calculations

The adsorption energies of the intermediates on the transition metals were calculated using plane wave density functional theory (DFT) code as implemented in Vienna ab initio simulation package (VASP-5.3.5version).[202] The core electrons were described using Vanderbilt ultrasoft pseudopotentials.[203] Kohn Sham one electron valence states were expanded in a plane wave basis function which was truncated at a cut-off energy of 396 eV. A Monkhorst-Pack k point grid with 3 x 3 x 1 mesh was used to sample the Brillouin zones.[204] Revised Perdew-Burke-Ernzerhof (RPBE) exchange correlation functional developed by Hammer et al.[205] was used. Different configurations of the adsorbates were studied and configuration with lowest energy was taken as the most stable configuration as reported in Section 4 and 5 of the supporting information (SI). The convergence criteria for force and energy were set to 0.05 eV/Å and 10⁻⁴ eV respectively.

Methodology of Ab-initio Microkinetic Modeling

A comprehensive MKM was developed using the reaction energetics obtained from DFT calculations on (111) surface of the transition metals; Au, Ag, Cu, Pt, Pd, Rh, Ru and Fe. DFT calculated energies of all reactants, intermediates and products were referenced to gas phase methane (CH₄), water (H₂O) and hydrogen (H₂) molecules and are given in Section 5 of SI. Energy of the transition state (E^{TS}) was calculated using the transition state scaling relationship ($E^{TS} = \gamma \sum E_{diss} + \beta$) with γ and β as the linear parameters as reported by Wang et al.[206] and Grabow et al.[207] for different bond dissociations. An error bar of 0.2 eV was used for interpreting trends

in binding energies of C and O, as suggested by Norskov et al.[208] A mean field descriptor-based approach was applied to construct the kinetic model without assuming a rate determining step. The governing differential equations for all the elementary steps (in Section 1 of SI) were solved using a multidimensional Newton's root finding method from the python mpmath library to obtain the steady state solution. Further details about the MKM methodology are available in previously reported work of Grabow et al.[207] and Medford et al.[208] Frozen adsorbate assumption was taken which ensured negligible change in entropy for the surface reaction steps. Shomate gas parameters for the gaseous species were obtained from the NIST database.[209] The model included two different sites for adsorption, one for hydrogen and another for all other adsorbates. Adsorbed hydrogen was assumed not to compete for the surface sites because of small size and negligible interaction to itself and other adsorbates, as proposed by Hammer [210], Vlachos [211], Norskov and co-workers. [212-214] The ratio of hydrogen sites (H-site) and terrace sites was considered to be 1. The energetics of the H-site is same as the (111) terrace sites. Similar model for hydrogen adsorption have been successfully employed by us for hydro-deoxygenation and dehydrogenation reactions.[215, 216] Microkinetic model was run at a temperature of 473 K and atmospheric pressure ($P = 1$ bar) with a stoichiometric flow of ethylene glycol and oxygen. A sample MKM script have been shown in the SI section S3.

Results of Density Functional Theory (DFT) Calculations.

A MKM was developed to explain the trend in reactivity of monometallic activity of selective oxidation of ethylene glycol to glycolic acid and oxalic acid on various transition metal surfaces. The reaction can proceed by either initial O-H bond cleavage or initial C-H bond cleavage for further oxidation to take place.[217] Using DFT calculations, Neurock and co-workers[218] showed that the activation barrier for initial O-H bond scission was lower than that of C-H bond

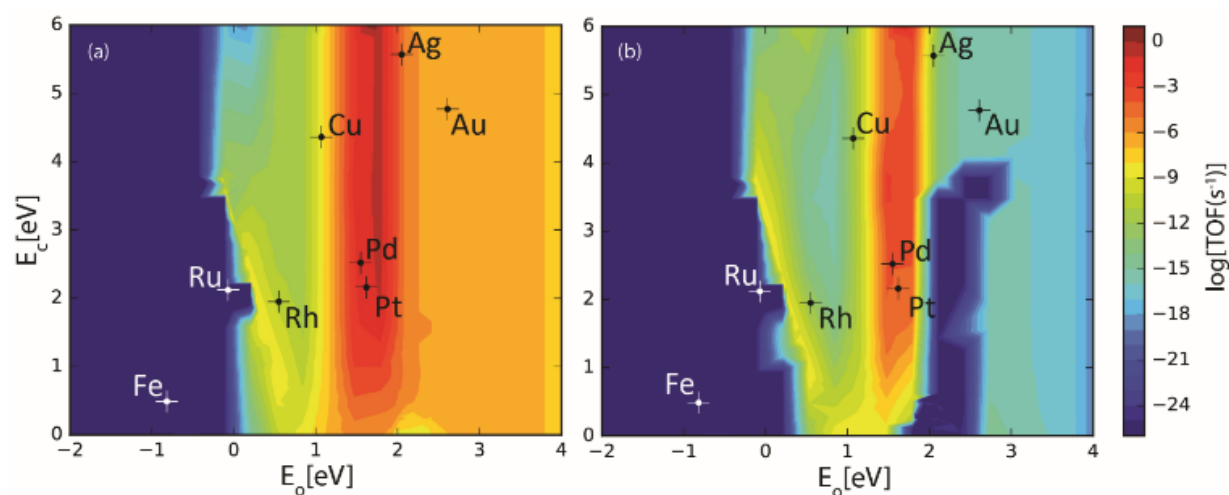
scission in ethanol oxidation on Pt and Au surfaces. Present work followed a similar mechanism where oxidation of EG proceeds by the initial H abstraction from a terminal O atom as shown in the reaction scheme diagram, Figure 2.[127, 149, 154, 219] Further H abstraction from C and addition of hydroxyl results in the primary oxidation product; i.e., glycolic acid which on further oxidation gives oxalic acid. The role of water in the formation of surface hydroxyl is reported by Kim et al.[220] for CO oxidation and by Davis et al.[154] for glycerol oxidation where the formation of surface hydroxyl takes place via a peroxide intermediate. The MKM model used in this work followed an identical approach for generation of OH by combining H_2O and O_2 as illustrated in SI-1 of SI. The adsorption energies of all intermediates were scaled in terms of the binding energies of C (E_C) and O (E_O) as suggested by Jones et al.[221] and Abild-Pedersen et al.[207] This gives the TOFs of the reaction products on all metal catalysts in terms of the energies of the two descriptors, thereby reducing the descriptor space to two variables. C and O binding energies were used as descriptors for the reaction because all the adsorbates bind either through C or O or both (shown in SI-4 of SI) making them a suitable choice for descriptors.

Steady state solution of the MKM model gave rates of production of the two products; glycolic acid and oxalic acid at 473 K as a function of E_C and E_O as shown in Figure 3. Theoretical maximum turnover of glycolic acid that can be achieved at the given reaction conditions was calculated to be 3.14sec^{-1} at $E_C = 6\text{ eV}$ and $E_O = 1.67\text{ eV}$. Although, none of the metals lied at the Sabatier maxima; Pt and Pd showed highest glycolic acid TOF ($\sim 10^{-1}\text{ sec}^{-1}$) among all the transition metals studied. Experiments under alkaline conditions also showed high TOFs of glycolic acid on Pt (TOF= 0.83 sec^{-1}) and Pd (TOF= 0.32 sec^{-1}). Noble metals, Ag and Au showed moderate reactivity with TOF $\sim 10^{-5}\text{ sec}^{-1}$ and 10^{-7} sec^{-1} respectively. Both experiments and computational simulations suggested Ag as the potential catalyst for the oxidation reaction after Pt and Pd.

Negligible TOFs values of $\sim 10^{-8}$ and $10^{-11} \text{ sec}^{-1}$ were observed for glycolic acid on transition metals like Cu and Rh respectively. High binding metals like Fe and Ru showed negligible production rates for both glycolic and oxalic acid because of desorption limitations.

Figure A - 1. Production rate for (a) Glycolic acid (b) Oxalic acid as a function of C and O binding energies at 473 K and 1 bar (50% Ethylene Glycol and 50% Oxygen). Error bar = 0.2 eV

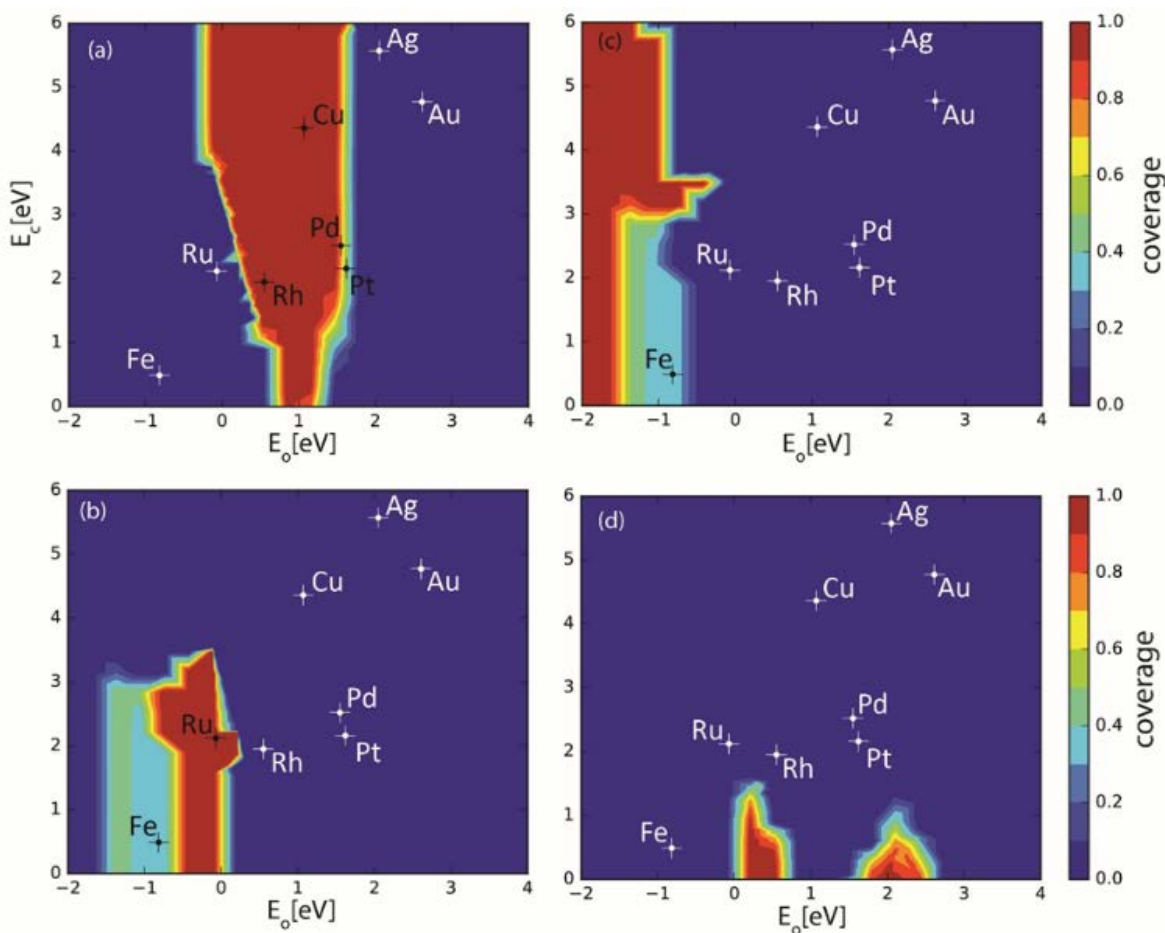
In order to understand the activity trends of the transition metals, detailed coverage analysis



was performed and coverage plots of the most abundant surface intermediates has been shown in Figure 4. Among all the adsorbates only O, OCHCO, OOH were found to have appreciable coverage over the transition metals. Among the transition metals; Rh and Cu were found to display full coverage ~ 1 monolayer (ML) by oxygen, while Pt and Pd also displayed partial albeit still significant coverage (> 0.4 ML) as can be seen in Figure 4 (a). Other transition metals studied here (Au, Ag, Ru and Fe), display negligible coverage of oxygen. As seen in Figure 2(b), only Ru and Fe showed significant coverage of OCHCO species, with Ru showing full coverage (~ 1 ML) and Fe displaying partial (~ 0.3 ML) coverage of OCHCHO. Similar coverage of OOH (~ 0.3 ML) was also observed over Fe, while the remaining transition metals displayed negligible OOH

coverage, as can be seen in Figure 4 (c). Coverage of H over the transition metal surface was negligible as can be seen in Figure 4 (d).

Figure A - 2. Coverage of (a) O (b) OCHCO (c) OOH (d) H as a function of C and O binding



energies at 473 K and 1 bar (50% Ethylene Glycol and 50% Oxygen). Error bar = 0.2 eV

Figure 5 illustrates the selectivity trends for both glycolic acid and oxalic acid. All the transition metals studied showed greater selectivity (> 0.9) for glycolic acid over oxalic acid. Although Pt and Pd showed moderate production rates for oxalic acid (TOF $\sim 10^{-5}$ and 10^{-4} sec^{-1} respectively), the mono acid selectivity (~ 1) was significantly high.

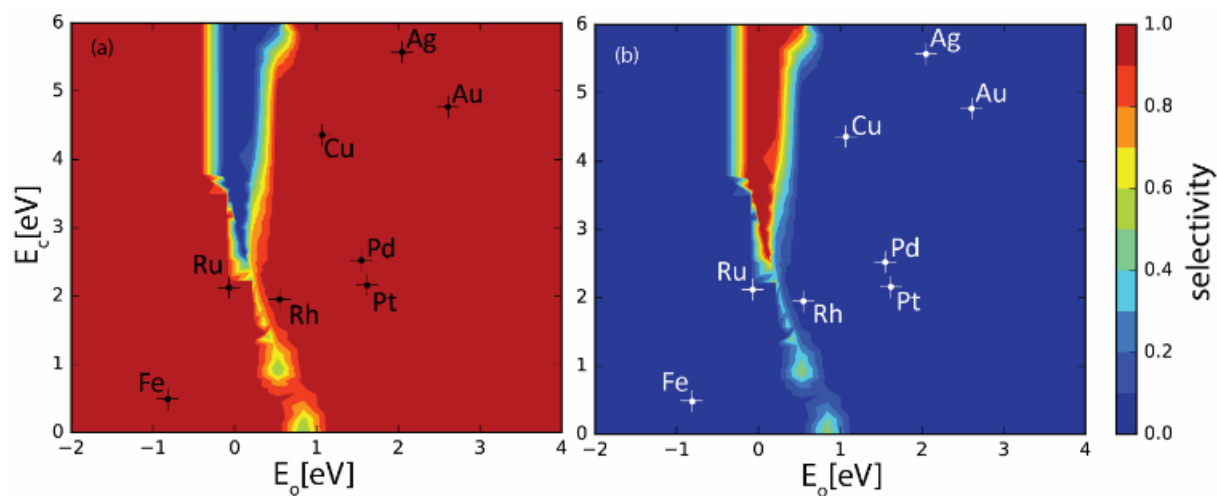


Figure A - 3. Selectivity for (a) Glycolic acid (b) Oxalic acid as a function of C and O binding energies at 473 K and 1 bar (50% Ethylene Glycol and 50% Oxygen). Error bar = 0.2 eV.

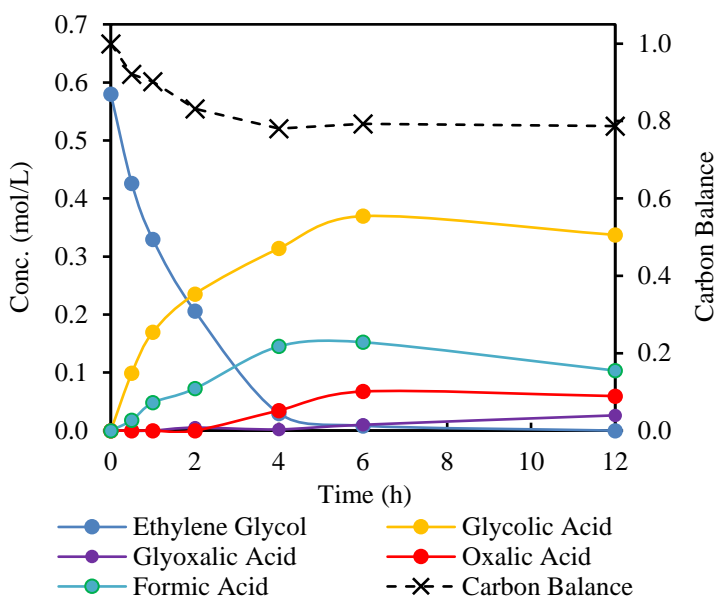


Figure A - 4. Concentration-time profile of testing Pt-Mn/CeO₂ catalysts on the reaction of ethylene glycol oxidation

Appendix II Supplementary Information for Chapter 3

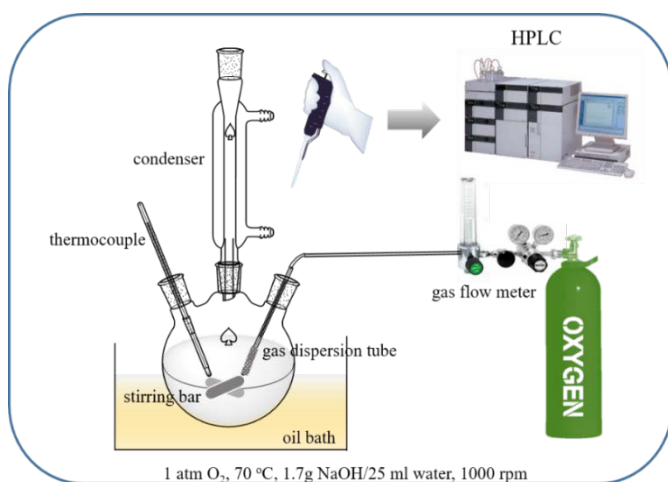


Figure A - 5. Oxidation experimental set-up under ambient O₂ pressure

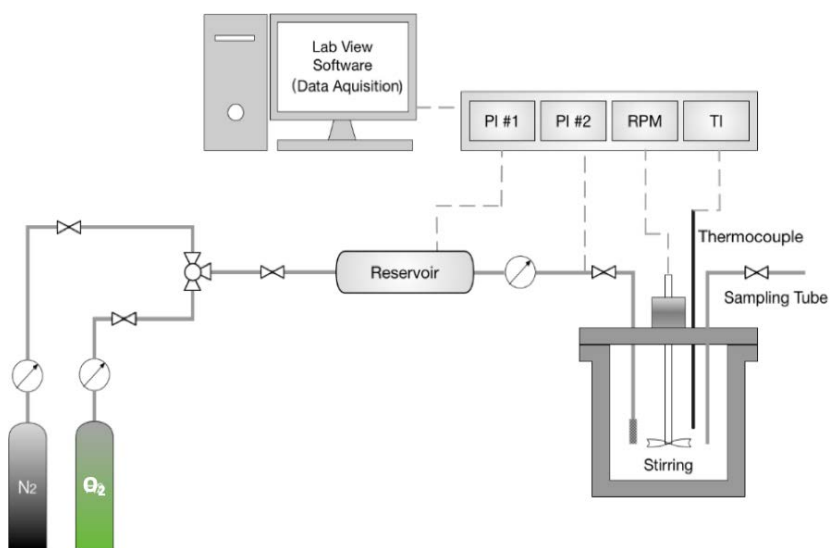
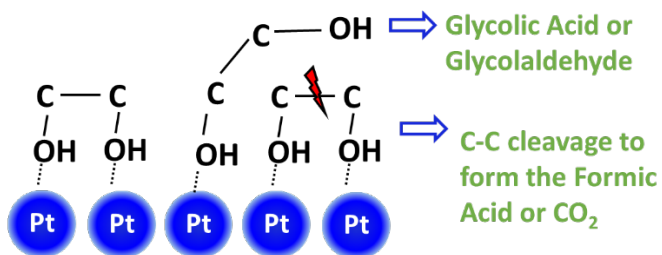


Figure A - 6. Stirred semi-batch slurry reactor for the parametric effect studies

Moderate Amount of Base



Large Amount of Base

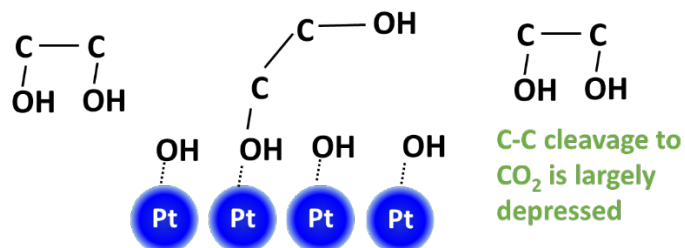


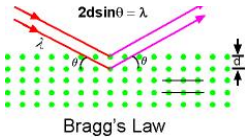
Figure A - 7. Scheme of base effect on product distribution



Figure A - 8. CaCO_3 precipitation to prove the $\text{CO}_2/\text{CO}_3^{2-}$ formation in the reaction with significant carbon balance loss. Test procedure is to add clear CaCl_2 aqueous solution to the centrifuged reaction solution after one batch of oxidation experiment.

Table A - 1. Details of XRD calculations to identify the Pt-Fe alloy structure

FCT structure									
a	0.379	nm							
c	0.370	nm							
λ	0.154	nm							

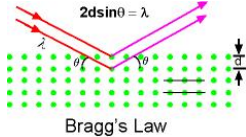


Bragg's Law

• Tetragonal:

$$\frac{1}{d^2} = \frac{h^2 + k^2}{a^2} + \frac{l^2}{c^2}$$

h	k	l	(h ² +k ²)/a ² + l ² /c ²	PtFe (FCC) - d	sin(θ)	θ	2θ	sin ² (θ)/((h ² +k ²)/a ² + l ² /c ²)
1	0	0	7.0	0.379	0.203	11.74	23.48	0.005929
1	1	0	14.0	0.268	0.288	16.72	33.45	0.005929
1	1	1	21.2	0.217	0.355	20.80	41.59	0.005929
2	0	0	27.9	0.189	0.407	24.01	48.02	0.005929
0	0	2	29.2	0.185	0.416	24.58	49.17	0.005929
2	0	1	35.2	0.169	0.457	27.19	54.39	0.005929
1	1	2	43.1	0.152	0.506	30.39	60.77	0.005929
2	2	0	55.8	0.134	0.575	35.13	70.26	0.005929
2	0	2	57.1	0.132	0.582	35.59	71.17	0.005929
2	2	1	63.1	0.126	0.612	37.73	75.45	0.005929
1	3	0	69.8	0.120	0.643	40.04	80.09	0.005929
3	1	1	77.0	0.114	0.676	42.54	85.09	0.005929
1	1	3	79.6	0.112	0.687	43.40	86.81	0.005929
2	2	2	85.0	0.108	0.710	45.24	90.48	0.005929
								constant



Bragg's Law

• Cubic:

$$\frac{1}{d^2} = \frac{h^2 + k^2 + l^2}{a^2}$$

h	k	l	h ² +k ² +l ²	PtFe (FCC) - d	sin(θ)	θ	2θ	sin ² (θ)/(h ² +k ² +l ²)
1	0	0	1	0.386	0.199	11.51	23.02	0.039793015
1	1	0	2	0.273	0.282	16.39	32.79	0.039793015
1	1	1	3	0.223	0.346	20.22	40.45	0.039793015
2	0	0	4	0.193	0.399	23.53	47.05	0.039793015
2	2	0	8	0.136	0.564	34.37	68.73	0.039793015
3	1	1	11	0.116	0.662	41.44	82.89	0.039793015
2	2	2	12	0.111	0.691	43.73	87.47	0.039793015
4	0	0	16	0.097	0.798	52.96	105.92	0.039793015
								constant

The conversion of EG and selectivity of products were calculated using the following formulas:

$$N_{surface\ metal} = \frac{catalyst\ weight \cdot bulk\ metal\ content(\%)}{metal\ molecular\ mass} \cdot metal\ dispersion\ (\%)$$

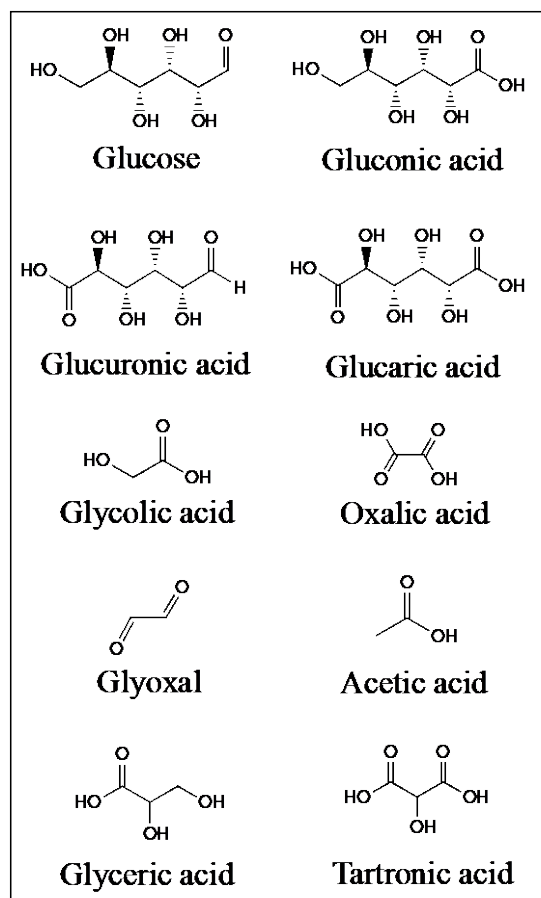
$$Conversion = \frac{C_{i,EG} - C_{f,EG}}{C_{i,EG}}$$

$$Selectivity = \frac{C_{f,p}}{C_{c,EG}}$$

$$Carbon\ balance = \frac{\sum C_{f,p} + C_{f,EG}}{C_{i,EG}}$$

$$Initial\ TOF = \frac{N_{c,EG}}{N_{surface\ metal} \cdot Time}$$

where, $C_{i,EG}$, $C_{f,EG}$, $C_{c,EG}$ represent the number of carbons in the initial EG, final EG and converted EG respectively, in the unit of mol; $C_{f,p}$ represents the carbon numbers in the final products, in the unit of mol; $N_{c,EG}$ is the mole of converted EG and $N_{surface\ metal}$ is the mole of Pt exposed on the catalyst surface

Appendix III Supplementary Information for Chapter 4**Figure A - 9.** Molecular structure of glucose and its derived products

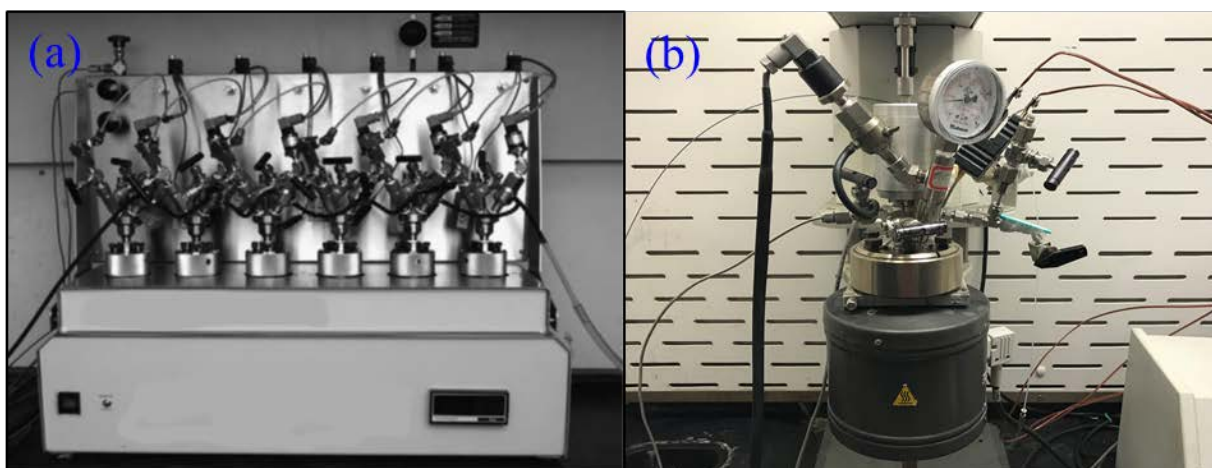


Figure A - 10. Oxidation reaction setup (a) Parr multiple reactors for catalyst performance tests (b) 100 ml semi-batch reactor for future kinetics study



Figure A - 11. (1) Mono-Pt catalyst and (2) bimetallic Pt-Pd catalysts prepared by the WC-2 method using NaBH_4 ; the metal particles were washed off from the TiO_2 -a support during centrifugation-washing procedure.

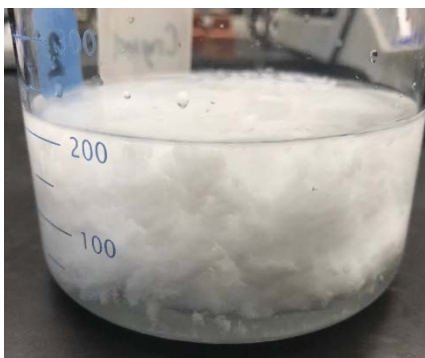


Figure A - 12. CaCO_3 precipitation to prove the CO_2 formation in the reactor outlet gas. Test procedure is to bubble reactor outlet gas slowly in NaOH aqueous solution, then add CaCl_2 aqueous solution.

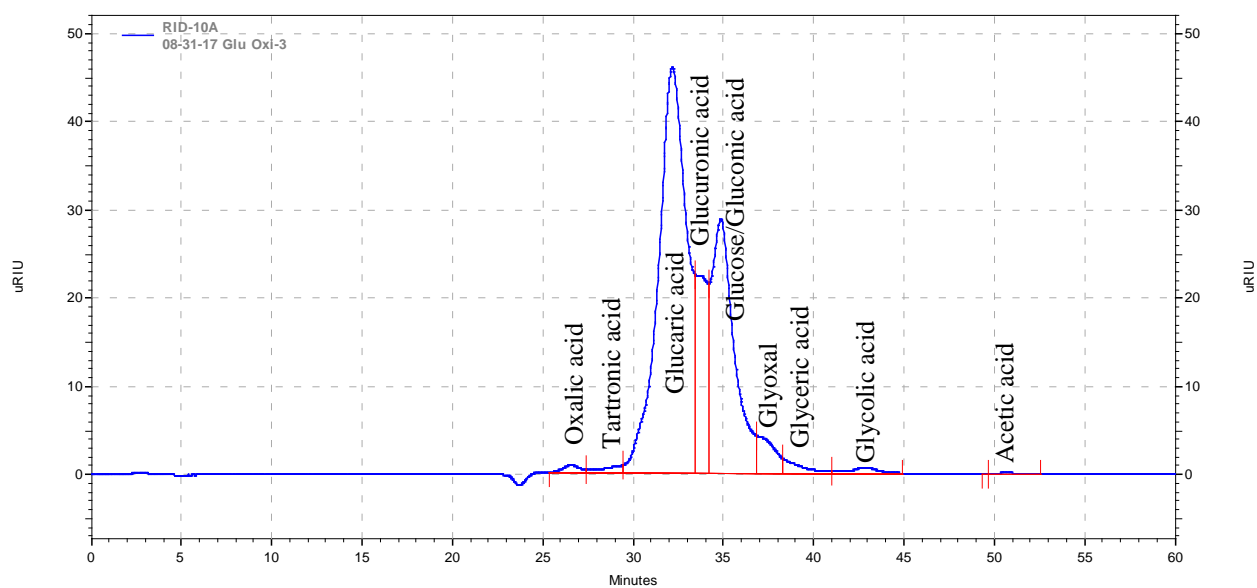


Figure A - 13. Example of the liquid products compositional analysis using the HPLC. Analysis conditions: Shodex SUGAR Series® 6 μm SH1011 HPLC column; column temperature 70 $^\circ\text{C}$, 0.005N H_2SO_4 aqueous solution as the mobile phase

Interphase Mass Transfer Limitation for Oxygen

(1) Gas-Liquid Mass Transfer Limitation: (Three phase catalytic reactors, Ramachandran & Chaudhari, 1983; J. Catal. 2008, 257, 1-4; J. Chem Eng Data. 1984, 29, 286-287; Hydrometallurgy 1998, 48, 327–342; Chem. Eng. Process, 2004, 43, 823-ss830)

$$\frac{R_{oxidation} \cdot d_{bubble}}{6 \cdot \varepsilon \cdot k_{g-l} \cdot C_{O_2,l}} = \frac{0.103 \left(\frac{kmol}{m^3 \cdot h} \right) \times 0.000002 (m)}{6 \times 0.09 \times 1.44 \left(\frac{m}{h} \right) \times 0.0195 \left(\frac{kmol}{m^3} \right)} = 1.36 \times 10^{-5} < 0.1$$

(2) Liquid-Solid Mass Transfer Limitation: (Three phase catalytic reactors, Ramachandran & Chaudhari, 1983; J. Catal. 2008, 257, 1-4; TiO₂ nanopowder (assume d_p is 100 nm))

$$\frac{R_{oxidation} \cdot \rho_p \cdot d_p}{6 \cdot \omega_{cat} \cdot k_{l-s} \cdot C_{O_2,l}} = \frac{0.103 \left(\frac{kmol}{m^3 \cdot h} \right) \times 3.9 \times 10^3 \left(\frac{kg}{m^3} \right) \times 10^{-7} m}{6 \times 2 \left(\frac{kg}{m^3} \right) \times 72.1 \left(\frac{m}{h} \right) \times 0.0195 \left(\frac{kmol}{m^3} \right)} = 2.38 \times 10^{-6} < 0.1$$

(3) Internal Diffusion: (Three phase catalytic reactors, Ramachandran & Chaudhari, 1983; J. Catal. 2008, 257, 1-4; Perry's Handbook: Table 5-16)

$$\frac{R_{oxidation} \cdot \rho_p \cdot d_p}{6 \cdot \omega_{cat} \cdot De \cdot C_{O_2,l}} = \frac{0.103 \left(\frac{kmol}{m^3 \cdot h} \right) \times 3.9 \times 10^3 \left(\frac{kg}{m^3} \right) \times (10^{-7} m)^2}{4 \times 2 \left(\frac{kg}{m^3} \right) \times 0.094 \left(\frac{m^2}{h} \right) \times 0.0195 \left(\frac{kmol}{m^3} \right)} = 1.74 \times 10^{-10} < 1$$

Interphase Mass Transfer Limitation for Glucose

(1) **Liquid-Solid Mass Transfer Limitation:** (AIChE J. 1980, 26, 177-201; J. Catal. 2008, 1-4;

Perry's Handbook: Table 5-16); TiO₂ nanopowder (assume d_p is 100 nm)

$$\frac{R_{oxidation} \cdot \rho_p \cdot d_p}{6 \cdot \omega_{cat} \cdot k_{l-s} \cdot C_{glucose}} = \frac{0.103 \left(\frac{kmol}{m^3 \cdot h} \right) \times 3.9 \times 10^3 \left(\frac{kg}{m^3} \right) \times 10^{-7} m}{6 \times 2 \left(\frac{kg}{m^3} \right) \times 0.1 \left(\frac{m}{h} \right) \times 0.222 \left(\frac{kmol}{m^3} \right)} = 1.51 \times 10^{-4} < 0.1$$

(2) **Intraparticle Transfer Limitation:** (AIChE J. 1980, 26, 177-201; AIChE J. DOI:

10.1002/aic.15114; Three phase catalytic reactors, Ramachandran & Chaudhari, 1983)

$$\frac{10^{-7} m}{6} \cdot \left(\frac{(m+1) \cdot R_{oxidation} \cdot \rho_p}{2 \cdot \omega_{cat} \cdot De \cdot C_{glucose}} \right)^{0.5} = \frac{0.103 \left(\frac{kmol}{m^3 \cdot h} \right) \times 3.9 \times 10^3 \left(\frac{kg}{m^3} \right) \times (10^{-7} m)^2}{4 \times 2 \left(\frac{kg}{m^3} \right) \times 0.094 \left(\frac{m^2}{h} \right) \times 0.0195 \left(\frac{kmol}{m^3} \right)}$$

$$= 2.64 \times 10^{-16} < 0.2$$

Safety Check for the Experimental Conditions

By Raoult's Law, the mole fraction of glucose in gas phase is:

$$y_{glucose} = \frac{\gamma_{glucose} \cdot x_{glucose} \cdot P_{glucose}^{vap}}{P}$$

Where,

$\gamma_{glucose} \leq 1$, since glucose is less volatile;

$x_{glucose} = 4.97\%$, see experimental section;

the vapor pressure of D-glucose ($P_{glucose}^{vap}$) is measured as 0.00260 Pa at 122.4 °C;[222]

$$P \approx P_{glucose}^{vap} x_{glucose} + P_{water}^{vap} x_{water} + P_{oxygen} = 0.0026 \text{ Pa} \times 4.97\% + 214507 \text{ Pa} \times 95.03\% + 1500000 \text{ Pa} = 1,703,846.0022 \text{ Pa};$$

Therefore, $y_{glucose} \leq 7.5840 \times 10^{-11}$ at 122.4 °C. Since the mole fraction of glucose in the vapor phase mixture is so small, the possibility of forming flammable mixtures is also negligible under our reaction conditions.

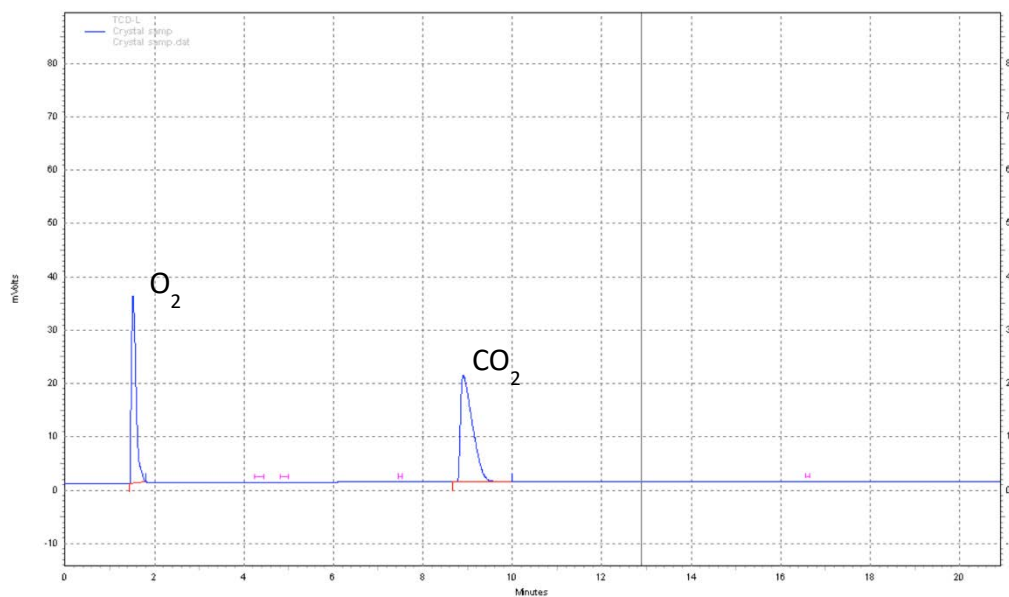


Figure A - 14. Gas chromatography results of gas products for glucose oxidation at 105 °C using Pt-Cu/TiO₂ catalyst (other reaction conditions see experimental descriptions in Table 5)

Table A - 2. Error analysis for carbon balance loss due to CO₂ formation

Product Name	Glucaric Acid	Gluconic Acid	Glyceric Acid	Acetic Acid	Oxalic Acid	CO ₂
Selectivity (%) based on carbon numbers ¹	26.0	3.2	1.2	1.1	0.3	67.0 ²
Theoretical Consumed O ₂ (mol) ³	1.44E-03	8.81E-05	6.87E-05	9.18E-05	4.91E-05	1.12E-02
Total Consumed O ₂ (mol)	1.29E-02					
Initial O ₂ partial pressure (Pa)	1500000					
Final O ₂ partial pressure (Pa)	860535					
Final CO ₂ partial pressure (Pa)	1106247					
Estimated CO ₂ mole fraction in gas (%)	56.25					
Experimental CO ₂ mole fraction in gas (%) ⁴	55					
Error%	2					

¹The selectivity is from the glucose oxidation test at 105 °C using PtCu/TiO₂ (other reaction conditions see Table 5)

²CO₂ selectivity is estimated from the carbon balance of 33%

³Moles of theoretical consumed O₂ is estimated by stoichiometry

⁴Experimental CO₂ mole fraction is measured by Shimatzu GC-2014 Gas Chromatography coupled with a TCD detector, see Figure S10 for details

Appendix IV Supplementary Information for Chapter 5

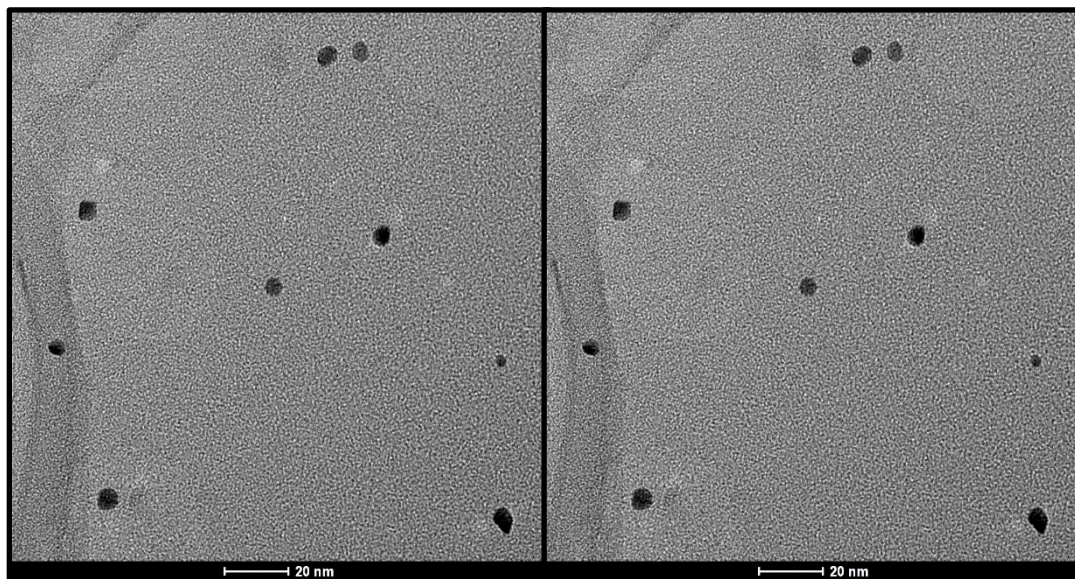


Figure A - 15. TEM images of unsupported Pt-Cu cubes

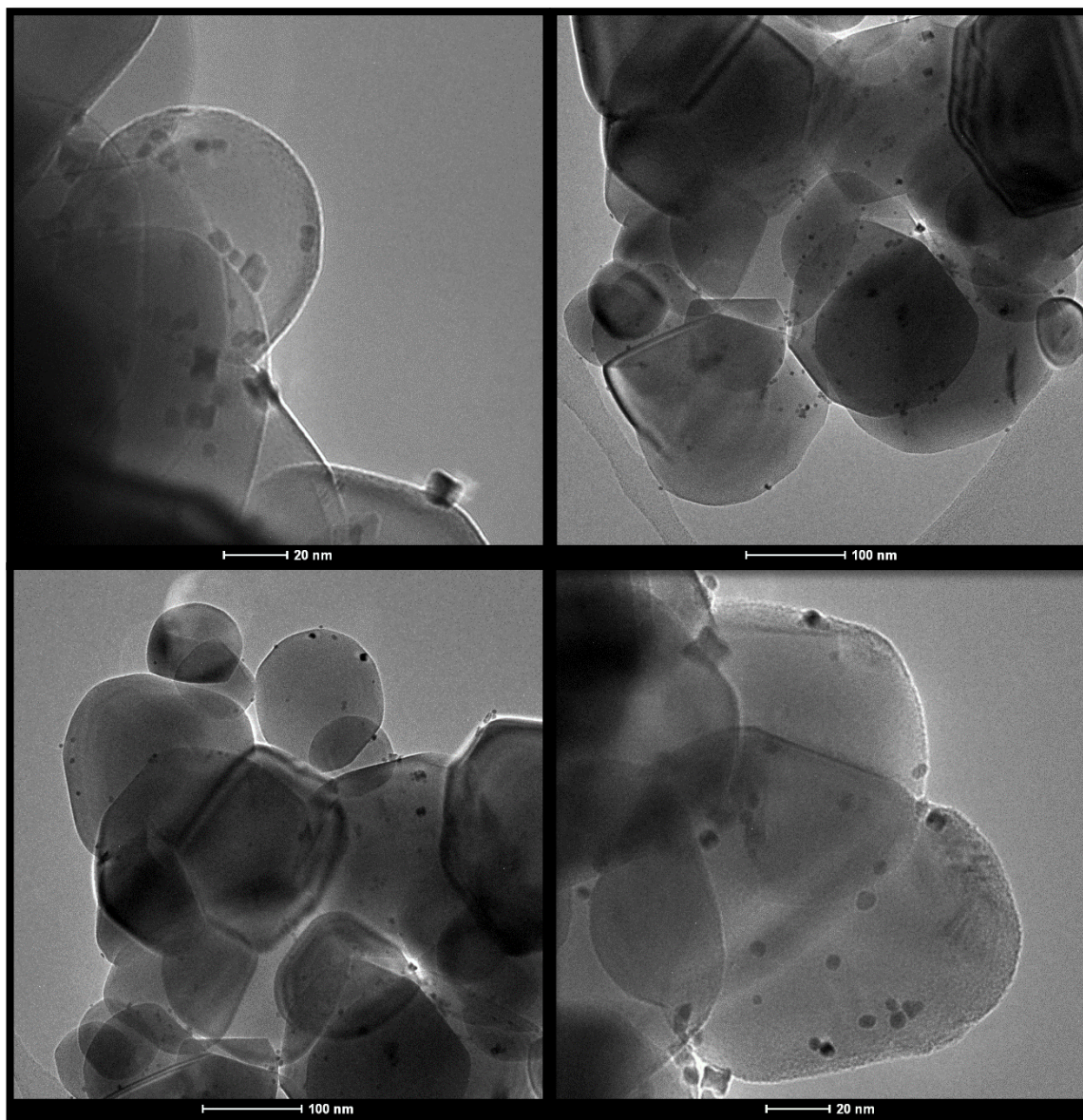


Figure A - 16. TEM of Pt-Cu cubes supported on TiO₂ by using PVP29

Table A - 3. Experimental results on glucose oxidation using Pt-Cu cube without PVP-removal treatment

Time (h)	Glucose Conversion (%)	Gluconic Acid Selectivity (%)	Carbon Balance (%)
1	1.0	100.0	1.03
2	1.4	100.0	1.04
3	3.3	100.0	1.04
4	4.2	100.0	1.04
6	6.1	100.0	1.04
8	8.2	100.0	1.05
12	8.4	100.0	1.03